The Impact of Dehydration and Initial HCl on HCl Null Cycles and Antarctic Stratospheric Ozone Loss in the Core of the Vortex

by
Yiran Zhang

Supervisor:
Prof. Dr. Eckart Rühl
Dr. Rolf Müller

Master Thesis
Master of Science in Chemistry

Freie Universität Berlin
Forschungszentrum Jülich
Monday 19th September, 2022

Eidesstattliche Erklärung

Hiermit versichere ich,

Yiran	Zhang	5044475
Vorname	Name	Matrikelnummer

13.07.1993	Hubei, China
geboren am	geboren in

,

an Eides statt, dass die vorliegende Arbeit von mir selbstständig und ohne unerlaubte Hilfe Dritter verfasst wurde und ich keine anderen als die angegebenen Quellen und Hilfsmittel verwendet sowie wörtliche und sinngemäße Zitate als solche kenntlich gemacht habe.

Diese Arbeit hat in gleicher oder ähnlicher Form noch keiner anderen Prüfungsbehörde vorgelegen und wurde bisher nicht veröffentlicht.

15.09.2022	Yiran Zhang
Ort, Datum	Unterschrift

Abstract

The Antarctic ozone hole is a phenomenon of substantially reduced polar ozone that reoccurs every winter and spring over Antarctica since many decades (Müller et al. 2018). Polar ozone depletion is driven by anthropogenic chlorine and bromine substances released to the atmosphere due to human activities. The Montreal Protocol has been successful in controlling stratospheric chlorine loading, the first signs of declination in stratospheric halogen and recovery of the Antarctic ozone hole are observed around year 2000. However due to the long lifetime of chlorine source gases, they are still causing and will be causing ozone depletion in the foreseeable future.

The characteristics of the global total column ozone field can be reproduced Chemistry-climate models, however the simulation of the Antarctic ozone hole is often not satisfactory due to deficiencies in the model dynamics or in the stratospheric chemistry scheme (Dhomse et al. 2018).

Chlorine species in the atmosphere exist mainly in the form of HCl and $ClONO_2$. Stratospheric ozone depletion requires these so-called reservoirs to convert into active chlorine species by heterogeneous reactions on polar stratospheric clouds (PSCs) and cold sulphate aerosol particles (WMO 2018). Ozone depletion occurs in the presence of light, which first returns in early spring in the Antarctica, this time period is characterised by further activation and maintenance of high levels of active chlorine(Müller et al. 2018.

In this thesis, we follow earlier work [Grooß et al., 2011, Müller et al., 2018, Zafar et al., 2018] on the chemical processes in the core of the vortex, in the lower stratosphere (16 – 18 km, 85–55 hPa, 390–430 K), where extremely low ozone mixing ratios are reached. In these studies the "HCl null cycles" were intensively studied. However, two aspects were neglected in the previous study: namely the impact of Antarctic dehydration (Kelly et al. 1989, Nedoluha et al. 2002, Poshyvailo et al. 2018, Rolf et al. 2015, Schoeberl and Dessler 2011, Vömel et al. 1995) and HCl destruction in Antarctic winter (the exact chemical process remains to be investigated, Grooß et al. 2018). To study the effects of these aspects, box-model simulations were performed. We used similar setup and initiations with small

variations that can represent the above-discussed circumstances. The validity of "HCl null cycles" and other previous studies are tested in these new simulations.
The studies so far were based on the recommendations of Sander et al. 2011. Since year 2011, two revised editions are published (Burkholder et al. 2020, 2015) in which the kinetic parameters of some important reactions are revised. We have conducted calculations that employed the most recent edition (Burkholder et al. 2020) and made comparison to those with Sander et al. 2011. This recommendation was also applied in multi-trajectory simulations.
Simulations with the projection of the future, namely less chlorine species, were also conducted using the recommendation Burkholder et al. 2020.
Overall the results have shown that neither of these two assumptions on the initial conditions has a strong effect on the simulated chemical ozone depletion, small changes have been observed and we have analyzed their causes. The simulations with the recommendation Burkholder et al. 2020 have also shown similar results to the previous studies, however the revised parameters do have a small impact on the patterns of the trajectory trends.

Acknowledgments

This work was done during my study in Freie Universität Berlin, Berlin, Germany and at Stratosphäre (IEK-7), Institut für Energie- und Klimaforschung (IEK), Forschungszentrum Jülich, Jülich.

I would like to thank Prof. Dr. Eckart Rühl, my supervisor in Freie Universität Berlin. His series of lectures on environmental chemistry have a great influence on me, they sparked my passion for atmospheric chemistry.

I owe my deepest gratitude to my supervisor Dr. Rolf Müller in Forschungszentrum Jülich. Dr. Müller has guided me patiently during this thesis, I would not have accomplished this work without him. Dr. Müller is an excellent role model in the academic aspect as well as in life. My stay in Jülich was an unforgettable experience.

Dr. Jens-Uwe Grooß and Ms. Verena Alishahi in Forschungszentrum Jülich have also provided me a lot of instructions in terms of technical setup and methodology. Their help has relieved pressure in my work and I appreciate the support a lot.

Finally yet importantly I would like to thank my parents and my boyfriend, who have supported me emotionally through tough times. I am very fortunate to have you in my life.

Contents

List of Figures

Chapter 1

Introduction

1.1 Ozone in Our Atmosphere

Ozone is an inorganic molecule with the chemical formula O_3. It is composed of three oxygen atoms, naturally it can be found in the atmosphere. The discovery and determination of its structure trace back to mid-1800s. The molecule has a bent structure (Figure 1.1), it is unstable compared to the more common oxygen O_2. Ozone is present in nature and also widely used in the industry. Although high concentration (above 0.1 ppm) ozone is potentially hazardous, ozone layer in the atmosphere is of critical importance in absorbing most of the sun's ultraviolet (UV) radiation.

Ozone can be found in two regions in the atmosphere. Figure 1.2 is a schematic profile

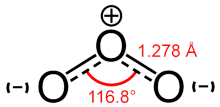

Figure 1.1: The structure of an ozone molecule.

of ozone abundance in relation to altitude in the tropics. In lower troposphere there exist about 10% of the atmospheric ozone, which is mainly a result of the human activities. The remaining 90% is located in the stratosphere, from 10 kilometers to up to 50 kilometers above Earth's surface, this region is commonly known as the "ozone layer". Although called "ozone layer", the ozone concentrations in this region are only two to eight parts per million.

The thickness of the ozone layer also largely depends on the regions and seasons. Total ozone varies intensely with latitude: Ozone production is high in the tropics due to strong solar ultraviolet radiation, but large-scale air circulation in the stratosphere transports ozone

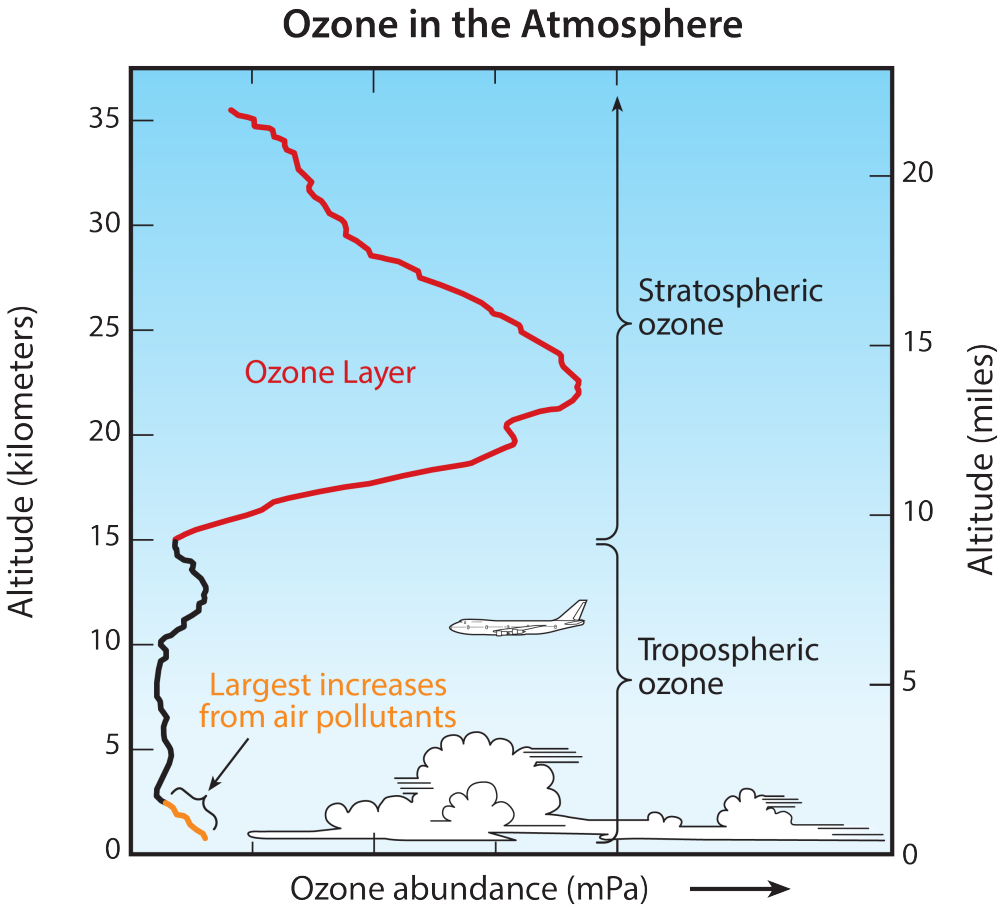

Figure 1.2: Ozone distribution along altitude. (WMO 2018)

to middle and high latitudes. Therefore the thickness is lowest at the equator and highest in polar regions. Figure 1.3 is a typical example of this phenomenon.

Figure 1.4 also shows the seasonal variation on the globe. Total ozone in the tropics (20°N - 20°S latitudes) over all seasons are relatively stable and at low level. Ozone-rich air travels from the tropics and accumulates at higher latitudes, hence ozone at higher latitudes shows higher dependence on the season. A maximum can be seen at high latitudes in the Northern Hemisphere during winter and spring season.
Figure 1.4 depicts an area of low total ozone values (known as the "Ozone Hole") over Antarctica in September, which is the consequence of the ozone-depleting substances produced by human activities.

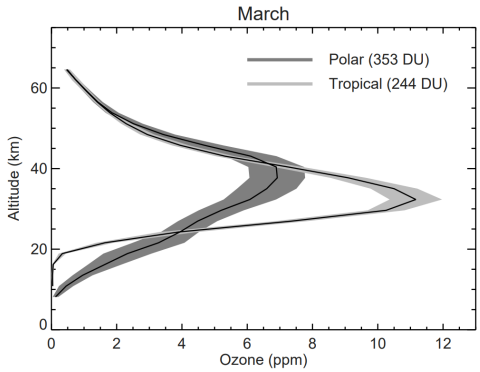

Figure 1.3: The vertical profile of ozone mixing ratio against altitude for polar (equivalent latitude 72.5°N) and tropical (equivalent latitude 2.5°N) conditions in March. The ozone data are from the climatology of Grooß and Russell III 2005. (Müller 2010)

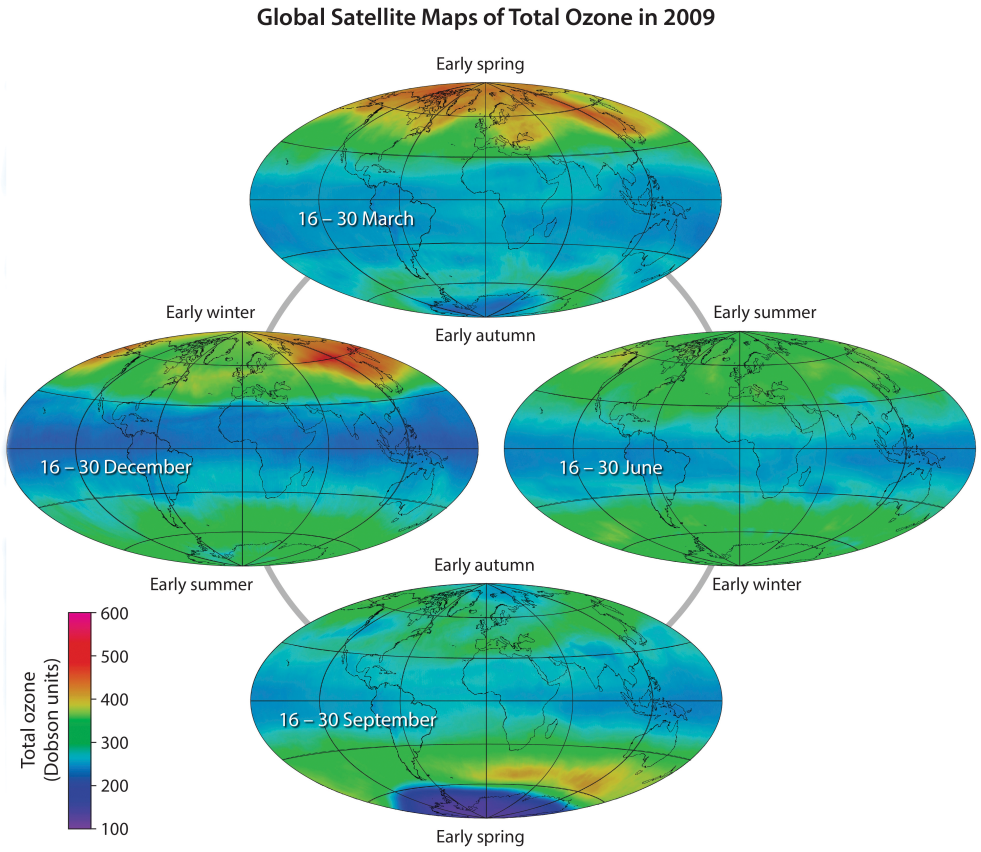

Figure 1.4: Global satellite maps of total ozone in 2009. (WMO 2018)

1.2 Ozone Formation and Ozone depletion

1.2.1 Ozone Formation

Stratospheric ozone formation The main source of formation is the natural chemical reaction of oxygen molecules under solar ultraviolet radiation (Chapman 1930). The process includes complex catalytic cycles and heterogeneous reactions which we will discuss in this thesis, in this introductory section only a very simplified version is described. At certain altitude (about 30 km), molecular oxygen photodissociates into oxygen atoms:

$$O_2 + h\nu \longrightarrow 2\,O$$

In the presence of another molecule M (usually oxygen or nitrogen molecules), oxygen atoms reacts with a unit of oxygen to form ozone:

$$O + O_2 + M \longrightarrow O_3 + M$$

Ozone can also decompose under ultraviolet radiation in the wavelength range of 240 to 320 nm or by reacting with an oxygen atom:

$$O_3 + h\nu \longrightarrow O_2 + O$$

$$O_3 + O \longrightarrow O_2 + O_2$$

Tropospheric ozone formation Ozone near Earth's surface often forms from pollution gases. The primary source of pollutant is fossil fuel combustion. Tropospheric ozone is small in amount and it usually does not transport to the stratosphere effectively.

1.2.2 The Ozone Depletion Process

Emission The main sources of emissions are manufactured halogen source gases, especially manufactured halocarbon refrigerants, solvents, propellants, and foam-blowing agents (chlorofluorocarbons (CFCs), HCFCs, halons), these chemicals are often referred to as ozone-depleting substances (ODS). CFCs were the most important materials in refrigeration and air conditioning systems, halons were used in fire extinguishers. Oceanic and terrestrial ecosystems also emit a large amount of some halogen sources gases, namely methyl chloride

(CH_3Cl) and methyl bromide (CH_3Br). Natural emissions make up about 17% to the total chlorine and 30% to the total bromine in the stratosphere (statistics from year 2012).
Non-halogen gases caused by human activities can also have a negative effect stratospheric ozone. Methane (CH_4) and nitrous oxide (N_2O) are the important emissions from human activities that can react in the stratosphere into water vapor and reactive hydrogen and nitrogen oxides. These are the substances that can destroy stratospheric ozone.

Accumulation and Transportation The lifetime of the halogen source gases is relatively long (from one year to several hundred years). Short living gases (HCFCs, methyl bromide, methyl chloride, etc.) are able to convert to other gases, which are effectively removed by the rain in the troposphere. Halogen source gases with long lifetime are stable in the lower atmosphere, therefore they accumulate in the lower atmosphere and are transported to the stratosphere by natural air motions.

Conversion and Reaction Under ultraviolet radiation, halogen source gases in the stratosphere convert to reactive halogen gases. These include chemical reservoirs like bromine nitrate ($BrONO_2$), hydrogen chloride (HCl) and chlorine nitrate ($ClONO_2$). Reservoirs do not directly react with ozone. Very reactive halogen gases like chlorine monoxide (ClO), bromine monoxide (BrO), bromine atoms (Br) and clorine atoms (Cl) take part in catalytic reaction cycles that decompose ozone directly.

$$
\begin{aligned}
\mathrm{Cl} + \mathrm{O_3} &\longrightarrow \mathrm{ClO} + \mathrm{O_2} \\
\mathrm{ClO} + \mathrm{O} &\longrightarrow \mathrm{Cl} + \mathrm{O_2} \\
\hline
\text{Net: } \mathrm{O_3} + \mathrm{O} &\longrightarrow 2\,\mathrm{O_2}
\end{aligned}
$$

$$
\begin{aligned}
\mathrm{ClO} + \mathrm{ClO} &\longrightarrow \mathrm{Cl_2O_2} \\
\mathrm{Cl_2O_2} + \mathrm{h}\nu &\longrightarrow \mathrm{ClOO} + \mathrm{Cl} \\
\mathrm{ClOO} &\longrightarrow \mathrm{Cl} + \mathrm{O_2} \\
2\,(\mathrm{Cl} + \mathrm{O_3} &\longrightarrow \mathrm{ClO} + \mathrm{O_2}) \\
\hline
\text{Net: } 2\,\mathrm{O_3} &\longrightarrow 3\,\mathrm{O_2}
\end{aligned}
$$

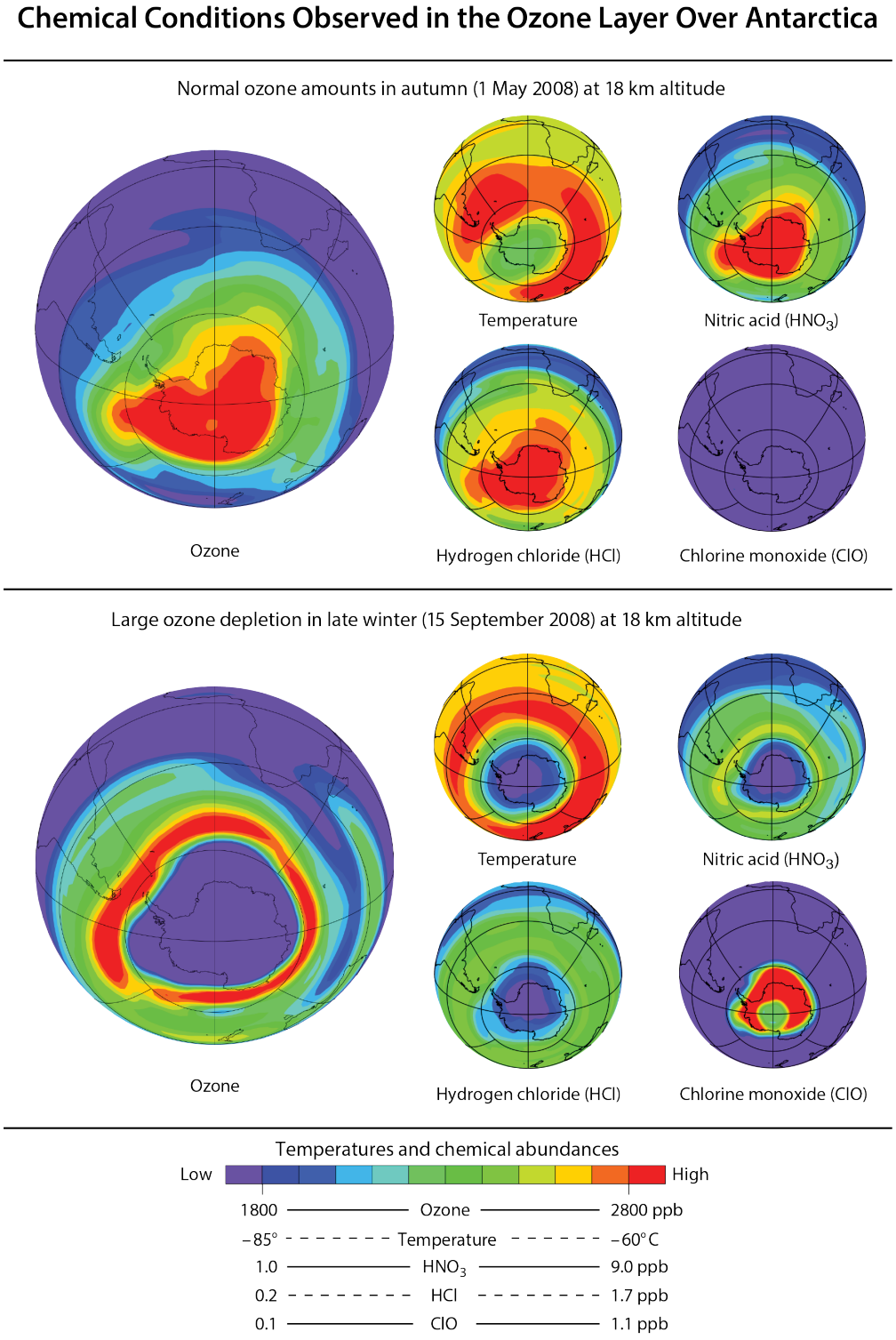

Figure 1.5: Chemical conditions in the ozone layer over Antarctica. Observations of the chemical conditions in the Antarctic region highlight the changes associated with the formation of the ozone hole. Satellite instruments have been routinely monitoring ozone, reactive chlorine gases, and temperatures in the global stratosphere. Results are shown here for autumn (May) and late winter (September) seasons in the Antarctic region, for a narrow altitude region near 18 km (11.2 miles) within the ozone layer. WMO 2018)

1.3 Ozone Hole

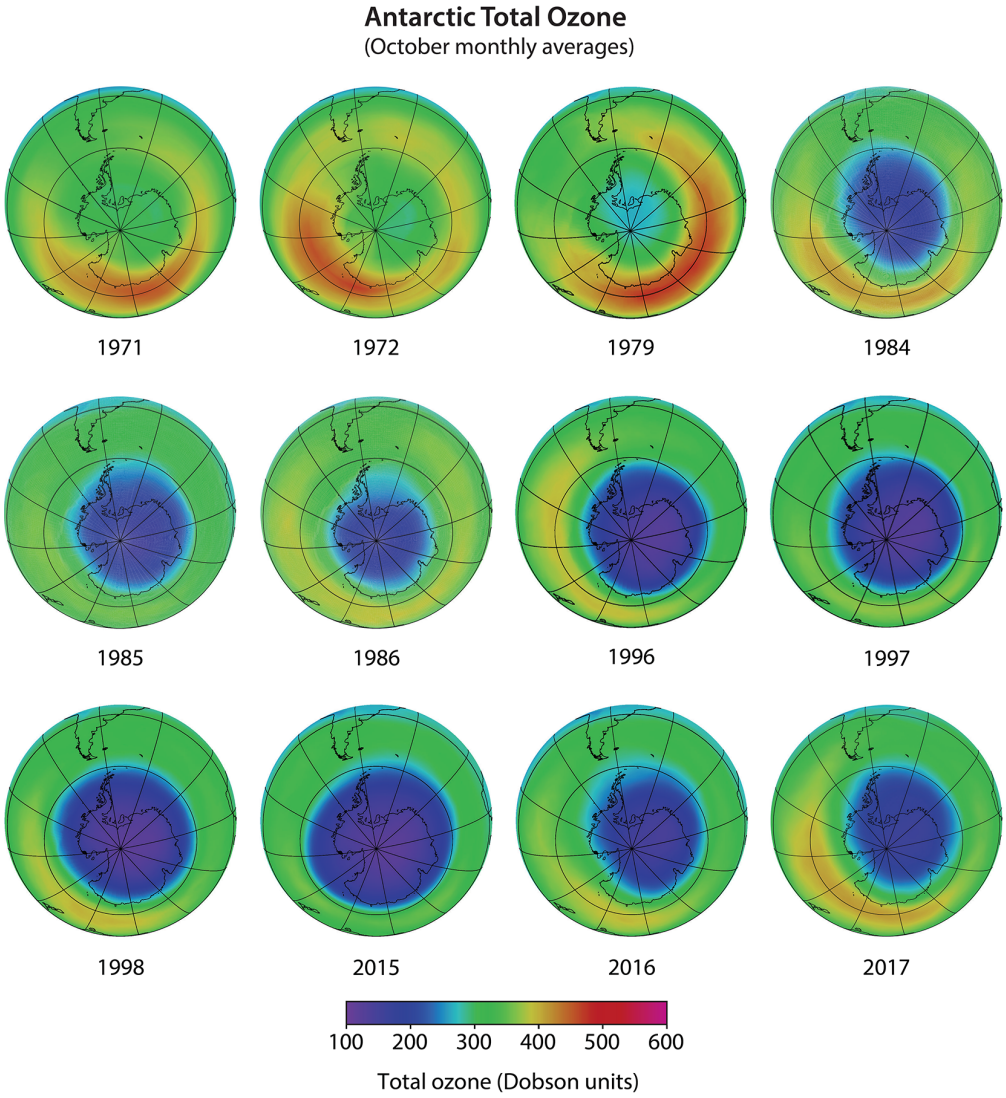

Figure 1.6: Antarctic total ozone. Long-term changes in Antarctic total ozone are demonstrated with this series of total ozone maps derived from satellite observations. Each map is an average during October, the month of maximum ozone depletion over Antarctica. In the 1970s, no ozone hole was observed, as defined by a significant region with total ozone values less than 220 DU (dark blue and purple colors). The ozone hole initially appeared in the early 1980s and increased in size until the early 1990s. A large ozone hole has occurred each year since the early 1990s.(WMO 2018)

In 1985, it was reported that in Antarctic spring strongly reduced total ozone values occurred at the British Antarctic Survey station at Halley (Mahieu et al. 2004, Rinsland

et al. 2003). It is one of the most astonishing examples of direct impact of human activities on the atmosphere. The term "ozone hole" for this phenomenon was first used in Stolarski 1988. Obviously, it is not a true "hole", there still exists some column ozone. In the core of the ozone hole, value of about 100 DU ozone still remains. The most recent satellite measurements of ozone hole from year 1971 to year 2017 is shown in figure 1.6.
Ozone-depleting substances are produced mostly in areas with high density on human activities. Air motions transport these substances throughout the stratosphere, yet severe depletion of ozone layer is mostly only found in the Antarctic. The Antarctic ozone layer has a very special meteorological and chemical conditions. In Autumn, a large vortex forms over Antarctica as the polar stratosphere radiatively cools, creating a thermal contrast between polar and mid-latitude air. As the cooler polar air descends, mid-latitude air moves in the direction of pole and a strong wind jet forms, when the Coriolis force deflects the air eastward. This wind jet is the reason why the Antarctic polar vortex is strongly isolated from the mid-latitude stratosphere (Yokouchi et al. 2005). The isolated vortex ensured a stably low enough temperature increased effectiveness of ozone destruction by reactive chlorine-containing gases. In spring, temperatures in the polar lower stratosphere increase, stopping the most effective chemical cycles that destroy ozone.

1.4 Implications of Ozone Depletion and the Montreal Protocol

Ozone depletion is not the principal cause of global climate change. However, both ozone-depleting substances and their substitutes are greenhouse gases, ozone depletion and global climate change are closed linked. Ozone itself is also a greenhouse gas, stratospheric ozone depletion leads to surface cooling. On the other hand, escalating tropospheric ozone and other greenhouse gases level lead to surface warming. The cooling effect from ozone depletion is small compared to the warming from the greenhouse gases responsible for observed global climate change.
The important consequence of a hole in the ozone layer is an increased flux of UV radiation at the earth's surface and in the top layers of the ocean (Smith et al. 1992). Ozone depletion does not simply increase all UVB-related effects, because adaptive reactions will dampen or even neutralize the impact of an increase in UVB radiation even if sun-exposure behaviour remains the same (de Gruijl and Leun 2000). Changes in stratospheric ozone and climate over the past 40-plus years have already altered the solar ultraviolet (UV) radiation condi-

tions at the Earth's surface. These changes are interacting in complex ways to affect human health, food and water security, and ecosystem services (Barnes et al. 2019).

In response to the growing concern on ozone hole, in 1987 **the Montreal Protocol on Substances that Deplete the Ozone Layer** was signed and entered into force in 1989. The Montreal Protocol was strengthened with Amendments and Adjustments with the development of researches on ozone depletion as well as substitutes and alternatives. Each Amendment is named after the city where the Meeting of the Parties to the Montreal Protocol took place and by the year. Montreal Protocol controls are based on several factors that are considered separately for each ODS. The factors include (1) ozone depleting potential, (2) the availability of suitable substitutes for domestic and industrial use, and (3) the potential impact of controls on developing nations (UNEP 1987).

The Montreal Protocol has most certainly been successful in reducing ozone-depleting substances in the atmosphere. Figure 1.7 shows the development of stratospheric halogen loading measured as the equivalent effective stratospheric chlorine. The past increases of CFCs, along with those of carbon tetrachloride, methyl chloroform, halon-1211, and halon-2402, have slowed and reversed in the last three decades. The abundances of most HCFCs, which are used as transitional substances to replace CFCs, will likely continue to increase in the next one to two decades before production and consumption are completely phased out. The abundance of halon-1301 has nearly peaked and is expected to decline in coming decades. Future decreases in methyl bromide are expected to be modest, since industrial production is now much smaller than occurred in the 1990s. The abundance of methyl chloride is projected to be constant in the future as it is not controlled under the Montreal Protocol.

Equivalent effective stratospheric chlorine values (EESC) are a measure of the potential for ozone depletion in the stratosphere, obtained by summing over adjusted amounts of all chlorine and bromine gases. Effective stratospheric chlorine levels as shown here for mid-latitudes will return to 1980 values around 2050. The return to 1980 values will occur around 2065 in polar regions (Newman et al. 2007). Overall emissions and atmospheric concentrations have decreased and will continue to decrease given international compliance with the provisions of the Montreal Protocol.

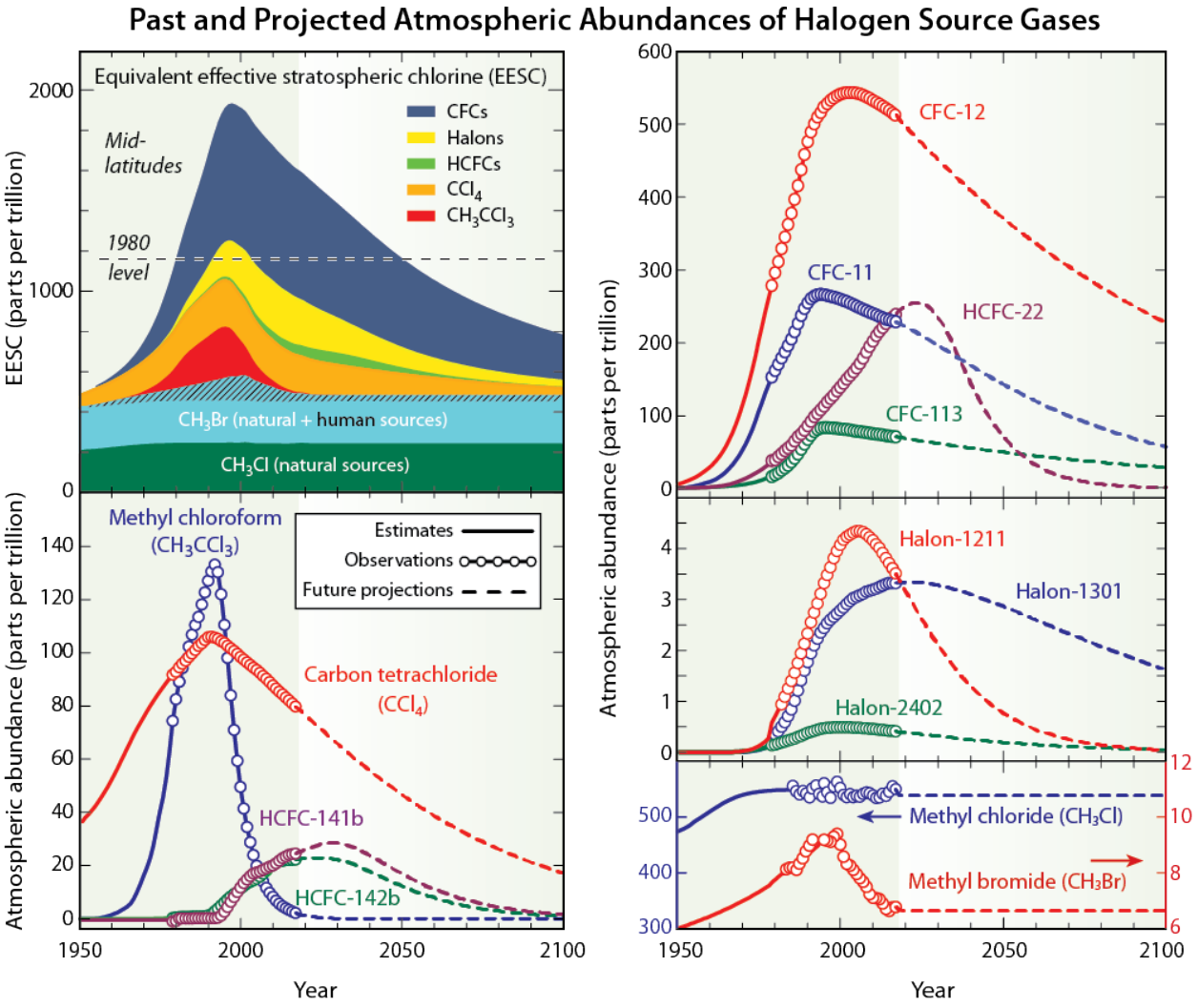

Figure 1.7: Halogen source gas changes. The surface abundances of individual gases shown here were obtained using a combination of direct atmospheric measurements, estimates of historical abundances, and future projections of abundances assuming compliance with the Montreal Protocol. The gases are all ODSs except for methyl chloride, which is produced by natural processes. (WMO 2018)

1.5 Stratosphere Ozone in the 21st Century

Around the middle of 21st century, we expect a substantial recovery of the ozone layer. As ODSs and reactive halogen gases in the stratosphere decreases, ozone recovery is also observable in the presence. On the other hand, as a result of climate change, the ozone layer will not return precisely to its unperturbed state when the abundance of halogens returns to background levels. Furthermore, climate change complicates the attribution of ozone recovery to the decline of ODSs (Waugh et al. 2009).

To project the future evolution of stratospheric ozone and attribute its change in response to the different constraints, numeric models that can adequately represent the chemistry and the dynamics of the ozone layer are practical. These models include inputs of historical and projected concentrations of ODSs, CO2, CH4, N2O, air pollutant gases, as well as solar output, they evaluate the complex interactions of the processes that control ozone and climate involving radiation, chemistry, and transport. Thus we are able to analyze how changes in ozone are expected to vary across geographic regions.

Such Chemistry-Climate Models (CCMs) are three dimensional atmospheric circulation models with fully coupled chemistry. CCMs are key tools for the detection, attribution and projection of the response of stratospheric ozone and solar ultraviolet (UV) radiation levels to be studied (Eyring et al. 2007).

Over the past decade several international projects evaluating stratospheric CCMs as well as related General Circulation Models (GCMs) were developed. Most of them are organized under the auspices of the WCRP's (World Climate Research Programme) SPARC (Stratospheric Processes and their Role in Climate) project. For example, the GCM-Reality Inter-comparison Project (GRIPS) and the Chemistry-Climate Model Validation (CCM-Val) Activity (Eyring et al. 2005, Pawson et al. 2000). These multi-model projects have contributed directly to the assessment of CCMs during the preparation of the World Meteorological Organization/ United Nations Environment Programme (WMO/UNEP) Scientific Assessments of Ozone Depletion (CCMVal 2010, Eyring et al. 2005, 2006, 2007, 2010, Oman et al. 2010, Pawson et al. 2000).

The model used in this thesis is **the Chemical Lagrangian Model of the Stratosphere (CLaMS)**. It is a modular chemistry transport model (CTM) system developed at Research Centre Jülich, Germany.

CLaMS was first described in year 2000 and was expanded into three dimensions in Konopka et al. 2004. CLaMS has been employed in various European aircraft field campaigns including THESEO, EUPLEX, TROCCINOX, SCOUT-O3, RECONCILE and STRATOCLIM with

a focus on simulating ozone depletion and water vapour transport.
The advantage of CLaMS in comparison to other CTMs are (Krämer et al. 2003):

- its low diffusive Lagrangian transport scheme with the ability to reproduce small-scale structures and gradients of trace species;
- its applicability for reverse domain filling studies;
- its anisotropic mixing scheme;
- its integrability with arbitrary observational data;
- comprehensive chemistry scheme.

The details of the model CLaMS are well documented and published in the scientific literature. The details of the model is described in the following chapter.

Chapter 2

Theoretical Fundation and Methods

2.1 Polar Stratospheric Clouds

Polar stratospheric clouds (PSCs) are clouds in the winter polar stratosphere at altitudes of 15 – 25km. Normally, the water vapour mixing ratio of stratospheric air is very low, because most of the moisture freezes out as the air transits the tropopause, where temperatures are extremely low (Peter and Grooß 2012b). Further cloud formation is usually impossible due to the extremely dryness of the air, except in the polar winter stratosphere, where ice saturation is approached at 188 K ± 4 K as the Antarctic is extremely cold. There are two main types of PSCs: Type I clouds contain water, nitric acid (HNO_3) and sulfuric acid (H_2SO_4) and are a source of polar ozone depletion. Type II clouds consist solely of water ice, which are very rarely observed in the Arctic. The PSCs references in this thesis signify type I PSCs only.

Solid water ice particles can exist only below the frost point T_{ice} (typically below 188 K in the lower stratosphere), because only then the vapor pressure of ice drops below water partial pressures prevalent in the lower stratosphere. However, below the so-called "NAT-temperature", T_{NAT} = 195 K, crystalline nitric acid trihydrate (NAT) particles can nucleate and exist steadily (Hanson and Mauersberger 1988, Peter and Grooß 2012a). Balloon-borne mass spectrometric measurements have confirmed the stoichiometric $HNO_3 : H_2O = 1 : 3$ inside solid PSCs (Voigt et al. 2000).

NAT-PSCs can form in different pathways, depending on whether solid inclusion exists: they nucleate heterogeneously on pre-existing sold inclusion at or slightly below T_{NAT} = 195 K, subsequently ice nucleates heterogeneously below T_{ice} = 188 K; Or NAT nucleate heterogeneously on ice below (T_{ice} - 3 K) without previous solid inclusions. Different hypotheses

remain to be proven for the detailed mechanisms behind. Although the nucleation process is not identified, the estimated nucleation rates have been used to simulate the vertical redistribution of HNO_3. The simplified assumption is that, if T drops lower than T_{NAT}, the NAT nucleation rate is a constant. Davies et al. 2002, Grooß et al. 2005 have adapted this assumption.

Figure 2.1 shows profiles of NO_y redistribution measured (crosses) in January 2003 and

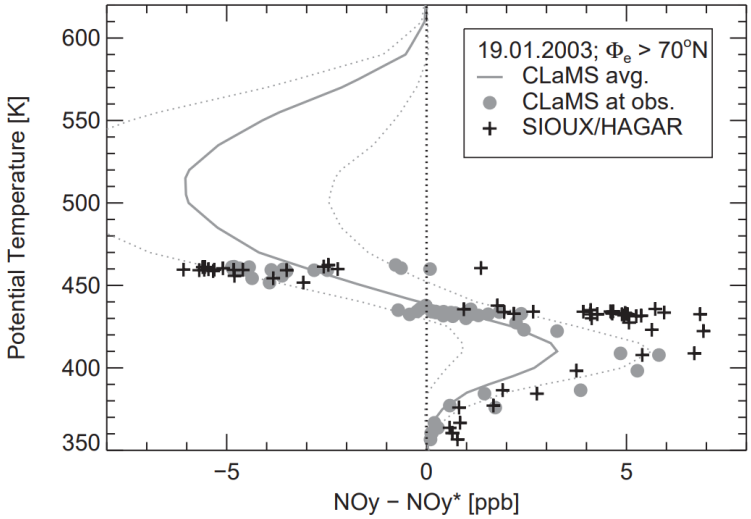

Figure 2.1: Denitrification derived from measurements (black crosses) and model simulations (lines and gray circles). (Grooß et al. 2005)

simulated by CLaMS (lines and gray circles). The vertical axis is roughly linear in geometric altitude with 350 K potential temperature corresponding to ≈ 14 km, and 600 K to ≈ 24 km. The model uses a constant nucleation rate of 7.8×10^{-6} cm^{-3} air h^{-1}. The thick gray line corresponds to the modeled vortex average and the dotted lines indicate the standard deviation (variability is massive due to the sedimentation process, despite the generally widespread nucleation wherever T is smaller than T_{NAT}. Crosses show measurements onboard the Geophysica high-altitude aircraft. Results from the CLaMS simulations for the location of these observations are shown as gray circles(Grooß et al. 2005).

This figure shows that the vertical redistribution of NO_y can be generally well described by the model, although the model can miss specific measurement points by more than 50%. Simulations in this thesis continue to apply this assumption.

2.2 Stratospheric Halogen Chemistry

Before we dive into details, first the concept of "active chlorine" ClO_x needs to be defined:

$$ClO_x = ClO + 2 \times Cl_2O_2 + Cl \tag{E1}$$

Active chlorine, contrary to chlorine reservoir species (HCl, $ClONO_2$), reacts with ozone molecules directly.
As already shortly discussed in section 1.2.2 Chapter 1, the decomposition of anthropogenically emitted source gases releases chlorine in the stratosphere. In the presence of sunlight, ozone is depleted by catalytic cycles involving several chlorine species.
The most fundamental ozone destroying catalytic cycle is:

$$\begin{aligned} O_3 + h\nu &\longrightarrow O_2 + O \\ XO + O &\longrightarrow X + O_2 \\ X + O_3 &\longrightarrow XO + O_2 \\ \hline \text{Net(X1): } 2\,O_3 &\longrightarrow 3\,O_2 \end{aligned}$$

The X in cycle (X1) could be any halogen atom. Fluorine reacts with CH_4, due to the high stability of reservoir gas HF, the loss of Fluorine in the stratosphere takes place fast. The concentration of iodine in the stratosphere is insignificant. Therefore, X is mainly chlorine and bromine (von Hobe and Stroh 2011).
More complex catalytic cycles exist as radicals like HO_x or NO_x interact with halogens. For example, chlorine monoxide can react with HO_2, the cycles is commonly called as HOCl cycle(Johnson et al. 1995, Kovalenko et al. 2007, Poulet et al. 1992), the same works for Br and accordingly HOBr cycle:

$$\begin{aligned} O_3 + OH &\longrightarrow O_2 + O_2 \\ XO + HO_2 &\longrightarrow HOX + O_2 \\ HOX + h\nu &\longrightarrow X + OH \\ X + O_3 &\longrightarrow XO + O_2 \\ \hline \text{Net(X2): } 2\,O_3 &\longrightarrow 3\,O_2 \end{aligned}$$

The production of a halogen atom upon photolysis of the reservoir gases $ClONO_2$ (Toumi et al. 1993) also leads to ozone destruction cycle (X3). In this cycle, the presence of sufficient

aerosol surface area is necessary as these reactions are not purely gas phase but heterogeneous. They also need to have the potential to simultaneously generate HO_x from HCl (Lary et al. 1996).

$$\begin{aligned}
NO + O_3 &\longrightarrow NO_2 + O_2 \\
XO + NO_2 + M &\longrightarrow XONO_2 + M \\
XONO_2 + h\nu &\longrightarrow X + NO_3 \\
NO_3 + h\nu &\longrightarrow NO + O_2 \\
X + O_3 &\longrightarrow XO + O_2 \\
\hline
\text{Net(X3): } 2\,O_3 &\longrightarrow 3\,O_2
\end{aligned}$$

In addition to cycle (X3), ClO_x and NO_x could interact in gas-phase catalytic cycle:

$$\begin{aligned}
O_3 + h\nu &\longrightarrow O_2 + O \\
O + NO_2 &\longrightarrow NO + O_2 \\
NO + ClO &\longrightarrow NO_2 + Cl \\
Cl + O_3 &\longrightarrow Cl + O_2 \\
\hline
\text{Net(X4): } 2\,O_3 &\longrightarrow 3\,O_2
\end{aligned}$$

The relative contribution to ozone depletion of cycle (X3) and (X4) in different regions and under different conditions has been studied thoroughly in Grenfell et al. 2006.

2.3 Heterogeneous Chemistry

The abundance of atomic oxygen is sufficiently low at high latitudes in the lower stratosphere to limit the rate of ozone depletion. The catalytic cycles explained in the previous section are inadequate to fully explain the formation of ozone hole. Molina and Molina 1987 and McElroy et al. 1986 have proposed two further catalytic cycles that does not require atomic oxygen, yet they remove ozone from the stratosphere effectively: the ClO dimer cycle and the ClO/BrO cycle. Figure 2.2 shows the reaction schemes and the interactions between them.

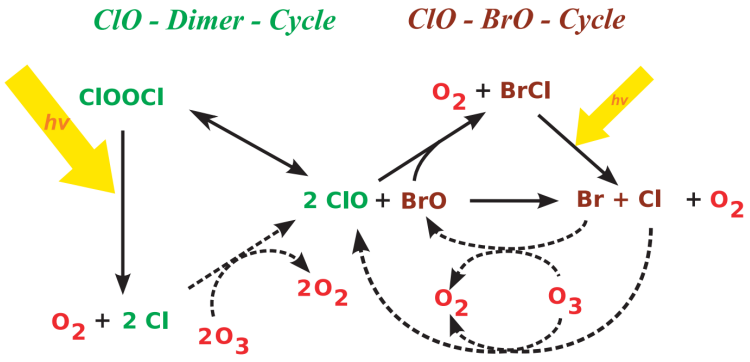

Figure 2.2: Schematic of the two most important catalytic cycles and their interaction. (von Hobe and Stroh 2011)

The ClO Dimer Cycle The ClO dimer cycle (X5) starts with the recombination of two ClO radicals. In the polar stratosphere in winter, PSCs leads to significant growth of ClO concentration, this favors the initialization of (X5):

$$
\begin{array}{rcl}
\mathrm{ClO} + \mathrm{ClO} + \mathrm{M} & \longleftrightarrow & \mathrm{Cl_2O_2} + \mathrm{M} \\
\mathrm{Cl_2O_2} + \mathrm{h}\nu & \longrightarrow & \mathrm{Cl} + \mathrm{ClO_2} \\
\mathrm{ClO_2} + \mathrm{M} & \longrightarrow & \mathrm{Cl} + \mathrm{O_2} + \mathrm{M} \\
2\ [\ \mathrm{Cl} + \mathrm{O_3} & \longrightarrow & \mathrm{ClO} + \mathrm{O_2}\ ] \\
\hline
\mathrm{Net(X5):}\ 2\,\mathrm{O_3} & \longrightarrow & 3\,\mathrm{O_2}
\end{array}
$$

The heterogeneous reaction of ClOO proceed principally instantaneously with $\mathrm{Cl} + \mathrm{O_3}$, therefore they do not limit the overall rate of the catalytic cycle. Of importance is the photolysis rate of $\mathrm{Cl_2O_2}$, because under twilight conditions, it is the rate determining step of (X5).

The ClO/BrO Cycle In this cycle (X6), ClO and BrO recombination forms Cl, Br atoms BrCl and OClO, no mixed diner formation occurs.

$ClO + BrO$	$\longrightarrow$	$Cl + Br + O_2$ (a)
	$\longrightarrow$	$BrCl + O_2$ (b)
	$\longrightarrow$	$OClO + Br$ (c)
$BrCl + h\nu$	$\longrightarrow$	$Br + Cl$
$Cl + O_3$	$\longrightarrow$	$ClO + O_2$
$Br + O_3$	$\longrightarrow$	$BrO + O_2$
Net(X6): $2\,O_3$	$\longrightarrow$	$3\,O_2$

Reaction (c) in (X6) does not result in ozone depletion, as OClO is photolysed upon formation, which yields an oxygen atom afterwards. Oxygen atom react with O_2 to produce an ozone molecule. Therefore, the branching of this reaction is one of the key parameters in this catalytic cycle in terms of quantifying ozone loss.

2.4 HCl Null Cycles

The initial step of chlorine activation proceeds via the heterogeneous reaction /Solomon et al. 1986):

$$ClONO_2 + HCl \longrightarrow Cl_2 + HNO_3 \tag{R1}$$

As temperature drops low enough for heterogeneous chlorine activation to occur, reaction (R1) proceeds very rapidly during polar night (mid May). Initial $ClONO_2$ concentration is extremely low (Jaeglé et al. 1997, Santee et al. 2008), therefore the production of Cl_2 through (R1) is constraint (Crutzen et al. 1992, Salawitch et al. 1988). $ClONO_2$ or HOCl are required for heterogeneous reactions with HCl. It is crucial that, heterogeneous reaction

$$HOCl + HCl \longrightarrow Cl_2 + H_2O \tag{R2}$$

as well as the gas-phase reaction (Crutzen et al. 1992)

$$CH_3O_2 + ClO \longrightarrow CH_3O + ClOO \tag{R3}$$

occur for the efficacy of HCl null cycles. The product ClOO in (R3) decomposes rapidly to Cl and oxygen. Additionally, the formation of HO_x from CH_3O is also necessary.

The maintenance of chlorine activation Crutzen et al. 1992 first formulated cycle (C1) to explain the importance of (R3). Together with the CH_3 formed in (R4), they form a radical HO_2.

$$\begin{aligned}
CH_4 + Cl &\longrightarrow HCl + CH_3 && \text{(R4)}\\
CH_3 + O_2 + M &\longrightarrow CH_3O_2 + M && \text{(R5)}\\
CH_3O_2 + ClO &\longrightarrow CH_3O + ClOO && \text{(R3)}\\
CH_3O + O_2 &\longrightarrow HO_2 + HCHO && \text{(R6)}\\
ClO + HO_2 &\longrightarrow HOCl + O_2 && \text{(R7)}\\
HOCl + HCl &\longrightarrow Cl_2 + H_2O && \text{(R2)}\\
Cl_2 + h\nu &\longrightarrow 2\,Cl && \text{(R8)}\\
2\,[\,Cl + O_3 &\longrightarrow ClO + O_2\,] && \text{(R9)}\\
\hline
\text{Net(C1):}\ CH_4 + 2\,O_3 &\longrightarrow HCHO + H_2O + 2\,O_2 && \text{(R10)}
\end{aligned}$$

Both reactions (R4) and (R11) produce HCl, for each molecule formed, an HO_2 is generated (via (R6) in cycle C1 and via (R12) in cycle C2). Each HO_2 proceed to form one HOCl molecule. As HOCl and HCl undergoes heterogeneous reaction R2 with 1:1 stoichiometry, there is no net production of HCl.

$$\begin{aligned}
HCHO + Cl &\longrightarrow HCl + CHO && \text{(R11)}\\
CHO + O_2 &\longrightarrow CO + HO_2 && \text{(R12)}\\
ClO + HO_2 &\longrightarrow HOCl + O_2 && \text{(R7)}\\
HOCl + HCl &\longrightarrow Cl_2 + H_2O && \text{(R2)}\\
Cl_2 + h\nu &\longrightarrow 2\,Cl && \text{(R8)}\\
Cl + O_3 &\longrightarrow ClO + O_2 && \text{(R9)}\\
\hline
\text{Net(C2):}\ HCHO + O_3 &\longrightarrow CO + H_2O + O_2 && \text{(R10)}
\end{aligned}$$

Therefore we call cycles C1 and C2 the "HCl null cycles". In these cycles, Reaction (R3) dominates the loss of CH_3O_2. Müller and Crutzen 1994 have also proposed alternative reactions for CH_3O_2, the competition of these different reactions were analyzed in Lehmann

2004.
The effectiveness of these HCl null cycles in maintaining the HCl level is confirmed in Müller et al. 2018. The simulations have shown no net production of HCl despite the fact that the reaction rate of (R4) and (R11) increased and thus the production increased by two orders of magnitude in September, 2003. Cycles C1 and C2 constitute the chemical mechanism responsible for the maintenance of high levels of active chlorine.

Full activation of HCl Lehmann 2004, Müller et al. 2018 identified two further chemical cycles that are responsible the the activation of HCl.

$HCHO + h\nu$	$\longrightarrow$	$CHO + H$	(R14a)
$H + O_2 + M$	$\longrightarrow$	$HO_2 + M$	(R15)
$CHO + O_2$	$\longrightarrow$	$CO + HO_2$	(R12)
$2\ [\ ClO + HO_2$	$\longrightarrow$	$HOCl + O_2\ ]$	(R7)
$2\ [\ HOCl + HCl$	$\longrightarrow$	$Cl_2 + H_2O\ ]$	(R2)
$2\ [\ Cl_2 + h\nu$	$\longrightarrow$	$2\,Cl\ ]$	(R8)
$4\ [\ Cl + O_3$	$\longrightarrow$	$ClO + O_2\ ]$	(R9)
Net(C3): $HCHO + 2\,HCl + 4\,O_3$	$\longrightarrow$	$CO + 2\,ClO + 2\,H_2O + 4\,O_2$	(R10)
$O_3 + h\nu$	$\longrightarrow$	$O(^1D) + O_2$	(R17)
$O(^1D) + H_2O$	$\longrightarrow$	$2\,OJ$	(R18)
$2\ [\ OH + O_3$	$\longrightarrow$	$HO_2 + O_2\ ]$	(R19)
$2\ [\ ClO + HO_2$	$\longrightarrow$	$HOCl + O_2\ ]$	(R7)
$2\ [\ HOCl + HCl$	$\longrightarrow$	$Cl_2 + H_2O\ ]$	(R2)
$2\ [\ Cl_2 + h\nu$	$\longrightarrow$	$2\,Cl\ ]$	(R8)
$4\ [\ Cl + O_3$	$\longrightarrow$	$ClO + O_2\ ]$	(R9)
Net(C4): $2\,HCl + 7\,O_3$	$\longrightarrow$	$2\,ClO + H_2O + 9\,O_2$	(R10)

Cycle C3 and C4 both require sufficiently fast heterogeneous reactions to be present. In contrast to cycles C1 and C2, the production of HO_2 proceeds without simultaneous HCl

formation. Therefore, as HO_2 forms HOCl via (R7), it result in net loss of HCl via (R2). Reactions (R9), (R17) and (R19) are fast enough to sustain cycles C3 and C4 at extremely low ozone concentrations and are not rating-determining for cycles C3 and C4 (Müller et al. 2018). For Cycle C3, the photolysis reaction (R14a) is the rate-determining step, and for cycle C4 is reaction (R18).
The primary source of HO_x in polar lower stratosphere in late winter and in early spring is the photolysis of HCHO (reaction (R14a)). The photolysis consists of two channels, namely the radical channel and the molecular channel:

$$HCHO + h\nu \longrightarrow HCO + H \tag{R14a}$$

$$HCHO + h\nu \longrightarrow H_2 + CO \tag{R14b}$$

The molecular channel produces hydrogen and carbon monoxide, which does not continue to take part in the production of HO_x (Crowley et al. 1994, Crutzen et al. 1992, Müller and Crutzen 1994). The sensitivity of the ozone in relation to the branching ratio of HCHO is studied in Müller et al. 2018.

2.5 Pathway Analysis

When the output of a complex chemical model is analysed, a typical topic is the determination of pathways, i.e., reaction sequences, that produce or destroy a chemical species of interest. A representative example is the investigation of catalytic ozone destruction cycles in the stratosphere. An algorithm for the automatic determination of pathways in any given reaction system is presented in Lehmann 2004 and is employed here. Reaction rates are assumed to be given, the algorithm finds all pathways with a rate above a predetermined threshold. The algorithm forms pathways step by step, starting from single reactions. The chemical species in the system are consecutively considered as "branching points". For every branching-point species, each pathway producing it is connected with each pathway consuming it. Rates proportional to "branching probabilities" are calculated. Pathways with a rate that is smaller than a prescribed threshold are discarded. If a newly formed pathway contains sub-pathways, e.g., null cycles, it is split into these simpler pathways.
(Special acknowledgement: note that in this thesis, the pathway analysis results are the contribution of Ralph Lehmann from his unpublished research on "Rapid net HCl formation in the Antarctic spring stratosphere despite counteracting heterogeneous chemistry, and implications for minimum ozone concentration".

Some results and discussions of Chapter 4 are based on the calculations of pathway analysis of this work. By the time of completion of this thesis, the above-said work is still in the planning phase of publishing.)

Chapter 3

Model Description

3.1 ClaMS

The details of the model CLaMS are well described in McKenna et al. 2002a,b and Grooß et al. 2014. Major updates and developments are: Calculation of photolysis rates by Becker et al. 2000); Extension to 3-dimension model version by Konopka et al. 2004; Improved agrangian sedimentation by Tritscher et al. 2019; Extension to the (upper) troposphere using hybrid vertical coordinate zeta by Konopka et al. 2007; Incorporation of the concept of air mass origin tracers by Günther et al. 2008; Climatological simulation and simplified chemistry by Pommrich et al. 2014; Integration of Lagrangian transport into the climate model EMAC by Hoppe et al. 2014; Tropospheric mixing and parametrization of unresolved convective updrafts by Konopka et al. 2019.The model grid points are air parcels that follow trajectories and are therefore distributed irregularly in space. Mixing between the air parcels is calculated by an adaptive grid algorithm that depends on the large-scale horizontal flow deformation (McKenna et al. 2002a). The change of composition by chemistry and especially heterogeneous chemistry is calculated along the trajectories (Grooß et al. 2014, McKenna et al. 2002b). The replacement of previous chemistry solver routine IMPACT by a Newton-Raphson method derived from Wild and Prather 2000 is also updated. In Grooß et al. 2014 the Lagrangian PSC particle sedimentation scheme only include simulation for NAT particles, from Tritscher et al. 2019 on, an improvement that also simulates ice particles. This parameterisation should allow the model to sufficiently reproduce the observed PSC types and distribution.
The simulations in this thesis focus on air parcel trajectories in the Antarctic of time period late winter to early spring, where the ozone hole appears (WMO 2018). Wind and tempera-

ture data for the single air parcel trajectory are subtracted from the ERA-Interim reanalysis with 1°× 1 °resolution (Dee et al. 2011). Diabatic descent rates use the radiation code from Morcrette 1991, Zhong and Haigh 1995, they assume cloud free atmosphere based on temperatures from the ERA-Interim reanalysis and climatological ozone and water vapour profiles (Grooß and Russell III 2005, Grooß et al. 2011).
The chemical kinetics of the trajectory are based on Sander et al. 2006. Dimer Cl_2O_2 cross section is taken from von Hobe et al. 2009, but scaled by a factor of 1.48 so that the results fit the study of Lien et al. 2009. The photolysis rates are calculated for spherical geometry (Becker et al. 2000, Meier et al. 1982) using climatological ozone profile and ozone hole conditions from HALOE measurements (Grooß and Russell III 2005, Grooß et al. 2011). Heterogeneous chemistry is calculated on ice, NAT, liquid ternary particles ($H_2O/H_2SO_4/HNO_3$) and cold liquid binary aerosols (Grooß et al. 2011). The temperature dependent uptake coefficients of heterogeneous reactions on liquid ternary and binary aerosols are parameterized by Shi et al. 2001. The uptake coefficients of reactions on NAT are parameterized by Carslaw et al. 1997, Hanson and Ravishankara 1993. The NAT number density is 0.003 cm^{-3}.
SVODE solver (Brown et al. 1989) is applied in the simulations of the thesis. It is applied so that different reactions with different rates do not proceed the next time step before the previous time step is finished. SVODE allows for a higher accuracy in the interpolated results.
The CLaMS model contains a wide range of reactions, including full chlorine and bromine chemistry, photolysis and heterogeneous reactions in the stratosphere. The model chemistry is integrated from Atmospheric Chemistry Code (ASAD) by Carver et al. 1997, which provides subroutines to time dependent problems in the atmospheric chemistry as well as a chemical reaction database. In Appendix A.1 all the reactions that are involved in the stratosphere in this model are listed. These reactions are organized in four groups: binary reactions (numbered with B), ternary reactions (numbered with T), photolysis reactions (numbered with J) and heterogeneous reactions (numbered with H). The reaction rates are calculated by temperature and pressure dependent routines from Burkholder et al. 2020, 2015, Sander et al. 2011 respectively, which will be discussed in details in the next section. Reaction rates are updated on an hourly basis in the simulations.

3.2 JPL Recommendations

The Jet Propulsion Laboratory, California Institute of Technology and NASA publish and update chemical kinetics and photochemical data regularly. These data are used primarily to model stratospheric and upper tropospheric processes, with particular emphasis on the ozone layer and its possible perturbation by anthropogenic and natural phenomena.
The CLaMS model also employ this recommendation. There are three versions of recommendations that were applied in this thesis, namely JPL2011 (Sander et al. 2011), JPL2015 (Burkholder et al. 2015) and JPL2020 (Burkholder et al. 2020). JPL2015 is no longer the most recent edition and it contains a typo in the publication (see detail in the following subsection), therefore only a couple of exemplary simulations using this recommendation are presented in the Appendix A.3 and will not be discussed in Chapter 4.

3.2.1 A Comparison of JPL2011, JPL2015 and JPL2020

Below are the tables of the reactions which are involved in the CLaMS model that have been changed from JPL2011 to JPL2015 and JPL2020:

Adjusted reactions from JPL2011 to JPL2015	
$Cl + CH_4 \longrightarrow HCl + CH_3$	(R4)
$ClO + CH_3O_2 \longrightarrow Cl + HCHO + HO_2$ (This adjustment has typo)	(R3)
$CFC_{12} + O(^1D) \longrightarrow$ Products	–
$HCFC_{22} + O(^1D) \longrightarrow$ Products	-
$CFC_{113} + O(^1D) \longrightarrow$ Products	-
$HCFC_{22} + OH \longrightarrow$ Products	-
$CH_3Cl + OH \longrightarrow$ Products	-
$HO_2 + NO_2 \longrightarrow HO_2NO_2$	-
$HO_2NO_2 \longrightarrow HO_2 + NO_2$	(CR1)
$NO_2 + NO_3 \longrightarrow N_2O_5$	(CR2)
$ClO + ClO \longrightarrow Cl_2O_2$	(CR3)

$Cl_2O_2 \longrightarrow ClO + ClO$	(CR4)
$BrO + NO_2 \longrightarrow BrONO_2$	-
$OH + CO \longrightarrow CO_2 + H$	(CR5)
$CH_2O + h\nu \longrightarrow$ Products	(R14)

Table 3.1: Changes from JPL2011 to JPL2015

Adjusted reactions from JPL2015 to JPL2020	
$ClO + CH_3O_2 \longrightarrow Cl + HCHO + HO_2$ (The typo in JPL2015 is removed)	(R3)
$CO + OH \longrightarrow CO_2 + H$	(CR6)
$O(^3P) + NO_2 \longrightarrow NO + O_2$	(CR7)
$HO_2 + HO_2 \longrightarrow H_2O_2 + O_2$	(CR8)
$HNO_3 + OH \longrightarrow NO_3 + H_2O$	(CR9)
$HO_2 + NO \longrightarrow NO_2 + OH$	(CR10)
$NO + NO_3 \longrightarrow NO_2 + NO_2$	(CR11)
$H + O_2 \longrightarrow HO_2$	(R15)
$CH_3O_2NO_2 + h\nu \longrightarrow CH_3O_2 + NO_2$	(CR12)

Table 3.2: Changes from JPL2015 to JPL2020

The rate of $ClO + CH_3O_2$ This paragraph is dedicated to the reaction $ClO + CH_3O_2 \longrightarrow Cl + HCHO + HO_2$. The role of this reaction for "ozone hole" chemistry is important to a certain degree (Crutzen et al. 1992, Zafar et al. 2018), the adjustments are discussed in this

paragraph. The temperature dependent rate constant in Sander et al. 2011 is listed as:

$$k_{\mathrm{jpl11}}(T) = 3.3 \times 10^{-12} \cdot \exp\left(-\frac{1}{115} \cdot \frac{1}{T}\right) \tag{A1}$$

where T is temperature. This recommendation was updated and the correct equation is:

$$k_{\mathrm{jpl15/20}}(T) = 1.8 \times 10^{-11} \cdot \exp\left(-\frac{1}{600} \cdot \frac{1}{T}\right) \tag{A2}$$

however in both Burkholder et al. 2015 and (unchanged) in Burkholder et al. 2020 the A-factor is listed as $A = 1.8 \times 10^{-12}$. The correct value should be $A = 1.8 \times 10^{-11}$. This is confirmed by the author personally.

The calculation of room temperature rate with equation (A2) is consistent with earlier

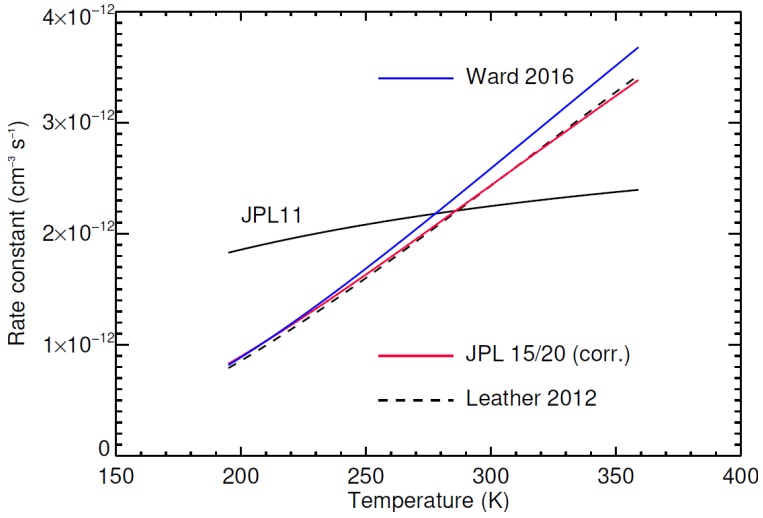

Figure 3.1: The temperature dependent rate constant for reaction $ClO + CH_3O_2 \longrightarrow Cl + HCHO + HO_2$ from a variety of sources. Note that the results for Burkholder et al. 2020, 2015 (line color red) is calculated with the corrected value $A = 1.8 \times 10^{-11}$. (Plot courtesy Rolf Müller)

work and also reproduces the k(298 K) value given in Burkholder et al. 2020, 2015, these are listed in the table below. The formulation with equation (A2) as well as the recommendation Sander et al. 2011 and other measurements (Leather et al. 2012, Ward and Rowley 2016) are presented in the same figure 3.1. Using the incorrect value $A = 1.8 \times 10^{-12}$ results in inconsistency with the laboratory measurements.

$k(298\,\mathrm{K})$	Source
2.2434510^{-12}	Sander et al. 2011
2.4035610^{-12}	Burkholder et al. 2020, 2015
2.3985410^{-12}	Leather et al. 2012
2.5515010^{-12}	Ward and Rowley 2016

Table 3.3: The rate constant k of reaction $\mathrm{ClO} + \mathrm{CH_3O_2} \longrightarrow \mathrm{Cl} + \mathrm{HCHO} + \mathrm{HO_2}$ at 298 K. The entry for Burkholder et al. 2015 and Burkholder et al. 2020 is for $A = 1.8 \times 10^{-11}$.

Cl_2O_2 Canty et al. 2016 has proven that the recent laboratory-determined absorption cross sections of Cl_2O_2 that report larger values than found by prior studies are more consistent with atmospheric measurements of Cl_2O_2 and ClO. Model results based on the JPL 2015 cross sections of Cl_2O_2 are in agreement with atmospheric observations for a wide range of $\mathrm{ClO} + \mathrm{ClO}$ dimerization reaction rate constant.

Other adjustments From JPL2011 to JPL2015 new bromine species are included but they should not interfere with the simulations as they are initialized with 0, from JPL2015 to JPL2020 they are once again removed. From JPL2015 to JPL2020 New formula for association/dissociation reactions are updated (namely $\mathrm{CO} + \mathrm{OH}$, $\mathrm{O}(^3\mathrm{P}) + \mathrm{NO_2}$, $\mathrm{HO_2} + \mathrm{HO_2}$ and $\mathrm{HNO_3} + \mathrm{OH}$). Temperature changed from 300 K by 298 K in all formulas.

Chapter 4

Results and Discussion

4.1 Standard Run

A series of research has been performed on the trajectory we employed in this work, namely in the study by Grooß et al. 2011, Müller et al. 2018 and Zafar et al. 2018. The results reported earlier indicate that at 16 - 18 km (85 - 55 hPa) in the core of the vortex, high levels of active chlorine are maintained by HCl null cycles, where the formation of HCl is balanced by immediate reactivation. In this section the calculations were performed under the same condition using JPL2011 recommendation (Sander et al. 2011) in order to reproduce the results in the studies.

The trajectory covers the time period when the ozone mixing ratios are the lowest, it is selected to study the stratospheric chemistry in the vortex core during late winter and early spring. The trajectory intersects an observation of South Pole Station of about 10 ppbv ozone at the pressure level 70 hPa on September 24th, 2003. The duration of the simulations performed by CLaMS is from June 1st to November 30th, 2003. The trajectory stays in the vortex core around 70° South with a standard deviation of 5°.

The initial values for the main trace gases on 1st June, 2003 are: O_3 = 2.2 ppm, H_2O = 4.1 ppm, CH_4 = 1.2 ppm, HNO_3 = 4.5 ppb, HCl = 1.05 ppb, ClO_x = 1.01 ppb, $ClONO_2$ = 12 ppt, HOCl = 5 ppt, Br_y = 17 ppt, CO = 16 ppb.

The assumptions in these initial conditions are: the initial step of heterogeneous activation has occurred in the air parcel, therefore the ClO_x values are high while HCl values are low. Secondly, denitrification is also represented in the initial conditions by assuming HNO_3 = 4.5 ppb. The sensitivity of the results of the simulations on the initial ozone and initial HNO_3 mixing ratios, as well as the impact of assumptions on the chemistry of methylhypochlorite

and the methyl peroxy radical has been discussed in previous work Müller et al. 2018.

A selection of the trajectory characters are presented in figure 4.1.

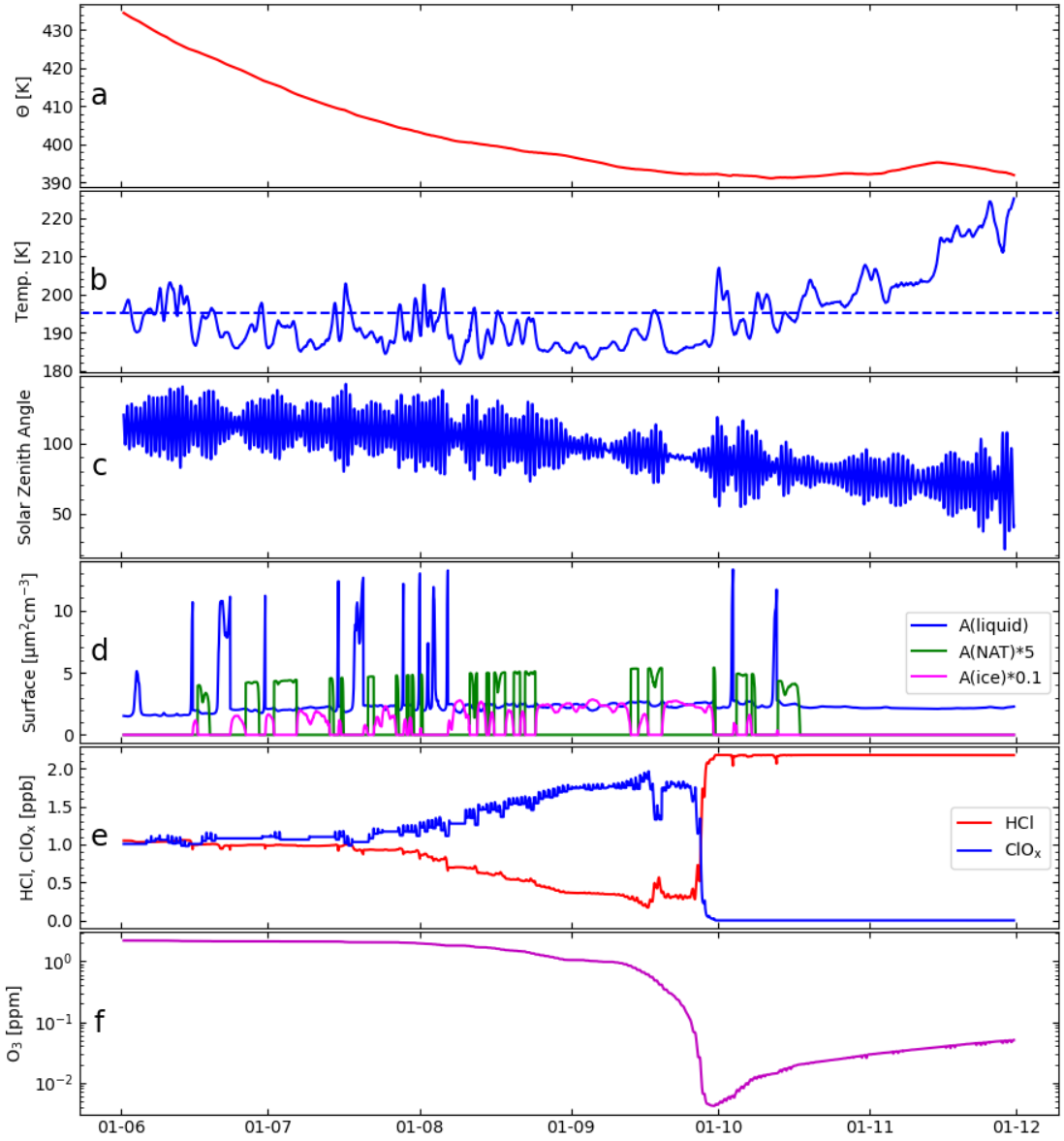

Figure 4.1: Box-model simulations along a trajectory passing through the location of the ozone sonde observation at South pole of 14 ppbv on 740 hPa (391 K) on 24th September, 2003 (with recommendations of Sander et al. 2011). The different panels show a time series of the relevant parameters: (a) potential temperature of the air parcel, (b) temperature, (c) solar zenith angle, (d) surface area density of ice (magenta, scaled by 0.1), NAT (green, scaled by 5) and liquid aerosol particles (blue), (e) ClO_x (blue) and HCl (red), (f) ozone.

Panel (a) shows that the potential temperature of the air parcel descends to 390 K when

lowest ozone concentrations are observed. Panel (b) shows temperature, where a dashed line of 195 K is also included. This temperature is the threshold temperature, below which crystalline nitric acid trihydrate (NAT) is thermodynamically stable and can exist if they nucleate (Hanson and Mauersberger 1988, Peter and Grooß 2012a). In winter and early spring the temperature is typically below this threshold. Panel (c) displays solar zenith angle along the trajectory. Panel (d) includes surface area density of ice, NAT and liquid aerosol particles. In Panel (e), HCl declines gradually and ClO_x increases as a result of the chlorine activation process in winter. In panel (f) ozone concentration is shown. The effect of ClO_x is minimum in winter, however in early spring, as solar zenith angle decreases, ozone begins to deplete rapidly. Accordingly, in panel (d) ClO_x is consumed while HCl increases significantly. Ozone depletion stops because ozone reached an extremely low value although temperatures are still low enough for PSCs and heterogeneous processing.

The calculations successfully reproduced those in the studies mentioned above. Based on this result we conducted further calculations with small variations to initial values of the trajectory, these will be discussed in the following section.

4.2 Impact of Initial Water Vapour Value (JPL2011)

In this section, we present further results that are based on the earlier recommendation JPL2011 (Sander et al. 2011) so that a straightforward comparison is possible.

The initial value $H_2O = 4.1$ ppm neglects the dehydration of the Antarctic stratosphere. It has already been reported for both in-situ and remote sensing measurements as well as for model simulations (Kelly et al. 1989, Nedoluha et al. 2002, Poshyvailo et al. 2018, Rolf et al. 2015, Schoeberl and Dessler 2011, Vömel et al. 1995), there exists strong dehydration in the Antarctic vortex in June, July and August.

Water vapour in the air is removed at sufficiently low temperatures through ice formation. Irreversible dehydration occurs every year through the sedimentation of ice particles. There is also a certain year-to-year variability in the extent and timing of the severity of Antarctic dehydration. Therefore, in this section we changed the initial mixing ratio of $H_2O = 2.05$ ppm, we believe that this constitutes a more realistic initial condition considering the dehydration in Antarctica.

The results in section 4.1 are compared with the simulation using this more realistic initial value. Figure 4.2 shows the result of the simulations.

In general the change in initial value does not result in significant change of the chlorine chemistry and ozone loss, the progression along the time are consistent. For initial value $H_2O = 2.05$ ppm, the minimum value of ozone is slightly higher that for $H_2O = 4.11$ ppm, which are separately plotted on a linear scale in figure 4.3. Ozone mixing ratio began to differentiate on August and reached the maximum difference of ozone on 19th September, after October there were no significant difference. The value of the difference is less than 0.09 ppm.

Although the differences are small, we dedicate the following subsections to a more detailed comparison on certain important reactions and cycles.

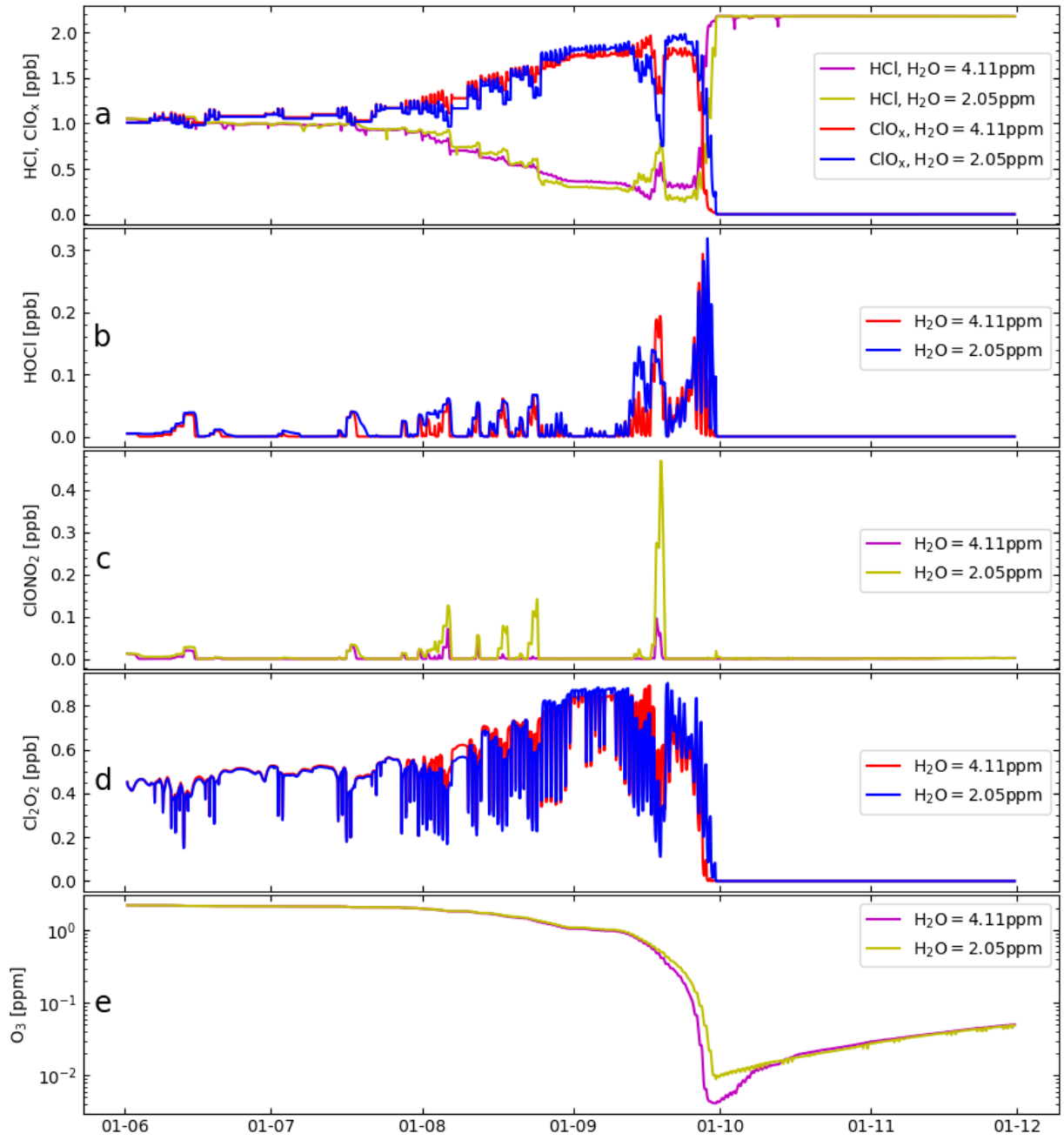

Figure 4.2: Box-model simulations along a trajectory passing through the location of the ozone sonde observation at South pole of 14 ppbv on 740 hPa (391 K) on 24th September, 2003 (with recommendations of Sander et al. 2011). The results for initial value $H_2O = 4.11$ ppm and $H_2O = 2.05$ ppm are both presented in the plot: (a) HCl and ClO_x, (b) HOCl, (c) $ClONO_2$, (d) Cl_2O_2, (e) ozone.

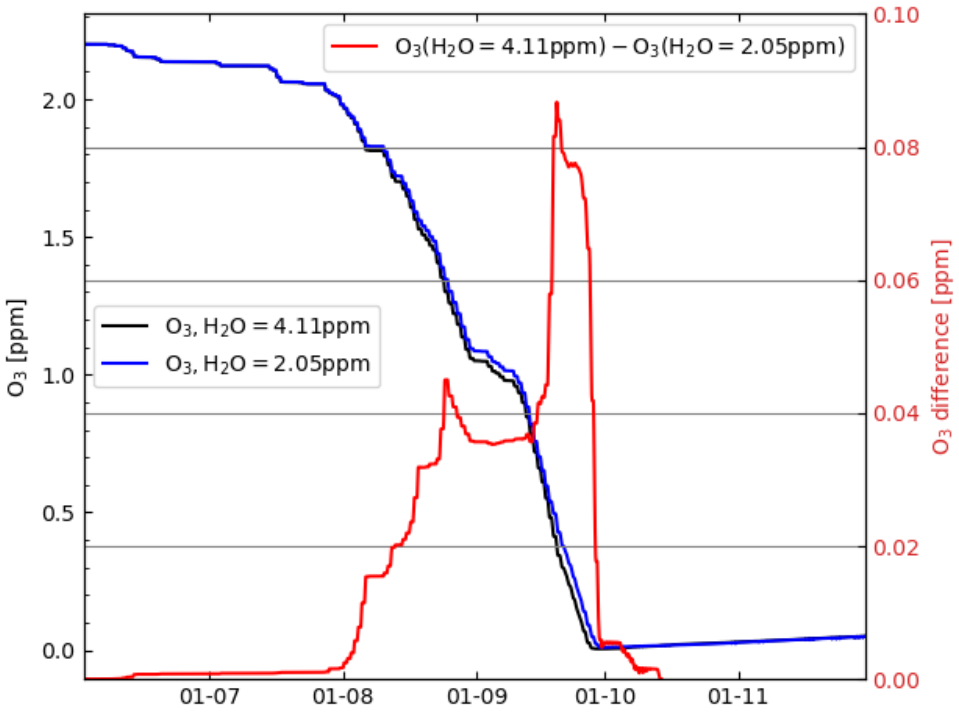

Figure 4.3: A different depiction of figure 4.2 panel (e). Ozone for initial value $H_2O = 4.11$ ppm and $H_2O = 2.05$ ppm on linear scale (black Y-scale on the left) and their difference (red Y-scale on the right).

4.2.1 PSCs and HNO_3

The ice PSCs and the mixing ratio of water vapour in the gas phase are shown in figure 4.4. For initial value $H_2O = 2.05$ ppm, ice surface is significantly lower than that for $H_2O = 4.11$ ppm. This difference has little impact on the development of HCl and active chlorine (figure 4.2 (a)). It is consistent with the notion that the specific rates of the heterogeneous reactions in the HCl null cycles are of little relevance for the efficacy of the HCl null cycles.
From figure 4.4 (a) and (b) we conclude that the change in initial water vapour value directly lead to huge difference in both surface density of ice PSCs and the mixing ratio of water vapour in the gas phase. Figure 4.4 (c) shows the concentration of HNO_3 in the gas phase. The results for initial value $H_2O = 2.05$ ppm displays a much higher HNO_3 concentration throughout the time period. This can be explained by ice particles absorption of HNO_3. Lower initial water vapour produces less ice and ice surface, leaving more HNO_3 in the gas phase. This results in a decrease in HCl and an increase in ClO_x, which is consistent with

figure 4.2 (a). NO_x species go through chemical reaction:

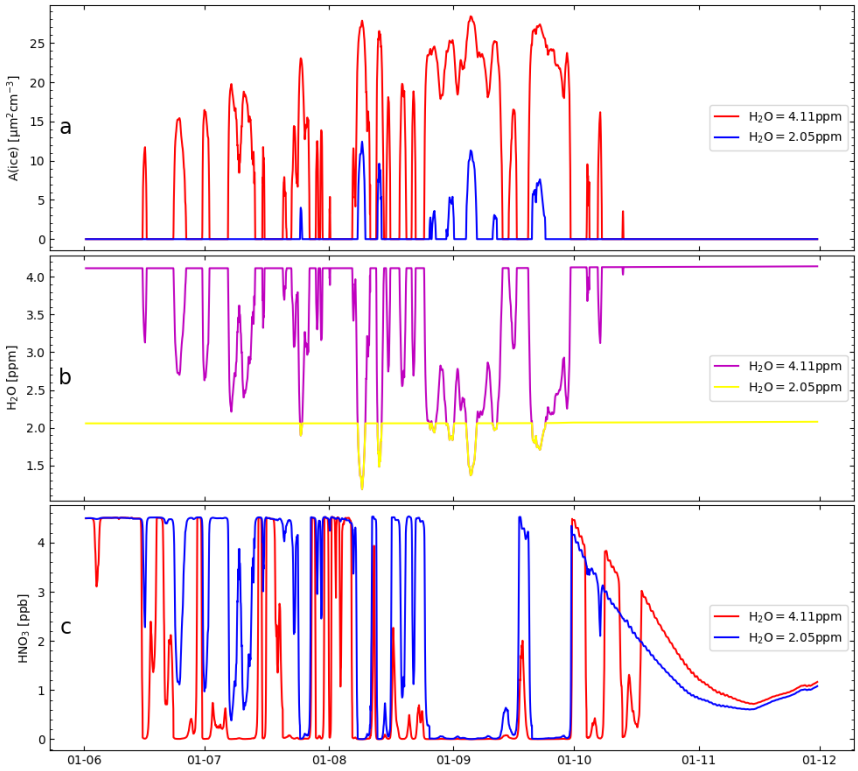

Figure 4.4: A comparison on simulations for initial value $H_2O = 4.11$ ppm and $H_2O = 2.05$ ppm with recommendation Sander et al. 2011: (a) Surface density of ice, (b) Water vapour in the gas-phase, (c) gas-phase HNO_3 concentrations.

$$ClO + NO_2 + M \longrightarrow ClONO_2 + M \tag{T9}$$

$ClONO_2$ then proceed to involve in reactions with chlorine species. However, these reactions are of little importance. Heterogeneous reaction $N_2O_5 + H_2O$ converts the majority of NO_x into HNO_3 in polar nights, furthermore, PSCs that have NAT exist continuously throughout the simulation, these leads to low NO_2 concentrations in both polar nights and in sunlight. The rate of $ClONO_2$ formation is rather slow, causing the rate of reactions $ClONO_2 + HCl$ significantly slower than $HOCl + HCl$ (up to four orders of magnitude slower). Therefore it is usally considered that the NO_x cycle plays only a rather small role in ozone depletion. Although we have changed the initial water vapour value, the significant decrease in HNO_3 does not result in any substantial changes in ozone depletion.

4.2.2 $O(^1D) + H_2O$

As the value of initial water vapour is modified, we want to consider the influence on reaction that directly involves water in the gas phase and produces OH, and its role in the O_3 depletion process.

$$O(^1D) + H_2O \longrightarrow OH + OH \tag{R18}$$

Two simulations were performed under the setting where the reaction rate of this reaction is set to zero, we call this "turning the reaction off". One simulation is for $H_2O = 4.11$ ppm and one is for $H_2O = 2.05$ ppm.

Figure 4.5 shows the difference between having the reaction rate unchanged and setting it to zero under the initial value $H_2O = 4.11$ ppm. The mixing ratio of OH is fundamentally identical under these two settings. It can be seen that, although water vapour is involved in the reaction directly, the reaction itself have a fairly minimal impact on the mixing ratio of HCl and ClO_x and other chlorine species. In consequence the change in O_3 is also negligible. Figure 4.6 shows the same comparison but for the simulation with initial value $H_2O = 2.05$ ppm. In this simulation there are less water vapour, therefore the relevance of the reaction to O_3 depletion is even more insignificant. As can be seen in the figure the progressions on every panel are almost identical.

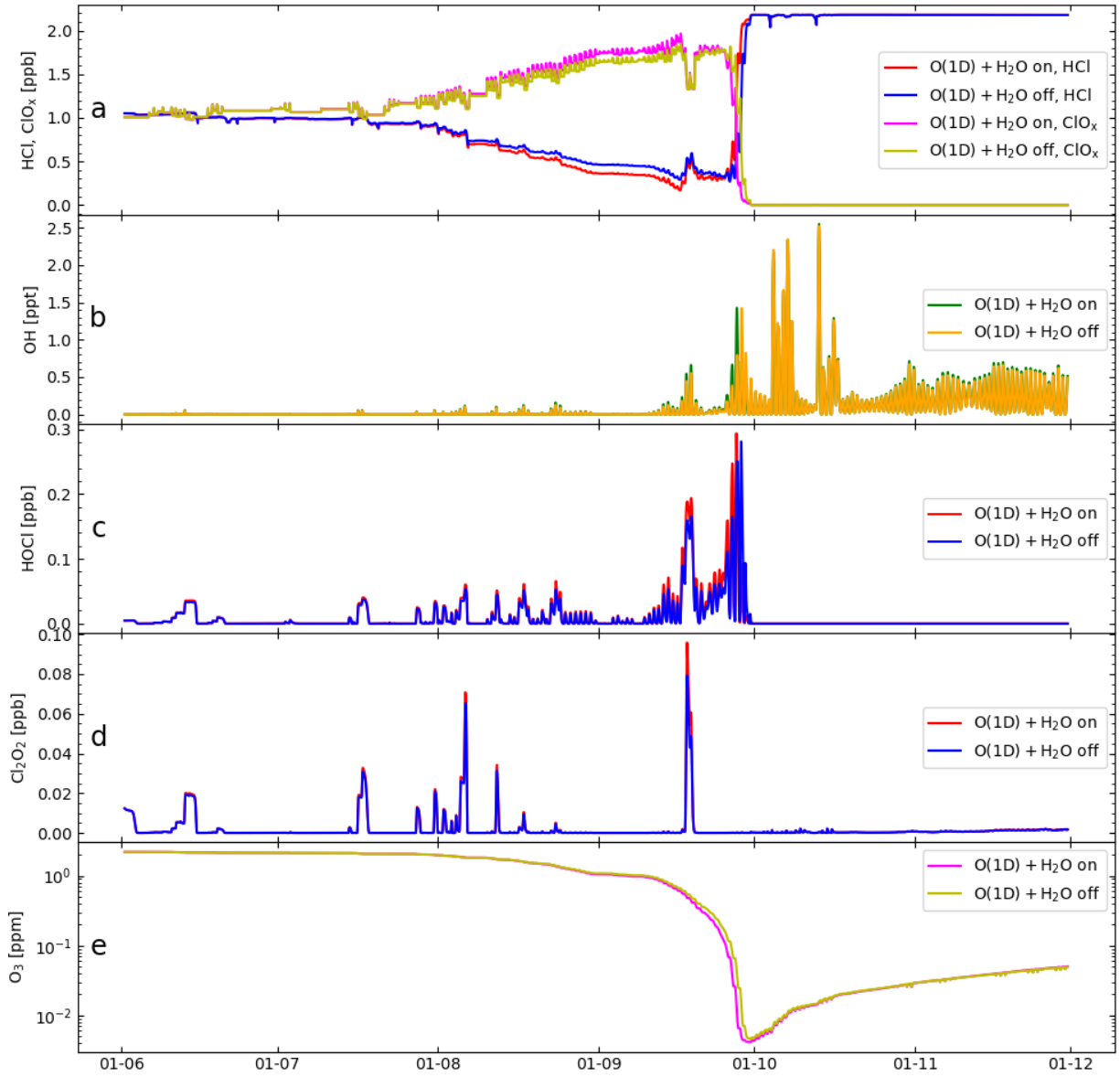

Figure 4.5: Box-model simulations for initial value H_2O = 4.11ppm. A comparison of different reaction rate settings for reaction $O(^1D) + H_2O \longrightarrow OH + OH$ (on, off) for (a) HCl and ClO_x, (b) OH, (c) HOCl, (d) Cl_2O_2, (e) ozone. JPL version uses recommendation Sander et al. 2011.

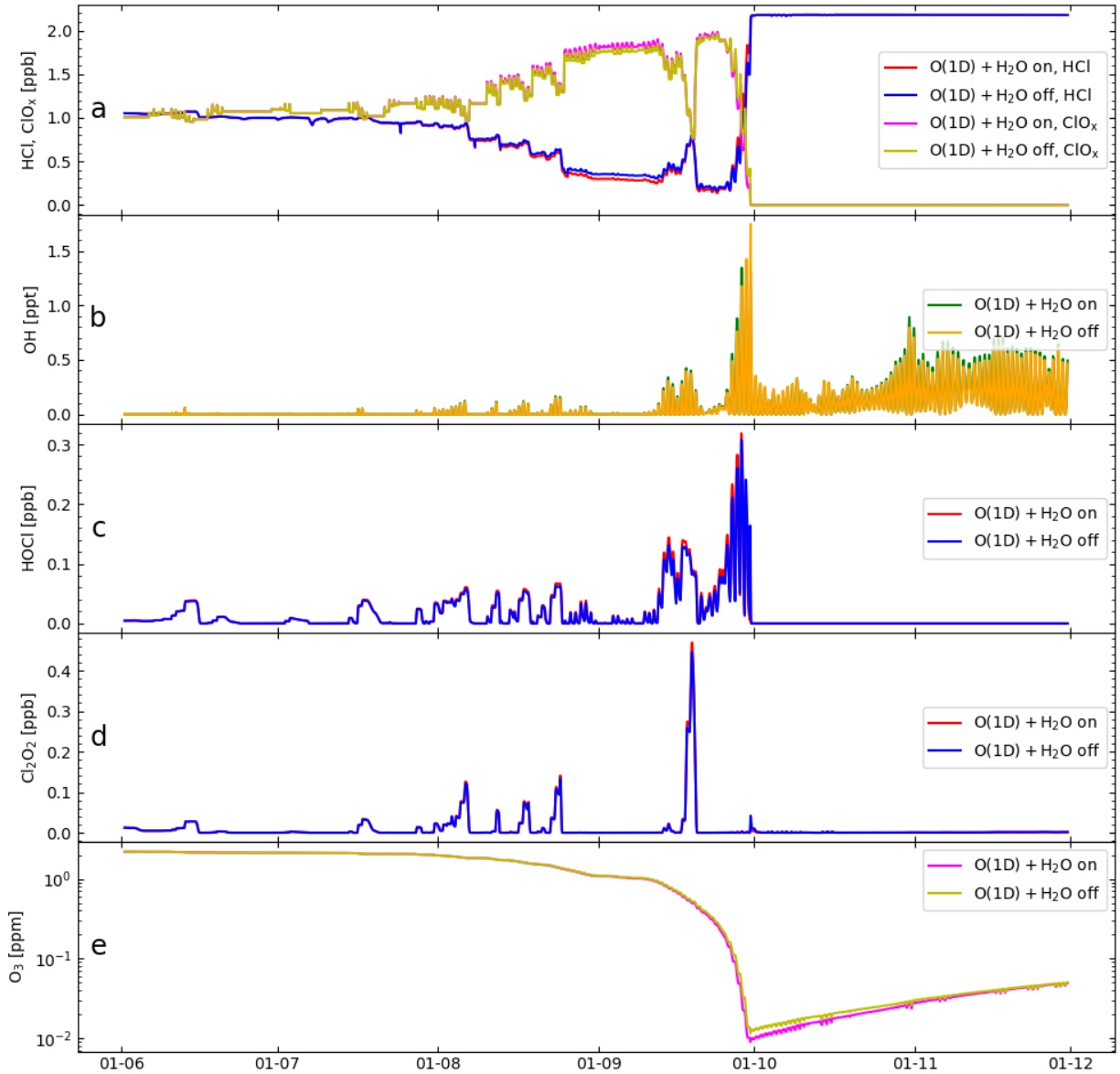

Figure 4.6: Box-model simulations for initial value H_2O = 2.05ppm. A comparison of different reaction rate settings for reaction $O(^1D) + H_2O \longrightarrow OH + OH$ (on, off) for (a) HCl and ClO_x, (b) OH, (c) HOCl, (d) Cl_2O_2, (e) ozone. JPL version uses recommendation Sander et al. 2011.

4.2.3 HCHO

It is concluded in the previous section that $O(^1D)$ radical reaction with H_2O has very limited impact. There is, however, another dominant source of HO_x that we could consider. The formaldehyde photolysis is an important step in the ozone hole chemistry. It consists of two channels, namely the radical channel and the molecular channel:

$$HCHO + h\nu \longrightarrow HCO + H \tag{R14a}$$

$$HCHO + h\nu \longrightarrow H_2 + CO \tag{R14b}$$

The molecular channel produces hydrogen and carbon monoxide, which does not continue to take part in the production of HO_x (Chapter 3 section 3.4). The radical channel product HCO undergoes oxidation and produces HO_x:

$$\begin{aligned} HCHO + h\nu &\longrightarrow HCO + H \\ H + O_2 &\longrightarrow HO_2 \\ CHO + O_2 &\longrightarrow CO + 2\,HO_2 \\ \hline \text{Net: } HCHO + 2\,O_2 &\longrightarrow CO + 2\,HO_2 \end{aligned}$$

To observe the difference in this process between $H_2O = 4.11$ ppm and $H_2O = 2.05$ ppm, the mixing ratio of HCHO and the reation rate of the radical channel are plotted in figure 4.7. Granted that the trends are similar in early stage of the simulation, two weeks before ozone minimum, the difference starts to become visible. For $H_2O = 2.05$ ppm the mixing ratio of HCHO increases slower than that for $H_2O = 4.11$ ppm, the reaction rate also grows slower and reaches peak later. It has been studied in Zafar et al. 2018 that, faster HO_2 production would result in faster HCl decline, which then leads to higher ClO_x. This is consistent with the slightly delayed plateau of HCl and ClO_x for $H_2O = 2.05$ ppm in figure 4.2 panel (a).

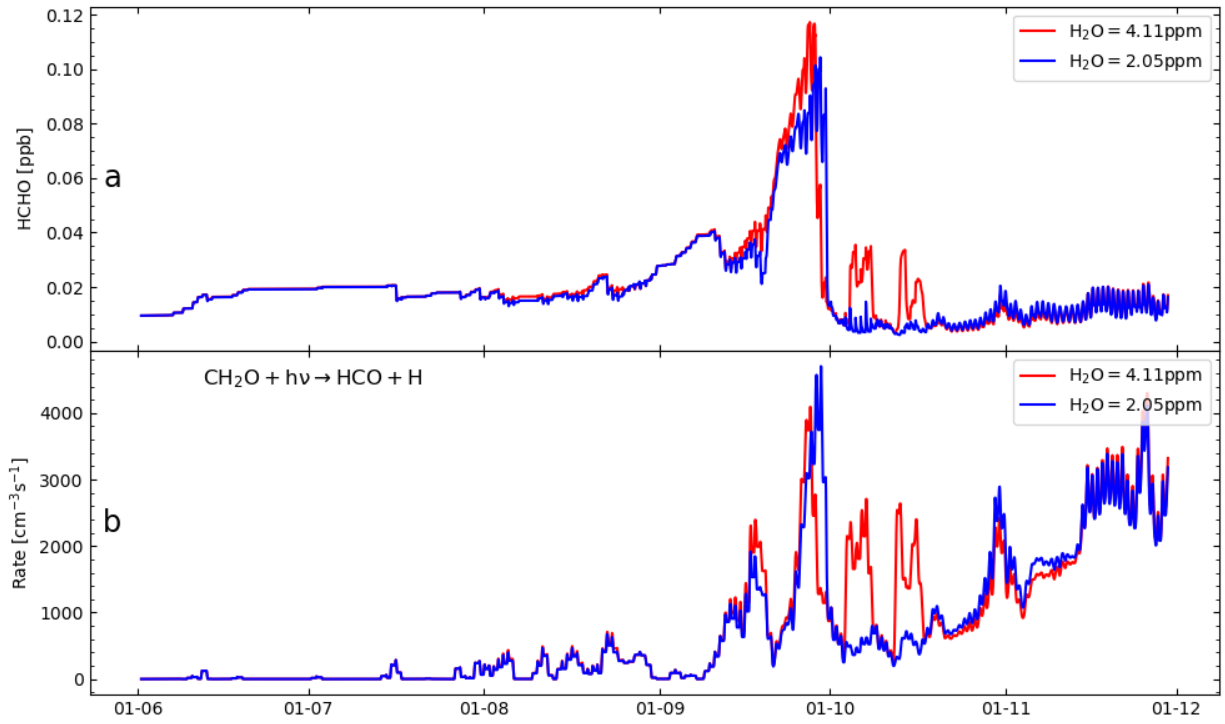

Figure 4.7: Box-model simulations for initial value H_2O = 4.11 ppm and H_2O = 2.05 ppm: (a) HCHO, (b) photolysis rate of HCHO + hν $\longrightarrow$ HCO + H. JPL version uses recommendation Sander et al. 2011.

4.2.4 Sensitivity on Ozone

In this section we conducted six further simulations with initial value $H_2O = 2.05$ ppm, where the initial ozone mixing ratios range from 2.0 to 2.6 ppm. This is to check if the sensitivity of the simulated development of chlorine chemistry and ozone mixing ratios behave like those for $H_2O = 4.11$ ppm in the previous settings.

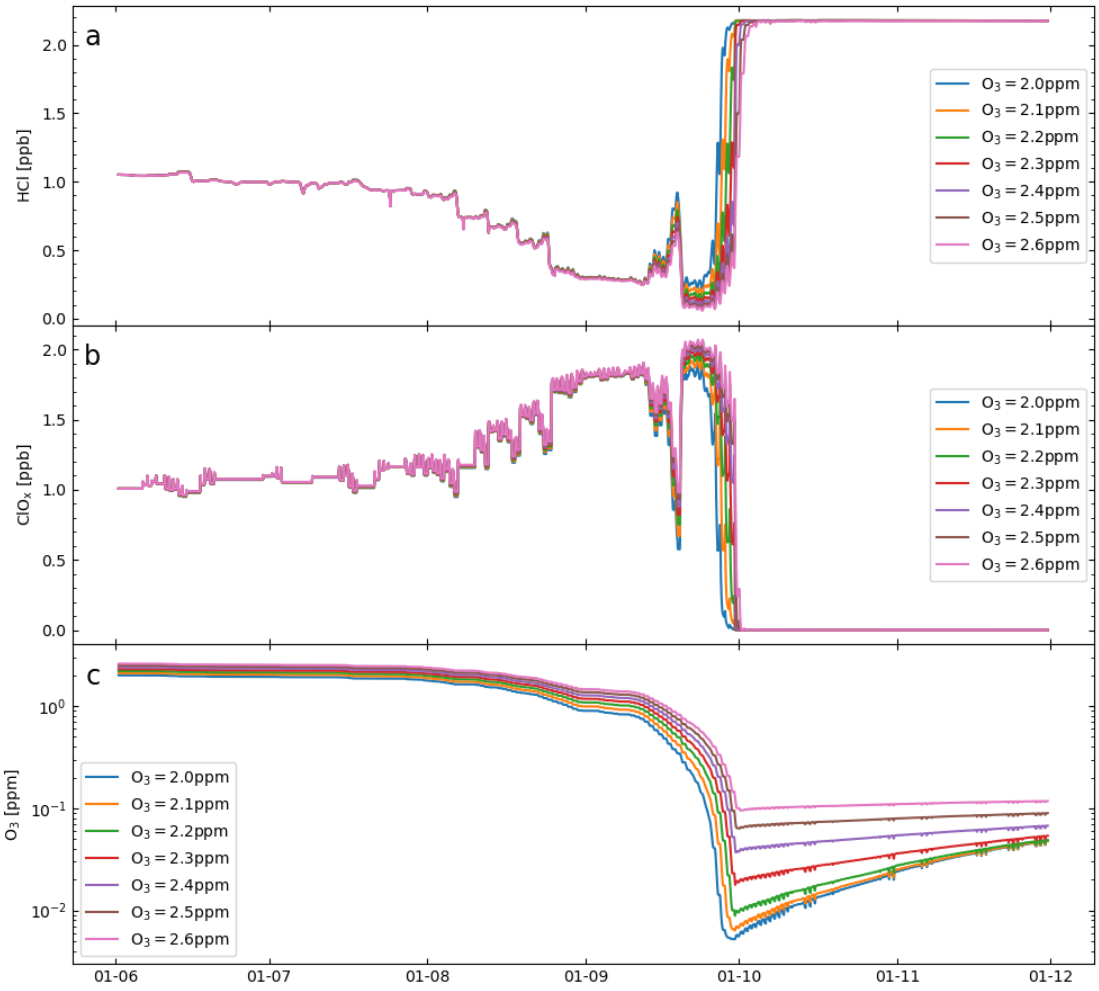

Figure 4.8: Simulations for different ozone initial value from $O_3 = 2.0$ ppm to $O_3 = 2.6$ ppm: (a) HCl, (b) ClO_x, (c) O_3.

The simulations are shown in figure 4.8. It is natural that the higher the initial value, the higher the minimum ozone mixing ratio. We can also see that the timing of the rapid increase in HCl and chlorine deactivation vary slightly for different initial values, but the

trends and patterns, especially before 20th of September, are almost identical. In the case of initial ozone $O_3 = 2.60$ ppm (line color magenta), maximum chlorine activation is achieved latest. The explanation for this could simply be that, there are more ozone to be depleted therefore it takes longer. In this case the ozone is abundant, it does not drop low enough that the HCl null cycles are disrupted. In the beginning of October, temperature rises to above 195 K, this disrupts HCl null cycles and HCl begins to increase.
For lower ozone abundance, for example $O_3 = 2.00$ ppm (line color cyan), it drops rapidly and reaches an sufficiently low value that HCl null cycles can not be maintained anymore. As HCl increases, O_3 depletion stops, the slow recovery of ozone already begins before temperatures rises above the threshold.
These results are consistent with the ozone sensitivity study for $H_2O = 4.11$ ppm. (Müller et al. 2018)

4.3 Impact of Initial HCl Value (JPL2011)

Grooß et al. 2018 reported a discrepancy between simulations and observations of HCl during the onset of chlorine activation (between May and July in the Antarctic), during this period model simulations significantly overestimate HCl. This section discusses the result and effects of modifying HCl and chlorine species.
The simulation is conducted for initial values H_2O = 2.05 ppm and HCl = 0 ppb. In order to maintain the total amount of total chlorine, an equivalent increase in initial Cl_2O_2 value is added:

$$Cl_2O_2(\text{new})_{\text{init}} = Cl_2O_2(\text{old})_{\text{init}} + \frac{1}{2}HCl(\text{old})_{\text{init}} \qquad \text{(Init. Adjustment)}$$

In this setting we have more active chlorine at the beginning of the simulation, the progressions along these trajectories are shown in figure 4.9. This simulation is also performed on initial value H_2O = 4.11 ppm (see appendix A.2).
From figure 4.9 (e) it can be concluded that more active chlorine leads to earlier and more ozone depletion. Table 4.1 lists the exact date when ozone reaches a minimum and its value for all four trajectories. The interpretation is that the more initial water vapour and the more initial active chlorine, the earlier (faster) and the more severe ozone depletion takes place.

	H_2O = 4.11 ppm	H_2O = 2.05 ppm
HCl = 1.05 ppb	Sep 30th,06:00 4.14×10^{-2} ppm	Sep 30th, 06:00 8.91×10^{-2} ppm
HCl = 0 ppb	Sep 26th, 11:00 3.28×10^{-2} ppm	Sep 26th, 14:00 3.01×10^{-2} ppm

Table 4.1: Day of reaching Ozone minimum and value

Panel (a) of figure 4.9 shows that the HCl and ClO_x species remain rather stable before August. From August, activation process slowly consumes HCl for the previously discussed setup, whereas for initial HCl =0, the mixing ratio remains steady.
Figure 4.9 (b) displays a substantially high HOCl mixing ratio for HCl = 0 ppb before September, around twice as much as that for HCl = 1.05 ppb in the time frame from mid

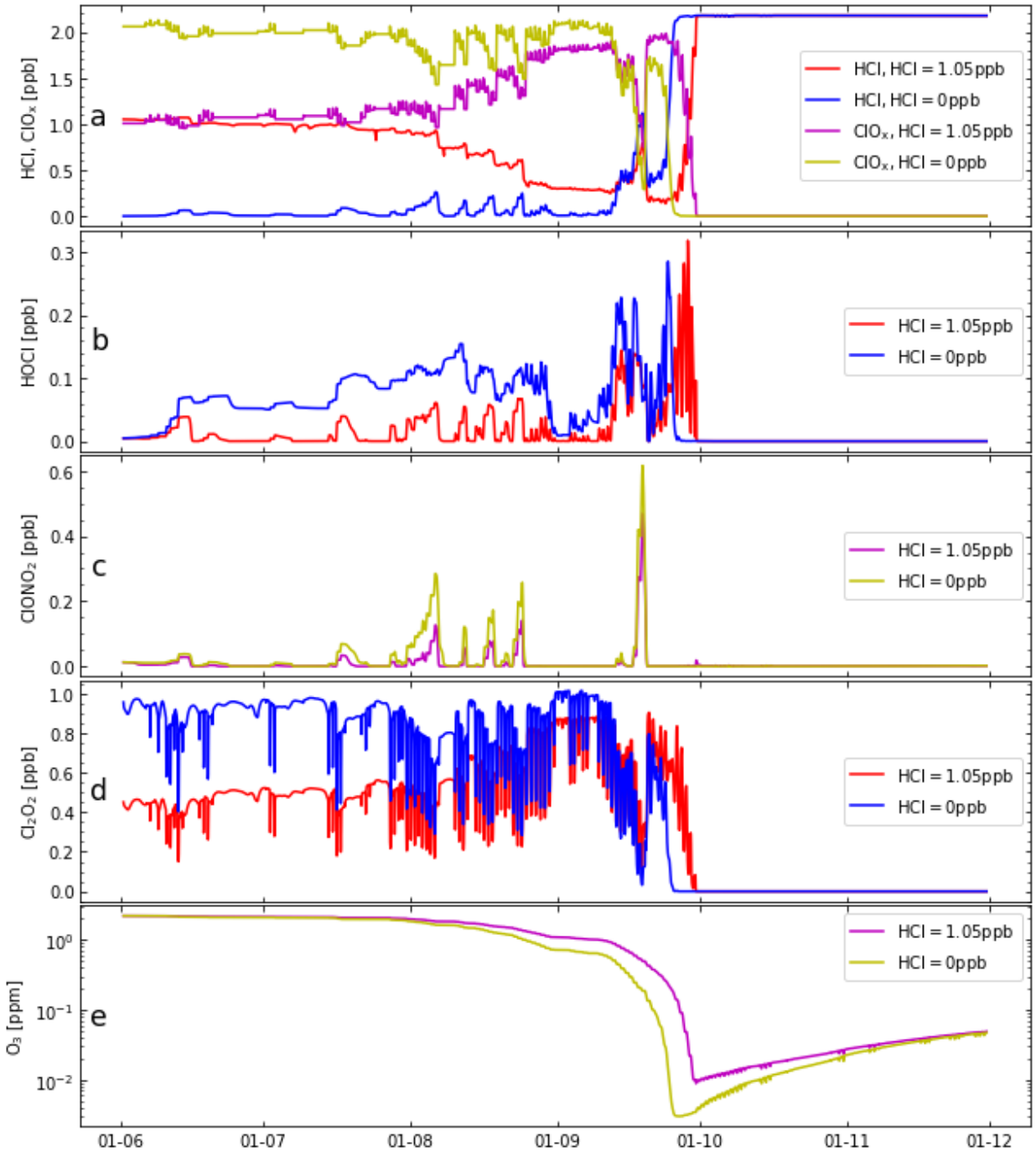

Figure 4.9: Box-model simulations along a trajectory passing through the location of the ozone sonde observation at South pole of 14 ppbv on 740 hPa (391 K) on 24 September 2003 (Sander et al. 2011). The results for initial value HCl = 1.05 ppb and HCl = 0 ppb are both presented in the plot: (a) HCl and ClO_x, (b) HOCl, (c) $ClONO_2$, (d) Cl_2O_2, (e) ozone.

June to September. The very low HCl mixing ratios also allow the abundance of HOCl to be greater than in a case with higher initial HCl value, especially from mid June to mid August. In this period HCl mixing ratio remains rather stable for both trajectories, we could infer that HCl null cycles keep HCl mixing ratio low. This is also the case for $H_2O = 4.11$ ppm.

4.3.1 HCl null cycles

In chapter 2 the HCl null cycles have been explained. The reactions

$$CH_4 + Cl \longrightarrow HCl + CH_3 \tag{R4}$$

$$CH_2O + Cl \longrightarrow HCl + CHO \tag{R11}$$

are of major importance in the maintenance of chlorine activation. After changing the initial value of HCl, we want to look closer into these key processes.
A comparison of the reaction rates are presented in figure 4.10 on logarithmic scales. It is straightforward that these reaction rates are higher for initial HCl = 0 almost at all times. The HCl null cycles ensure that the net production of HCl remains around zero. When the initial value is zero and ClO_x concentration is high, the speed of the above reactions are correspondingly higher, HCl level remains stable.

From middle September to October, the reaction rates increase substantially, up to two

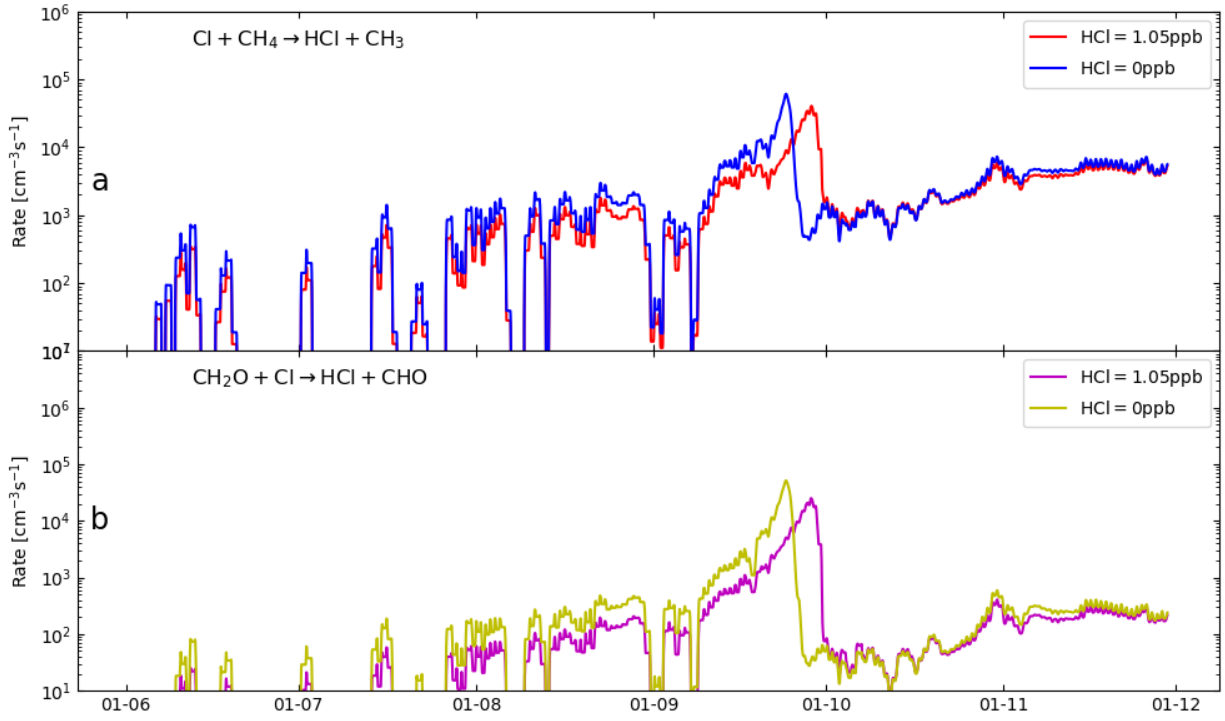

Figure 4.10: Simulation for initial value H_2O = 2.05 ppm, HCl = 1.05 ppb and 0 are plotted in comparison with ecommendation Sander et al. 2011: (a) HClRates of reaction of atomic chlorine with (a) CH_4, (b) CH_2O. The reaction rates in the panels are plotted as 24 h running averages.

orders of magnitude. For initial value HCl = 0, the growth of the reactions rates is faster and reaches peak value much earlier. Overall the HCl null cycles are maintained regardless of the initial values.

4.3.2 Activation of HCl

The increase in (R4) and (R11) reflects the consumption and reproduction of HCl, yet the cycles responsible for the full activation are (C3) and (C4). This again calls for attention on the study of HCHO photolysis. Figure 4.11 presents the HCHO mixing ratio and its

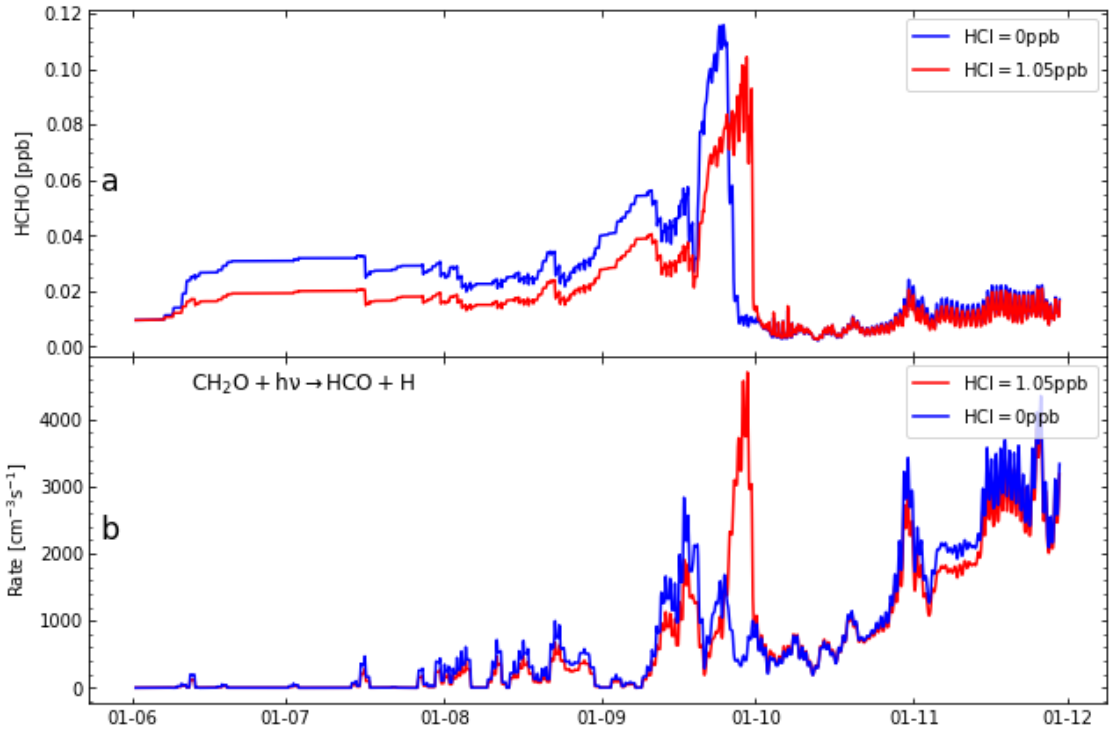

Figure 4.11: Box-model simulations for initial value H_2O = 2.05ppm, HCl = 1.05 ppb and HCl = 0: (a) HCHO, (b) photolysis rate of $HCHO + h\nu \longrightarrow HCO + H$. The reaction rates in the panels are plotted as 24 h running averages.

photolysis rate (radical channel). Shortly before October, the photolysis of HCHO rises intensely for initial HCl = 1.05 ppb, at the same time for initial HCl = 0, the photolysis rate remains steady with minor drop. In the case of initial HCl = 0, there is little activation taking place, as most of the chlorine species are already in the form of ClO_x. The interpretation could again confirm the earlier study for the full activation of HCl in Müller et al. 2018.

4.4 Simulations for JPL2020

In this section we use chemical kinetics and photochemical data from the recommendation JPL2020 (Burkholder et al. 2020), there remains a lot to be discussed on the simulations using this recommendation as this is the most recent one. The JPL2015 version (Burkholder et al. 2015) is not the main focus of this thesis, (some discussions were made, see Appendix A.3 for detail). Similar simulations like the previous sections as well as multi-trajectory simulations are discussed.

4.4.1 Impact of Revised Kinetic Parameters

The same trajectory in the section 4.2 is selected here as an example to study the difference between JPL2011 and JPL2020. The same initialization was used, namely H_2O = 2.05 ppm and HCl = 1.05 ppb. Figure 4.12 makes a comparison between these two recommendations.
Overall, the results are similar. The HCl level begins to sink lower in JPL2011 than JPL2020 from early August until the end of September. On the day where the simulation for JPL2011 reached O_3 minimum, O_3 mixing ratios for JPL2020 has not reached minimum yet. In the simulation of JPL2020, the O_3 mixing ratio already decreases fast from two weeks before September 28th, however it still continues to decrease, but slower, until reaching minimum on October 09th, 04:00, which is significantly later than JPL2011.
Panel (b), (c) and (d) show similar differences. In general, the HOCl, $ClONO_2$ and Cl_2O_2 mixing ratios at local peaks are higher in JPL2011 than in JPL2020. However after 28th of September, there exists a new peak for $ClONO_2$ which simulations for JPL2011 do not have. This is also visible in HOCl. The delay in HCl/ClO_x reaching plateau correspond these differences.

Difference on 18th to 19th September In figure 4.12 panel (c), $ClONO_2$ has a significantly higher peak in JPL2011, almost five times as much as in JPL2020. On this day, temperature shortly rises above T_{NAT} = 195 K, causing heterogeneous reactions on PSCs to reduce rapidly. In this time of year, solar zenith angle already began to decrease.
We extracted the reaction rates on this day. The rate of reaction (R1) is 2.8×10^2 ppb d^{-1} in JPL2020 and 1.2×10^3 ppb d^{-1} in JPL2011. Some of the reactions that have changed in the recommendations also exhibit differences. The rate of reaction (CR11) is 0.39 ppb d^{-1} for JPL2020 and 15.9 ppb d^{-1} for JPL2011. The same huge gap between rates are also found for (CR7): 0.7 ppb d^{-1} for JPL2020 and 29.7 ppb d^{-1} for JPL2011. Smaller differences are found for reaction (CR1) and (CR9), the values for JPL2011 are approximately three times

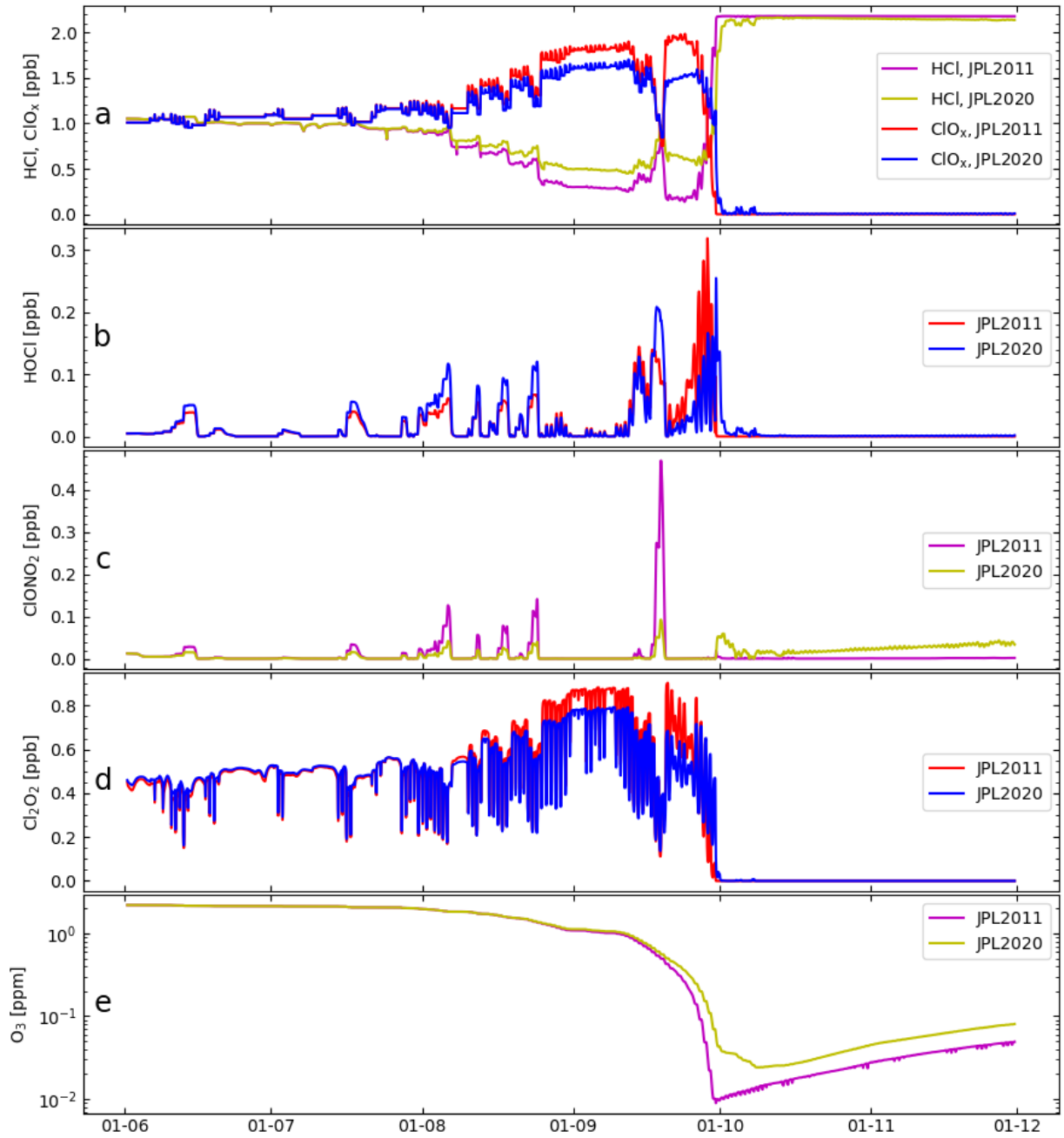

Figure 4.12: Box-model simulations along a trajectory passing through the location of the ozone sonde observation at South pole of 14 ppbv on 740 hPa (391 K) on 24th September, 2003. The results are both for initial value $H_2O = 2.05$ ppm, using recommendation Sander et al. 2011 and Burkholder et al. 2020 respectively: (a) HCl and ClO_x, (b) HOCl, (c) $ClONO_2$, (d) Cl_2O_2, (e) ozone.

the rates in JPL2020.

One deduction from these reaction rates is that, the lower value of $ClONO_2$ in JPL2020 is a result of lower NO_2 caused by changes in the recommendations. The validity of deduction is however challenged by the fact that the overall NO_2 turnover are very low for both cases, whether the differences at these low levels do have an impact on $ClONO_2$ remains to be tested.

Difference after September 28th This paragraph explores the behaviours of the trajectory using different recommendations after ozone hits minimum in JPL2011. As discussed in Chapter 2 section 2.4, the photolysis reaction (R14) is very important to understand the process of HCl full activation, especially that the parameters regarding this reaction has changed since JPL2015.

Already before 28th September the difference in radical channel becomes visible, the rate

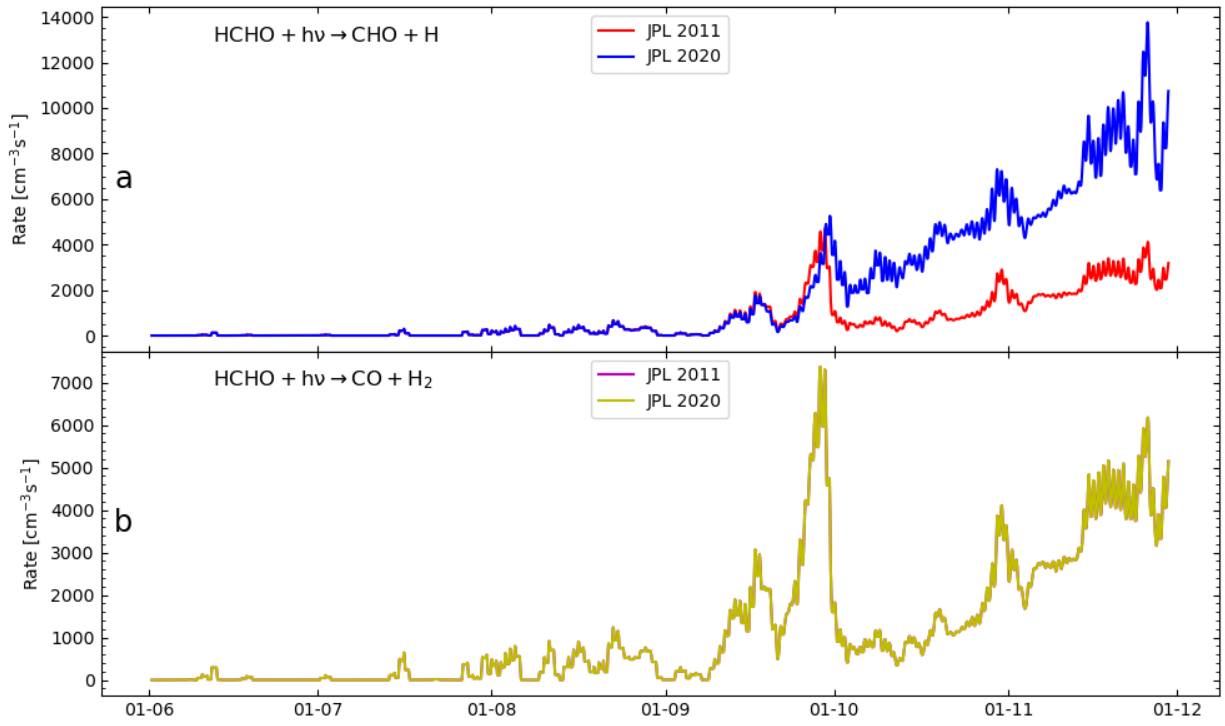

Figure 4.13: Photolysis rate of HCHO for H_2O = 2.05 ppm, using JPL2011 and JPL2020 respectively: (a) radical channel, (b) molecular channel. The reaction rates are plotted as 24 h running averages.

of photolysis increases slower in JPL2020 than in JPL2011 yet the peak value is higher. The rate of photolysis in JPL2020 reaches a local maximum value on 30th September, which then

decrease, but remains evidently higher than in JPL2011. The molecular channel of (R14) does not exhibit any noticeable difference between the two versions of recommendation. Fig-

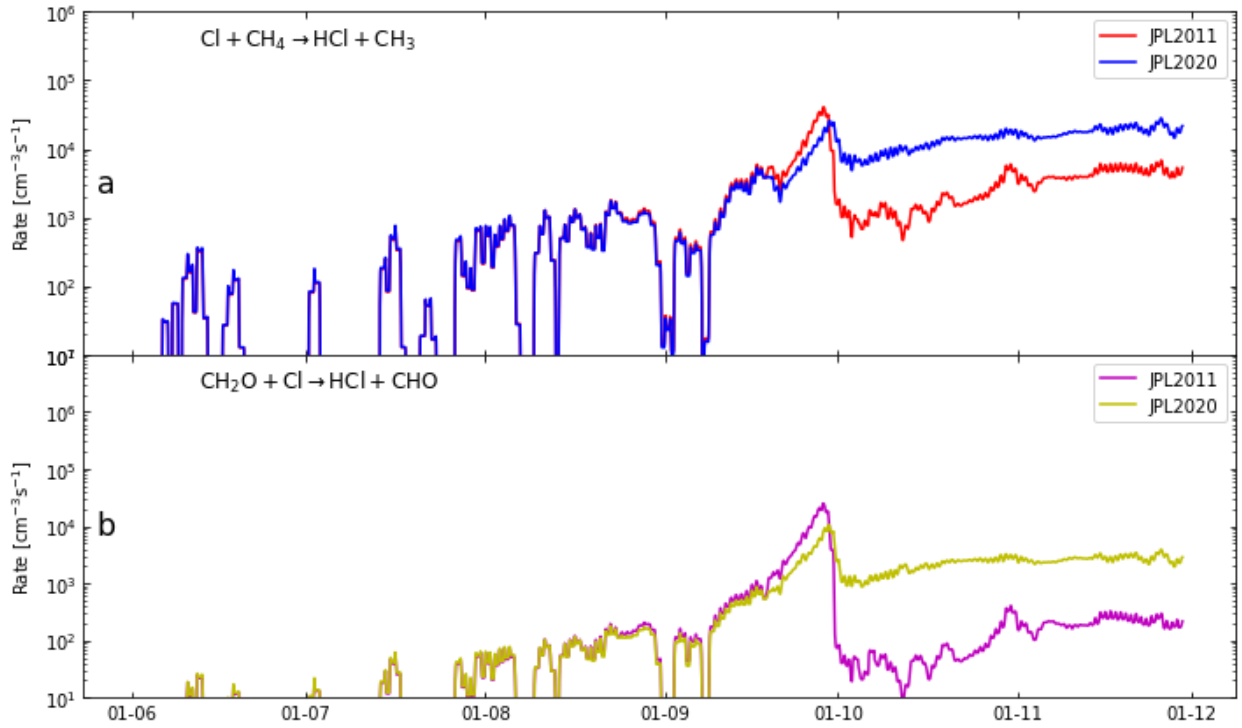

Figure 4.14: Simulation for initial value H_2O = 2.05 ppm, HCl = 1.05ppb using recommendation Sander et al. 2011 and Burkholder et al. 2020 respectively: (a) HClRates of reaction of atomic chlorine with (a) CH_4, (b) CH_2O. The reaction rates in the panels are plotted as 24 h running averages.

ure 4.14 displays the reaction rates for the important reactions (R4) and (R11) in HCl null cycles. Both reactions have the same characteristics: in JPL2020 both reaction rates rise slower, peak later and smaller in value. However, the decreases afterwards both stop at higher rates and remain steady and higher than in JPL2011. This does not affect the general efficacy of HCl null cycles, but the change in the rates of the cycle is rather interesting. Appendix A.4 lists a selection of the reactions that have been revised in the recommendation of roughly two weeks after 28th September, these reactions have shown visible differences, mainly linked with HO_x species and NO_x species.

4.4.2 Impact of Initial HCl Value (JPL2020)

The same setup in section 4.2 is used here for simulation but the recommendation JPL2020 (Burkholder et al. 2020) is employed. First we compare the results with those in section 4.4.1, the sole difference is the initial value of HCl.

Figure 4.15 shows that as the initial HCl value is set to zero, the transition in ozone depletion rate after October disappears. This is easily explained by the abundance of ClO_x at the beginning of the simulation. It allows a faster full HCl activation and thus faster ozone depletion. On 1st October ozone already reaches a value of 0.088 ppm, which is already too low a concentration for further ozone depletion process.

Figure 4.16 is a comparison of the version difference of the recommendation. It is similar to figure 4.12 but for the trajectory set up of H_2O = 2.05 ppm, HCl = 0 ppb. From this figure and some of the results in the previous section, that the recommendation Burkholder et al. 2020 leads to a generally milder ozone depletion. This is valid for different initial values of H_2O and HCl tested in this thesis.

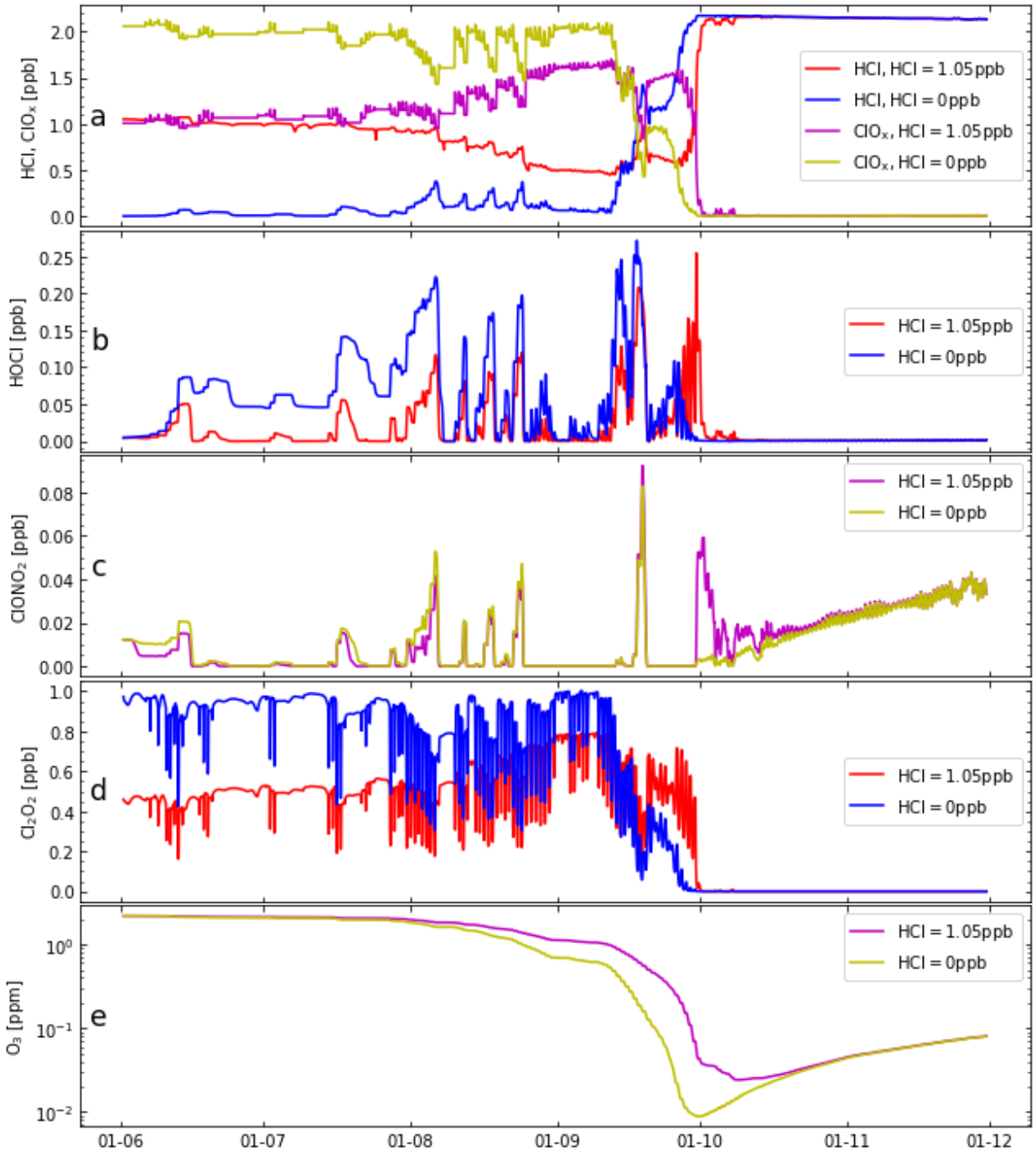

Figure 4.15: Box-model simulations along a trajectory passing through the location of the ozone sonde observation at South pole of 14 ppbv on 740 hPa (391 K) on 24 September 2003 (Burkholder et al. 2020). The results for initial value HCl = 1.05 ppb and HCl = 0 ppb are both presented in the plot: (a) HCl and ClO_x, (b) HOCl, (c) $ClONO_2$, (d) Cl_2O_2, (e) ozone.

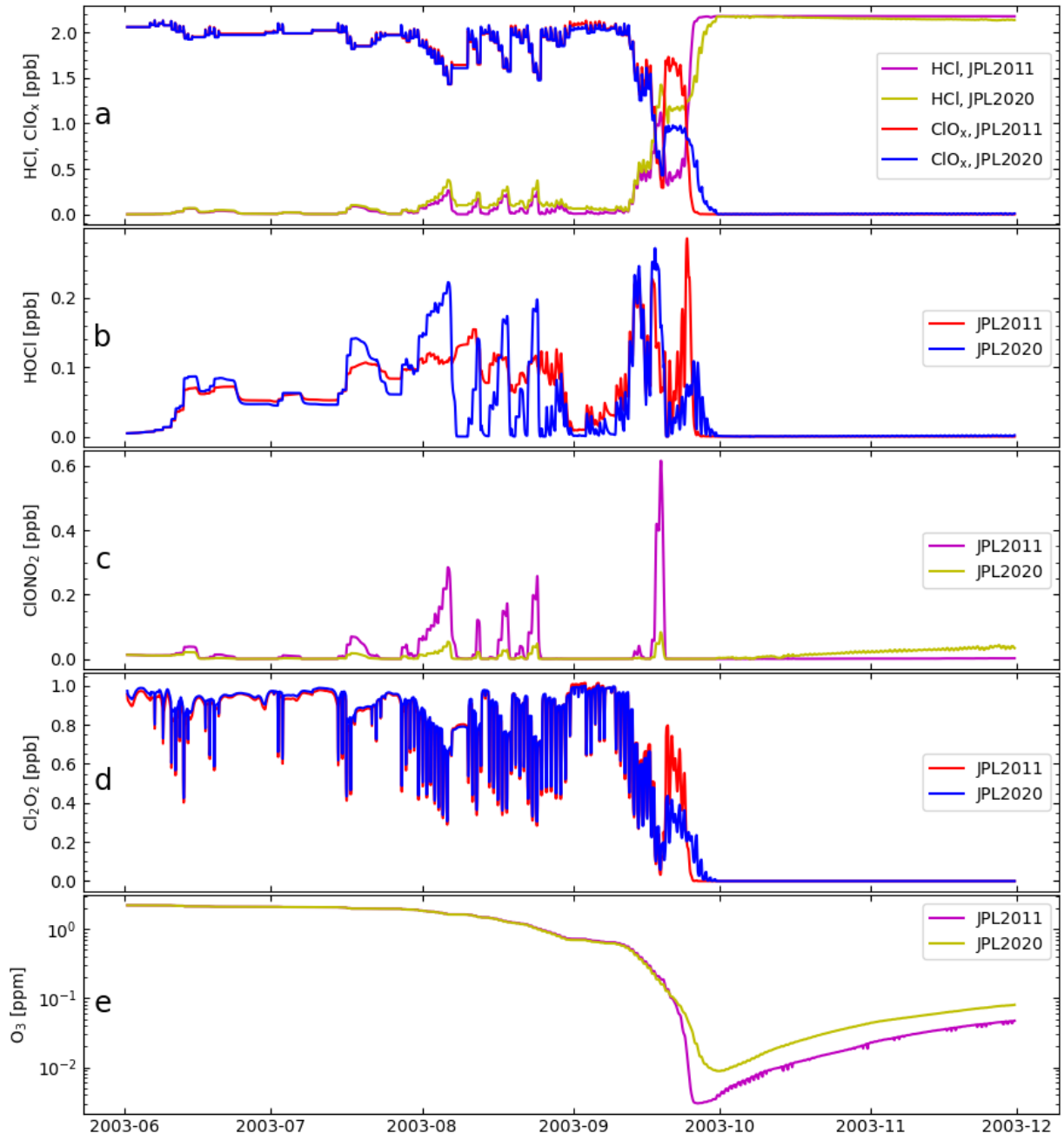

Figure 4.16: Box-model simulations along a trajectory passing through the location of the ozone sonde observation at South pole of 14 ppbv on 740 hPa (391 K) on 24 September 2003. The results for initial value $H_2O = 2.05$ ppm, HCl = 0 ppb are presented under both Sander et al. 2011 recommendation and Burkholder et al. 2020 recommendation: (a) HCl and ClO_x, (b) HOCl, (c) $ClONO_2$, (d) Cl_2O_2, (e) ozone.

4.4.3 Multi-trajectory simulation

Similar as in earlier work (Grooß et al. 2011, Müller et al. 2018), we present here results for several trajectories passing the South Pole (in late September/early October) at the 400 K potential temperature level; these trajectories include diabatic descent and latitude variation.

From early August to early October these trajectories show roughly the same diabatic descent of $\approx$ 10 K, similarly as for the single trajectory discussed in sections 4.1 and 4.2. However, over this period, the different trajectories show strong variations in latitude (and thus exposure to sunlight); the latitude varies between the South Pole and $\approx 65°$S with some equatorward excursions to $\approx 60°$S and, sometimes to $\approx 55°$S.

The initial values of HCl, ClO_x and H_2O were chosen consistently with the simulation presented in the previous sections. The same initial water vapour concentration (H_2O = 2.05 ppm) was employed for all trajectories, which approximately takes into account dehydration in the Antarctic lowermost stratosphere (see section 4.2). Further, we employ an initial value for HCl of zero (Grooß et al. 2018) and a corresponding increase in initialClO_x. The adjustment follows the principal of equation (Init. Adjustment) in section 4.3. The initial value of ClO_x is therefore different for the individual trajectories. The recommendations by (Burkholder et al. 2020) was used.

The results of the multi-trajectory simulations (4.17) show a certain variability in the ozone loss rate, which depends strongly on solar insulation and on the initial value of ClO_x; also note that initial ozone is different for the individual trajectories. The minimum ozone is reached for the individual trajectories between mid-September and early October. There is also a certain variability of the temporal development of HCl, with some trajectories showing intermittent rapid increases in HCl for certain periods.

However, all trajectories show strongly enhanced values of ClO_x over the period of strong ozone loss in August and September, consistent with suppressed values of HCl. Minimum ozone values for all trajectories are very low; below 50 ppb for all and below 10 ppb for several trajectories. The period of rapid ozone loss (driven by high levels of ClO_x) ends abruptly with chlorine deactivation through very rapid formation of HCl (Lehmann et al., 2022(see Chapter 2.5)). After deactivation, HCl values remain high and practically unchanged in the box model simulation.

.

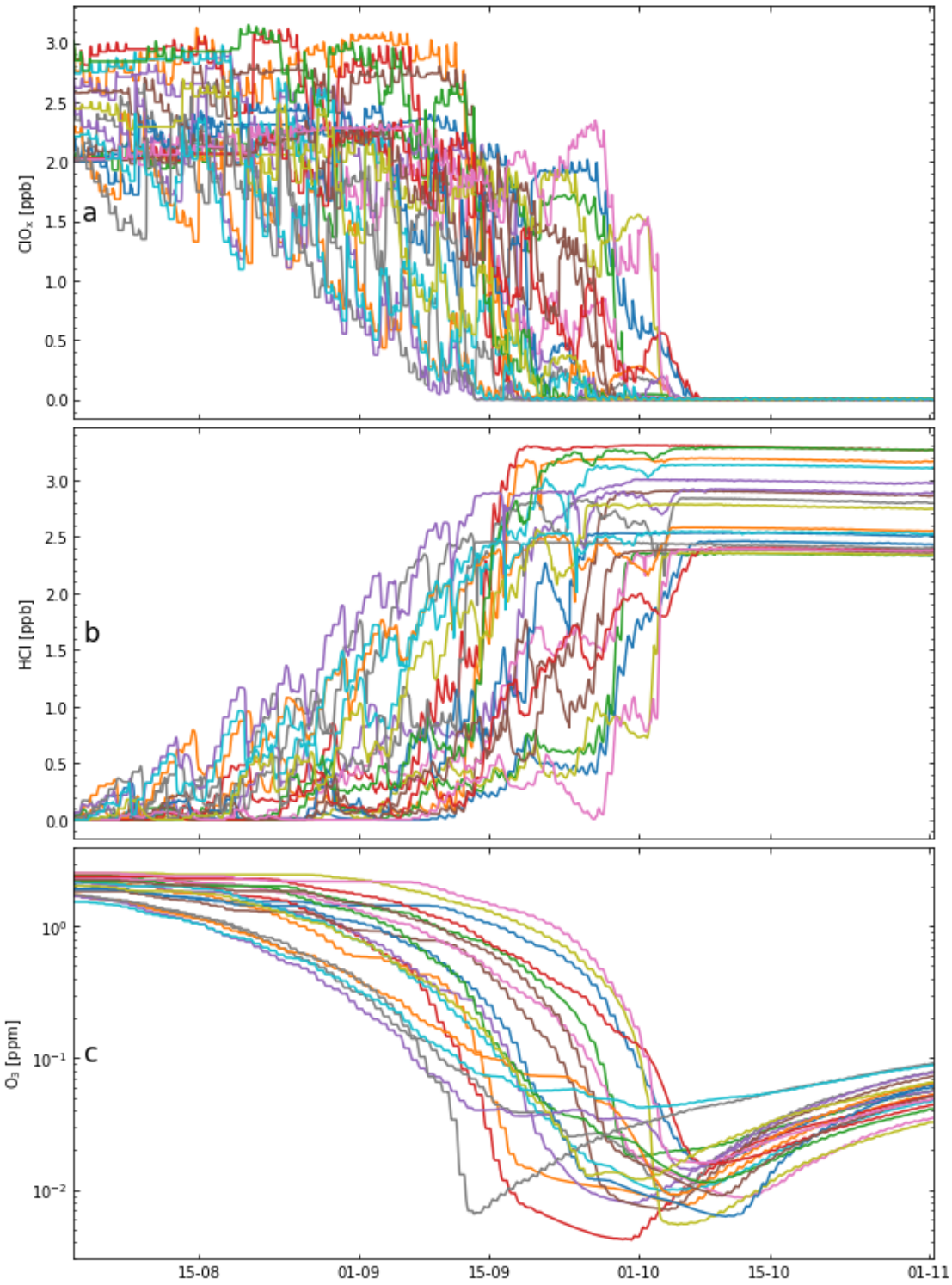

Figure 4.17: Results from multi-trajectory simulations of the CLaMS box-model. The trajectories are consistently initialised with HCl = 0 and H_2O = 2.05 ppm. Initial ClO_x and ozone are different (details are described above and in Grooß et al. 2011). Simulations were performed for a set of trajectories passing the South pole at 400 K (Grooß et al. 2011). The results are shown for the time period from 1st August to 1st November, 2003.A few trajectories showing very little diabatic descent (and thus much smaller values of total chlorine) were neglected. Individual trajectories are shown in different colours.

4.5 Impact of Initial Cl_y Value

Chlorine- and bromine-containing ozone-depleting substances (ODSs) are controlled by the 1987 Montreal Protocol. In consequence, atmospheric equivalent chlorine peaked in 1993 and has been declining slowly since then (Chipperfield et al. 2015). We expect that in the coming decades, the composition of the Antarctic lower stratosphere continue to change. Specifically, the stratospheric halogen loading should decrease continually. The impact of this expectation and its assessment are discussed in this section.

The term Cl_y in our model includes 10 chlorine species: Cl, BrCl, Cl_2, Cl_2O_2, $ClNO_2$, ClO, $ClONO_2$, HOCl, OClO and HCl. We performed sensitivity run based on initialization in section 4.2, where we adjusted Cl_y to the expectation unter Montreal Protocol. This means setting all the species in Cl_y to half of its initial value. Recommendation Burkholder et al. 2020 is employed. A setup like this is a typical anticipated condition around year 2050.

The results are presented in Figure 4.18. Lower active chlorine ClO_x and thus slower and smaller ozone depletion are observed as expected (Panel (f)). In the case of half Cl_y, the ozone depletion reaches a plateau of Ozone mixing ratio on 19th October around 0.54 ppm. Different from the cases (ozone minimum) in the previous section, the ozone mixing ratio does not recover afterwards but continues to decrease very slowly until the very end of the simulation to 0.49 ppm in December. The interpretation is that, the impact of reduced amount of Cl_y on ozone depletion is effective in September. This is consistent with the study in Solomon et al. 2016, in which observations and model calculations together indicated that healing of the Antarctic ozone layer has begun to occur during the month of September. For half Cl_y, ozone does not drop low enough that the depletion process stops, therefore the loss of ozone still continues after November at an extremely low rate.

Panel (c), (d) and (e) show that, the processes take place in the same pattern before October, merely at a lower level of mixing ratios. The differences are mainly observant in the month October. In the case of lower Cl_y, heterogeneous processing continues in correspondence to temperature fluctuation (Figure 4.19). Ozone depletion becomes significantly slower and rather stable as temperature grows significantly in late October and November.

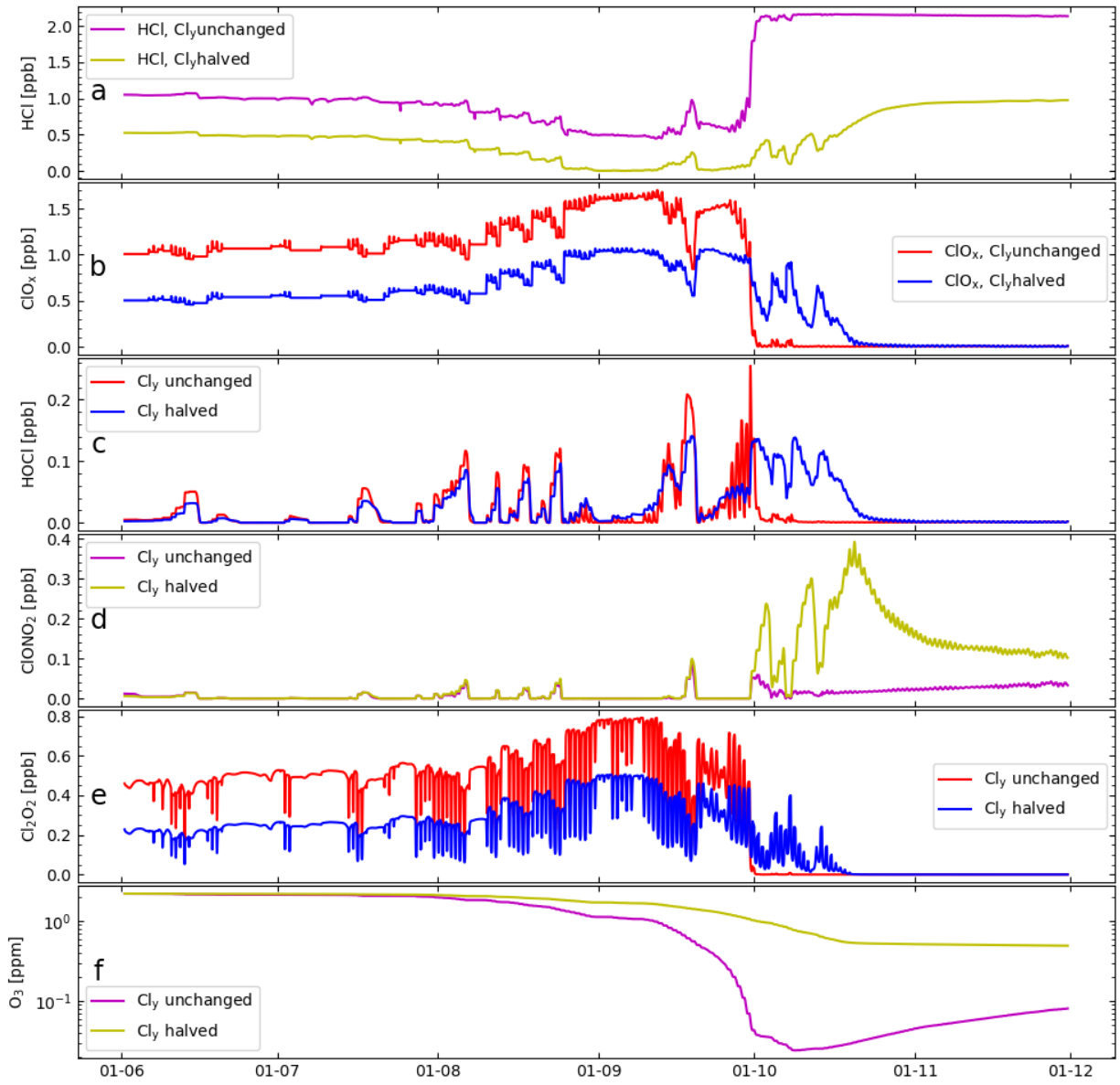

Figure 4.18: Sensitivity of the ozone hole chemistry on stratospheric chlorine levels: (a) radical channel, (b) molecular channel. Running average

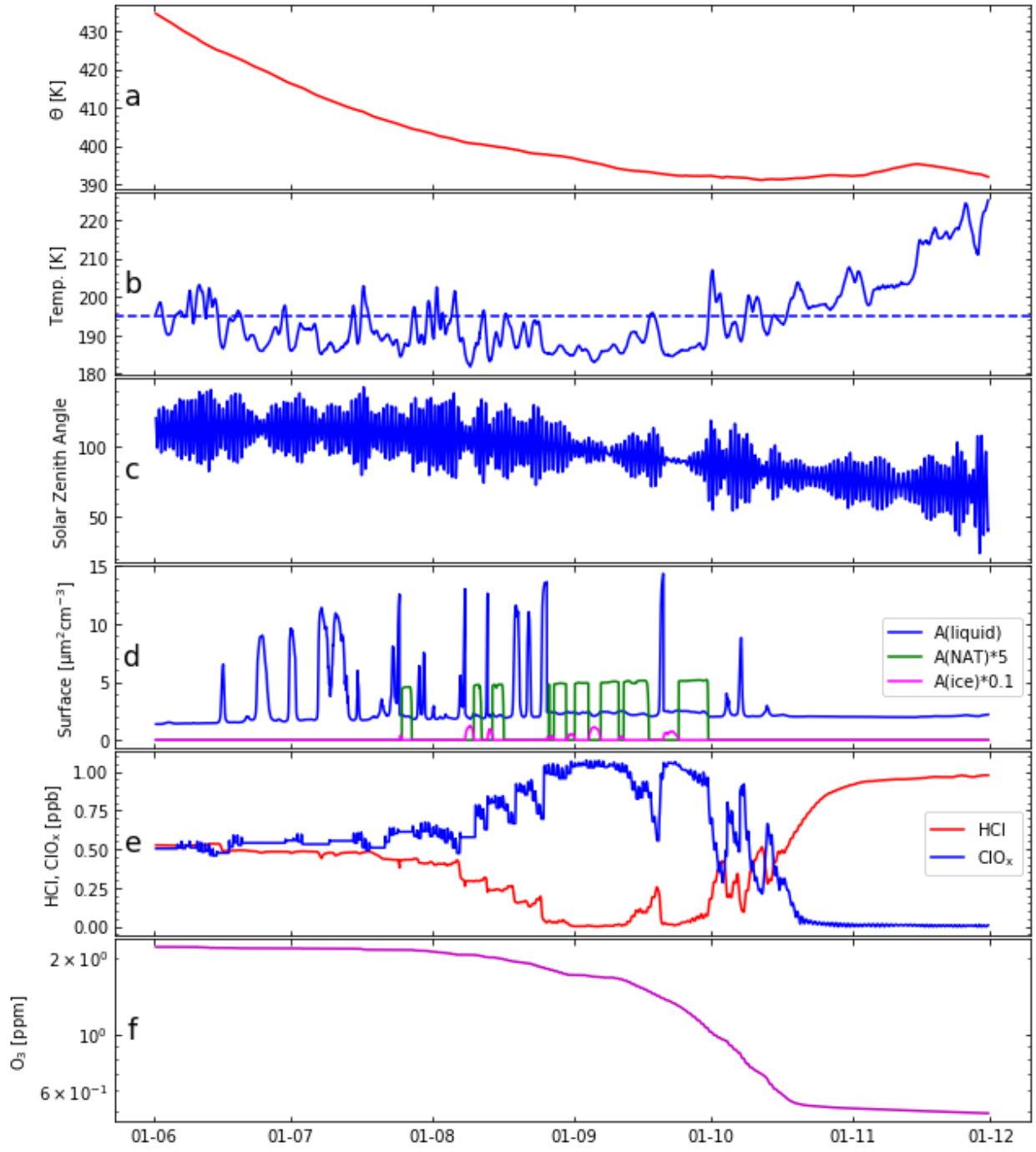

Figure 4.19: Sensitivity of the ozone hole chemistry on stratospheric chlorine levels: (a) radical channel, (b) molecular channel. Running average

Chapter 5

Summary and Outlook

The results of our simulations corroborate earlier findings that effective HCl null cycles (C1 and C2) allow high levels of active chlorine to be maintained in the Antarctic lower stratosphere during the period of strong ozone depletion. During this period, HCl production rates in the gas-phase are high and increase with decreasing ozone (Grooß et al. 2011, Müller et al. 2018). The HCl null cycles require the heterogeneous reaction (R2) to proceed at a substantial rate and further the gas-phase reaction (R3) is essential (Crutzen et al. 1992, Zafar et al. 2018).

The results from the simulations that take the observed dehydration in the Antarctic lower stratosphere in winter into account are similar to the unchanged simulations. The ice clouds are substantially reduced in the model, but does not affect strongly the overall results of chlorine chemistry and ozone loss. The most important impact of the simulated difference in ice clouds in the model is caused by the uptake of HNO3 from the gas-phase, which is different, when ice particle surface is available. Reaction (R18), which directs involves water, does not have an impact on the overall outcome of the simulated ozone loss.

Assuming an HCl mixing ratio of zero after polar night (consistent with Grooß et al. 2018) leads to a temporal development of the chlorine chemistry that is somewhat different than when assuming a higher initial HCl (in particular HOCl is enhanced from about mid-June to mid-August and HCl mixing ratios remain very low until chlorine deactivation into HCl). However the overall ozone depletion in the Antarctic lower stratosphere is not strongly affected (which is consistent with Grooß et al. 2018). Our simulations indicate extremely low minimum ozone values at the South Pole (below 50 ppb) in late September/early October in agreement with observations (Grooß et al. 2011).

Using the most recent recommendation for chemical kinetic and photochemical data (Burkholder et al. 2020), does not change the results of the simulations substantially compared to earlier

work (where Sander et al. 2011 was used). However there were some differences in terms of the rate of ozone loss and the amount of $ClONO_2$ on certain days, the cause for this lies in the reaction parameters that have been updated in Burkholder et al. 2020. A comparison of the updated reactions with respect to the change in ozone has been made but the detailed mechanism of these changes remains to be studied.

The results of the multi-trajectory simulations show a a certain variability in the ozone loss rate, which depends strongly on solar insulation and on the initial value of active chlorine. The initial ozone could also have an impact on the results as they are different for the individual trajectories. All of the trajectories show strongly enhanced values of ClO_x over the period of strong ozone loss in August and September, which is caused by the suppressed values of HCl at the start of the simulation.

Using an initial setup with the anticipation of 2050s under the Montreal protocol has shown that despite the overall declining chlorine species, ozone still decreases in a logarithmic scale. However the situation would already be significantly better than the current results from observation and simulation.

In conclusion, the results in this thesis have updated the previous studies with the consideration of dehydration and initial HCl values. The differences caused by the revised recommendation (Burkholder et al. 2020) have also been studied. The results have shown consistency with previous studies overall, however the underlying mechanism of small variations could require further research.

Bibliography

P. W. Barnes, C. E. Williamson, R. M. Lucas, S. A. Robinson, S. Madronich, N. D. Paul, J. F. Bornman, A. F. Bais, B. Sulzberger, S. R. Wilson, et al. Ozone depletion, ultraviolet radiation, climate change and prospects for a sustainable future. *Nature Sustainability*, 2 (7):569–579, 2019.

G. Becker, J.-U. Grooß, D. S. McKenna, and R. Müller. Stratospheric photolysis frequencies: Impact of an improved numerical solution of the radiative transfer equation. *Journal of atmospheric chemistry*, 37(3):217–229, 2000.

P. N. Brown, G. D. Byrne, and A. C. Hindmarsh. Vode: A variable-coefficient ode solver. *SIAM journal on scientific and statistical computing*, 10(5):1038–1051, 1989.

J. Burkholder, S. Sander, J. Abbatt, J. Barker, C. Cappa, J. Crounse, T. Dibble, R. Huie, C. Kolb, M. Kurylo, et al. Chemical kinetics and photochemical data for use in atmospheric studies; evaluation number 19. Technical report, Pasadena, CA: Jet Propulsion Laboratory, National Aeronautics and Space . . . , 2020.

J. B. Burkholder, S. P. Sander, J. P. D. Abbatt, J. R. Barker, R. E. Huie, C. E. Kolb, M. J. Kurylo, V. L. Orkin, D. M. Wilmouth, and P. H. Wine. Chemical kinetics and photochemical data for use in atmospheric studies, evaluation number 18. JPL Publication 15-10, 2015.

T. P. Canty, R. J. Salawitch, and D. M. Wilmouth. The kinetics of the cloocl catalytic cycle. *Journal of Geophysical Research: Atmospheres*, 121(22):13–768, 2016.

K. S. Carslaw, T. Peter, and S. L. Clegg. Modeling the composition of liquid stratospheric aerosols. *Reviews of Geophysics*, 35(2):125–154, 1997.

G. D. Carver, P. D. Brown, and O. Wild. The asad atmospheric chemistry integration package and chemical reaction database. *Computer Physics Communications*, 105(2-3): 197–215, 1997.

S. CCMVal. Sparc report on the evaluation of chemistry-climate models, edited by: Eyring, v., shepherd, tg, and waugh, dw. Technical report, SPARC report, 2010.

S. Chapman. Xxxv. on ozone and atomic oxygen in the upper atmosphere. *The London, Edinburgh, and Dublin Philosophical Magazine and Journal of Science*, 10(64):369–383, 1930.

M. P. Chipperfield, S. S. Dhomse, W. Feng, R. McKenzie, G. J. Velders, and J. A. Pyle. Quantifying the ozone and ultraviolet benefits already achieved by the montreal protocol. *Nature communications*, 6(1):1–8, 2015.

J. N. Crowley, F. Helleis, R. Müller, G. K. Moortgat, P. J. Crutzen, and J. J. Orlando. CH_3OCl: UV/Vis absorption cross-sections, j values and atmospheric significance. *J. Geophys. Res.*, 99:20683–20688, 1994.

P. J. Crutzen, R. Müller, C. Brühl, and T. Peter. On the potential importance of the gas phase reaction ch3o2+ clo→ cloo+ ch3o and the heterogeneous reaction hocl+ hcl→ h2o+ cl2 in "ozone hole" chemistry. *Geophysical research letters*, 19(11):1113–1116, 1992.

S. Davies, M. Chipperfield, K. Carslaw, B.-M. Sinnhuber, J. Anderson, R. Stimpfle, D. Wilmouth, D. Fahey, P. Popp, E. Richard, et al. Modeling the effect of denitrification on arctic ozone depletion during winter 1999/2000. *Journal of Geophysical Research: Atmospheres*, 107(D5):SOL–65, 2002.

F. de Gruijl and J. Leun. Environment and health: 3. ozone depletion and ultraviolet radiation. *Cmaj*, 163(7):851–855, 2000.

D. P. Dee, S. M. Uppala, A. J. Simmons, P. Berrisford, P. Poli, S. Kobayashi, U. Andrae, M. Balmaseda, G. Balsamo, d. P. Bauer, et al. The era-interim reanalysis: Configuration and performance of the data assimilation system. *Quarterly Journal of the royal meteorological society*, 137(656):553–597, 2011.

S. S. Dhomse, D. Kinnison, M. P. Chipperfield, R. J. Salawitch, I. Cionni, M. I. Hegglin, N. L. Abraham, H. Akiyoshi, A. T. Archibald, E. M. Bednarz, et al. Estimates of ozone return dates from chemistry-climate model initiative simulations. *Atmospheric Chemistry and Physics*, 18(11):8409–8438, 2018.

V. Eyring, N. Harris, M. Rex, T. G. Shepherd, D. Fahey, G. Amanatidis, J. Austin, M. Chipperfield, M. Dameris, P. D. F. Forster, et al. A strategy for process-oriented validation

of coupled chemistry–climate models. *Bulletin of the American Meteorological Society*, 86 (8):1117–1134, 2005.

V. Eyring, N. Butchart, D. W. Waugh, H. Akiyoshi, J. Austin, S. Bekki, G. E. Bodeker, B. A. Boville, C. Brühl, M. P. Chipperfield, et al. Assessment of temperature, trace species, and ozone in chemistry-climate model simulations of the recent past. *Journal of Geophysical Research: Atmospheres*, 111(D22), 2006.

V. Eyring, D. Waugh, G. Bodeker, E. Cordero, H. Akiyoshi, J. Austin, S. Beagley, B. Boville, P. Braesicke, C. Brühl, et al. Multimodel projections of stratospheric ozone in the 21st century. *Journal of Geophysical Research: Atmospheres*, 112(D16), 2007.

V. Eyring, I. Cionni, G. E. Bodeker, A. J. Charlton-Perez, D. E. Kinnison, J. F. Scinocca, D. W. Waugh, H. Akiyoshi, S. Bekki, M. P. Chipperfield, et al. Multi-model assessment of stratospheric ozone return dates and ozone recovery in ccmval-2 models. *Atmospheric Chemistry and Physics*, 10(19):9451–9472, 2010.

J. L. Grenfell, R. Lehmann, P. Mieth, U. Langematz, and B. Steil. Chemical reaction pathways affecting stratospheric and mesospheric ozone. *Journal of Geophysical Research: Atmospheres*, 111(D17), 2006.

J.-U. Grooß and J. M. Russell III. A stratospheric climatology for o 3, h 2 o, ch 4, no x, hcl and hf derived from haloe measurements. *Atmospheric chemistry and physics*, 5(10): 2797–2807, 2005.

J.-U. Grooß, G. Günther, R. Müller, P. Konopka, S. Bausch, H. Schlager, C. Voigt, C. Volk, and G. Toon. Simulation of denitrification and ozone loss for the arctic winter 2002/2003. *Atmospheric Chemistry and Physics*, 5(6):1437–1448, 2005.

J.-U. Grooß, K. Brautzsch, R. Pommrich, S. Solomon, and R. Müller. Stratospheric ozone chemistry in the antarctic: what determines the lowest ozone values reached and their recovery? *Atmospheric Chemistry and Physics*, 11(23):12217–12226, 2011. doi: 10.5194/acp-11-12217-2011. URL `https://acp.copernicus.org/articles/11/12217/2011/`.

J.-U. Grooß, I. Engel, S. Borrmann, W. Frey, G. Günther, C. R. Hoyle, R. Kivi, B. P. Luo, S. Molleker, T. Peter, et al. Nitric acid trihydrate nucleation and denitrification in the arctic stratosphere. *Atmospheric Chemistry and Physics*, 14(2):1055–1073, 2014.

J.-U. Grooß, R. Müller, R. Spang, I. Tritscher, T. Wegner, M. P. Chipperfield, W. Feng, D. E. Kinnison, and S. Madronich. On the discrepancy of hcl processing in the core of the wintertime polar vortices. *Atmospheric Chemistry and Physics*, 18(12):8647–8666, 2018.

G. Günther, R. Müller, M. Von Hobe, F. Stroh, P. Konopka, and C. Volk. Quantification of transport across the boundary of the lower stratospheric vortex during arctic winter 2002/2003. *Atmospheric chemistry and physics*, 8(13):3655–3670, 2008.

D. Hanson and K. Mauersberger. Laboratory studies of the nitric acid trihydrate: Implications for the south polar stratosphere. *Geophysical Research Letters*, 15(8):855–858, 1988.

D. Hanson and A. Ravishankara. Reaction of clono2 with hcl on nat, nad, and frozen sulfuric acid and hydrolysis of n2o5 and clono2 on frozen sulfuric acid. *Journal of Geophysical Research: Atmospheres*, 98(D12):22931–22936, 1993.

C. Hoppe, L. Hoffmann, P. Konopka, J.-U. Grooß, F. Ploeger, G. Günther, P. Jöckel, and R. Müller. The implementation of the clams lagrangian transport core into the chemistry climate model emac 2.40. 1: application on age of air and transport of long-lived trace species. *Geoscientific model development*, 7(6):2639–2651, 2014.

L. Jaeglé, D. J. Jacob, P. Wennberg, C. Spivakovsky, T. Hanisco, E. Lanzendorf, E. Hintsa, D. Fahey, E. Keim, M. Proffitt, et al. Observed oh and ho2 in the upper troposphere suggest a major source from convective injection of peroxides. *Geophysical Research Letters*, 24 (24):3181–3184, 1997.

D. Johnson, W. Traub, K. Chance, and K. Jucks. Detection of hbr and upper limit for hobr: Bromine partitioning in the stratosphere. *Geophysical research letters*, 22(11):1373–1376, 1995.

T. J. Kelly, S. E. Mclaren, and J. A. Kadlecek. Seasonal variations in atmospheric sox and noy species in the adirondacks. *Atmospheric Environment (1967)*, 23(6):1315–1332, 1989.

P. Konopka, H.-M. Steinhorst, J.-U. Grooß, G. Günther, R. Müller, J. W. Elkins, H.-J. Jost, E. Richard, U. Schmidt, G. Toon, et al. Mixing and ozone loss in the 1999–2000 arctic vortex: Simulations with the three-dimensional chemical lagrangian model of the stratosphere (clams). *Journal of Geophysical Research: Atmospheres*, 109(D2), 2004.

P. Konopka, G. Günther, R. Müller, F. Dos Santos, C. Schiller, F. Ravegnani, A. Ulanovsky, H. Schlager, C. Volk, S. Viciani, et al. Contribution of mixing to upward transport across

the tropical tropopause layer (ttl). *Atmospheric Chemistry and Physics*, 7(12):3285–3308, 2007.

P. Konopka, M. Tao, F. Ploeger, M. Diallo, and M. Riese. Tropospheric mixing and parametrization of unresolved convective updrafts as implemented in the chemical lagrangian model of the stratosphere (clams v2. 0). *Geoscientific model development*, 12(6): 2441–2462, 2019.

L. Kovalenko, K. Jucks, R. Salawitch, G. Toon, J.-F. Blavier, D. Johnson, A. Kleinböhl, N. Livesey, J. Margitan, H. Pickett, et al. Observed and modeled hocl profiles in the midlatitude stratosphere: Implication for ozone loss. *Geophysical research letters*, 34(19), 2007.

M. Krämer, R. Müller, H. Bovensmann, J. Burrows, J. Brinkmann, E. Röth, J.-U. Grooß, R. Müller, T. Woyke, R. Ruhnke, et al. Intercomparison of stratospheric chemistry models under polar vortex conditions. *Journal of atmospheric chemistry*, 45(1):51–77, 2003.

D. Lary, M. Chipperfield, R. Toumi, and T. Lenton. Heterogeneous atmospheric bromine chemistry. *Journal of Geophysical Research: Atmospheres*, 101(D1):1489–1504, 1996.

K. E. Leather, A. Bacak, R. Wamsley, A. T. Archibald, A. Husk, D. E. Shallcross, and C. J. Percival. Temperature and pressure dependence of the rate coefficient for the reaction between clo and ch3o2 in the gas-phase. *Physical Chemistry Chemical Physics*, 14(10): 3425–3434, 2012.

R. Lehmann. An algorithm for the determination of all significant pathways in chemical reaction systems. *Journal of atmospheric chemistry*, 47(1):45–78, 2004.

C.-Y. Lien, W.-Y. Lin, H.-Y. Chen, W.-T. Huang, B. Jin, I.-C. Chen, and J. J. Lin. Photodissociation cross sections of cloocl at 248.4 and 266 nm. *The Journal of chemical physics*, 131(17):174301, 2009.

E. Mahieu, P. Duchatelet, R. Zander, P. Demoulin, C. Servais, C. Rinsland, M. Chipperfield, and M. De Maziere. The evolution of inorganic chlorine above the jungfraujoch station: an update. In *20th Quadrennial Ozone Symposium*, 2004.

M. B. McElroy, R. J. Salawitch, S. C. Wofsy, and J. A. Logan. Reductions of antarctic ozone due to synergistic interactions of chlorine and bromine. *Nature*, 321(6072):759–762, 1986.

D. S. McKenna, J.-U. Grooß, G. Günther, P. Konopka, R. Müller, G. Carver, and Y. Sasano. A new chemical lagrangian model of the stratosphere (clams) 2. formulation of chemistry scheme and initialization. *Journal of Geophysical Research: Atmospheres*, 107(D15):ACH–4, 2002a.

D. S. McKenna, P. Konopka, J.-U. Grooß, G. Günther, R. Müller, R. Spang, D. Offermann, and Y. Orsolini. A new chemical lagrangian model of the stratosphere (clams) 1. formulation of advection and mixing. *Journal of Geophysical Research: Atmospheres*, 107(D16): ACH–15, 2002b.

R. Meier, D. Anderson Jr, and M. Nicolet. Radiation field in the troposphere and stratosphere from 240–1000 nm-i. general analysis. *Planetary and Space Science*, 30(9):923–933, 1982.

L. Molina and M. Molina. Production of chlorine oxide (cl2o2) from the self-reaction of the chlorine oxide (clo) radical. *Journal of Physical Chemistry*, 91(2):433–436, 1987.

J.-J. Morcrette. Radiation and cloud radiative properties in the european centre for medium range weather forecasts forecasting system. *Journal of Geophysical Research: Atmospheres*, 96(D5):9121–9132, 1991.

R. Müller. *Tracer-tracer Relations as a Tool for Research on Polar Ozone Loss*, volume 58. Forschungszentrum Jülich, 2010.

R. Müller and P. J. Crutzen. On the relevance of the methane oxidation cycle to "ozone hole" chemistry. In R. D. Hudson, editor, *Ozone in the troposphere and stratosphere*, Proceedings of the Quadrennial Ozone Symposium 1992, pages 298–301, 1994.

R. Müller, J.-U. Grooß, A. M. Zafar, S. Robrecht, and R. Lehmann. The maintenance of elevated active chlorine levels in the antarctic lower stratosphere through hcl null cycles. *Atmospheric Chemistry and Physics*, 18(4):2985–2997, 2018. doi: 10.5194/acp-18-2985-2018. URL `https://acp.copernicus.org/articles/18/2985/2018/`.

G. E. Nedoluha, R. M. Bevilacqua, and K. W. Hoppel. Poam iii measurements of dehydration in the antarctic and comparisons with the arctic. *Journal of Geophysical Research: Atmospheres*, 107(D20):SOL–33, 2002.

P. Newman, J. Daniel, D. Waugh, and E. Nash. A new formulation of equivalent effective stratospheric chlorine (eesc). *Atmospheric Chemistry and Physics*, 7(17):4537–4552, 2007.

L. Oman, D. Plummer, D. Waugh, J. Austin, J. Scinocca, A. Douglass, R. Salawitch, T. Canty, H. Akiyoshi, S. Bekki, et al. Multimodel assessment of the factors driving stratospheric ozone evolution over the 21st century. *Journal of Geophysical Research: Atmospheres*, 115(D24), 2010.

S. Pawson, K. Kodera, K. Hamilton, T. Shepherd, S. Beagley, B. Boville, J. Farrara, T. Fairlie, A. Kitoh, W. Lahoz, et al. The gcm-reality intercomparison project for sparc (grips): Scientific issues and initial results. *Bulletin of the American Meteorological Society*, 81(4): 781–796, 2000.

T. Peter and J. Grooß. Stratospheric ozone depletion and climate change, chapter 4. In *Roy. Soc*, page 144, 2012a.

T. Peter and J.-U. Grooß. Polar stratospheric clouds and sulfate aerosol particles: microphysics, denitrification and heterogeneous chemistry. *Stratospheric ozone depletion and climate change*, pages 108–144, 2012b.

R. Pommrich, R. Müller, J.-U. Grooß, P. Konopka, F. Ploeger, B. Vogel, M. Tao, C. Hoppe, G. Günther, N. Spelten, et al. Tropical troposphere to stratosphere transport of carbon monoxide and long-lived trace species in the chemical lagrangian model of the stratosphere (clams). *Geoscientific model development*, 7(6):2895–2916, 2014.

L. Poshyvailo, R. Müller, P. Konopka, G. Günther, M. Riese, A. Podglajen, and F. Ploeger. Sensitivities of modelled water vapour in the lower stratosphere: temperature uncertainty, effects of horizontal transport and small-scale mixing. *Atmospheric chemistry and physics*, 18(12):8505–8527, 2018.

G. Poulet, M. Pirre, F. Maguin, R. Ramaroson, and G. Le Bras. Role of the bro+ ho2 reaction in the stratospheric chemistry of bromine. *Geophysical research letters*, 19(23): 2305–2308, 1992.

C. Rinsland, E. Mahieu, R. Zander, N. Jones, M. Chipperfield, A. Goldman, J. Anderson, J. Russell III, P. Demoulin, J. Notholt, et al. Long-term trends of inorganic chlorine from ground-based infrared solar spectra: past increases and evidence for stabilization. *J Geophys Res*, 108:4252–72, 2003.

C. Rolf, A. Afchine, H. Bozem, B. Buchholz, V. Ebert, T. Guggenmoser, P. Hoor, P. Konopka, E. Kretschmer, S. Müller, et al. Transport of antarctic stratospheric strongly

dehydrated air into the troposphere observed during the halo-esmval campaign 2012. *Atmospheric chemistry and physics*, 15(16):9143–9158, 2015.

R. J. Salawitch, S. C. Wofsy, and M. B. McElroy. Chemistry of oclo in the antarctic stratosphere: Implications for bromine. *Planetary and space science*, 36(2):213–224, 1988.

S. Sander, D. Golden, M. Kurylo, G. Moortgat, P. Wine, A. Ravishankara, C. Kolb, M. Molina, B. Finlayson-Pitts, R. Huie, et al. Chemical kinetics and photochemical data for use in atmospheric studies evaluation number 15. Technical report, Pasadena, CA: Jet Propulsion Laboratory, National Aeronautics and Space ..., 2006.

S. P. Sander, R. R. Friedl, J. R. Barker, D. M. Golden, M. J. Kurylo, P. H. Wine, J. P. D. Abbatt, J. B. Burkholder, C. E. Kolb, G. K. Moortgat, R. E. Huie, and V. L. Orkin. Chemical kinetics and photochemical data for use in atmospheric studies. JPL Publication 10-6, 2011.

M. L. Santee, I. MacKenzie, G. Manney, M. Chipperfield, P. Bernath, K. Walker, C. Boone, L. Froidevaux, N. Livesey, and J. Waters. A study of stratospheric chlorine partitioning based on new satellite measurements and modeling. *Journal of Geophysical Research: Atmospheres*, 113(D12), 2008.

M. Schoeberl and A. Dessler. Dehydration of the stratosphere. *Atmospheric Chemistry and Physics*, 11(16):8433–8446, 2011.

Q. Shi, J. Jayne, C. Kolb, D. Worsnop, and P. Davidovits. Kinetic model for reaction of clono2 with h2o and hcl and hocl with hcl in sulfuric acid solutions. *Journal of Geophysical Research: Atmospheres*, 106(D20):24259–24274, 2001.

R. C. Smith, B. Prezelin, K. e. a. Baker, R. Bidigare, N. Boucher, T. Coley, D. Karentz, S. MacIntyre, H. Matlick, D. Menzies, et al. Ozone depletion: ultraviolet radiation and phytoplankton biology in antarctic waters. *Science*, 255(5047):952–959, 1992.

S. Solomon, R. R. Garcia, F. S. Rowland, and D. J. Wuebbles. On the depletion of antarctic ozone. *Nature*, 321(6072):755–758, 1986.

S. Solomon, D. J. Ivy, D. Kinnison, M. J. Mills, R. R. Neely III, and A. Schmidt. Emergence of healing in the antarctic ozone layer. *Science*, 353(6296):269–274, 2016.

R. S. Stolarski. The antarctic ozone hole. *Scientific American*, 258(1):30–37, 1988.

R. Toumi, R. Jones, and J. Pyle. Stratospheric ozone depletion by ciono2 photolysis. *Nature*, 365(6441):37–39, 1993.

I. Tritscher, J.-U. Grooß, R. Spang, M. C. Pitts, L. R. Poole, R. Müller, and M. Riese. Lagrangian simulation of ice particles and resulting dehydration in the polar winter stratosphere. *Atmospheric chemistry and physics*, 19(1):543–563, 2019.

UNEP. The montreal protocol on substances that deplete the ozone layer, 1987.

C. Voigt, J. Schreiner, A. Kohlmann, P. Zink, K. Mauersberger, N. Larsen, T. Deshler, C. Kroger, J. Rosen, A. Adriani, et al. Nitric acid trihydrate (nat) in polar stratospheric clouds. *Science*, 290(5497):1756–1758, 2000.

H. Vömel, S. Oltmans, D. Hofmann, T. Deshler, and J. Rosen. The evolution of the dehydration in the antarctic stratospheric vortex. *Journal of Geophysical Research: Atmospheres*, 100(D7):13919–13926, 1995.

M. von Hobe and F. Stroh. Stratospheric halogen chemistry. *Müller, R*, pages 78–107, 2011.

M. von Hobe, F. Stroh, H. Beckers, T. Benter, and H. Willner. The uv/vis absorption spectrum of matrix-isolated dichlorine peroxide, cloocl. *Physical Chemistry Chemical Physics*, 11(10):1571–1580, 2009.

M. K. Ward and D. M. Rowley. Kinetics of the clo+ ch 3 o 2 reaction over the temperature range t= 250–298 k. *Physical Chemistry Chemical Physics*, 18(19):13646–13656, 2016.

D. Waugh, L. Oman, S. Kawa, R. Stolarski, S. Pawson, A. Douglass, P. Newman, and J. Nielsen. Impacts of climate change on stratospheric ozone recovery. *Geophysical Research Letters*, 36(3), 2009.

O. Wild and M. J. Prather. Excitation of the primary tropospheric chemical mode in a global three-dimensional model. *Journal of Geophysical Research: Atmospheres*, 105(D20): 24647–24660, 2000.

WMO. Scientific assessment of ozone depletion: 2018, global ozone research and monitoring project-report no. 58, 2018.

Y. Yokouchi, F. Hasebe, M. Fujiwara, H. Takashima, M. Shiotani, N. Nishi, Y. Kanaya, S. Hashimoto, P. Fraser, D. Toom-Sauntry, et al. Correlations and emission ratios among bromoform, dibromochloromethane, and dibromomethane in the atmosphere. *Journal of Geophysical Research: Atmospheres*, 110(D23), 2005.

A. M. Zafar, R. Müller, J.-U. Grooss, S. Robrecht, B. Vogel, and R. Lehmann. The relevance of reactions of the methyl peroxy radical (ch3o2) and methylhypochlorite (ch3ocl) for antarctic chlorine activation and ozone loss. *Tellus B: Chemical and Physical Meteorology*, 70(1):1–18, 2018. doi: 10.1080/16000889.2018.1507391. URL `https://doi.org/10.1080/16000889.2018.1507391`.

W. Zhong and J. Haigh. Improved broadband emissivity parameterization for water vapor cooling rate calculations. *Journal of the atmospheric sciences*, 52(1):124–138, 1995.

Appendix A

Appendix

A.1 Reactions in CLaMS model

This section lists all the reactions included in the CLaMS Model: Gas-phase binary reactions (B1 - B64) (McKenna et al. 2002a), updated with gas-phase reactions (B65 - B 83) (Grooß et al. 2014); Ternary reaction (T13) and photolysis reactions (J28 - J36) updated from Grooß et al. 2014; Heterogeneous reactions (McKenna et al. 2002a).

	Binary Reaction
B1	$O(^3P) + O_3 \longrightarrow O_2 + O_2$
B2	$O(^1D) + O_2 \longrightarrow O(3\,^P) + O_2$
B3	$O(^1D) + H_2O \longrightarrow OH + OH$
B4	$O(^1D) + H_2 \longrightarrow OH + H^1$
B5	$O(^1D) + N_2 \longrightarrow O(^3P) + N_2$
B6	$O(^1D) + CH_4 \longrightarrow OH + CH_3$
B7	$OH + O_3 \longrightarrow HO_2 + O_2$
B8	$OH + HO_2 \longrightarrow H_2O + O_2$
B9	$OH + H_2O_2 \longrightarrow H_2O + HO_2$
B10	$HO_2 + O_3 \longrightarrow OH + 2\,O_2$

B11 $HO_2 + HO_2 \longrightarrow H_2O_2 + O_2$

B12 $O(^3P) + NO_2 \longrightarrow NO + O_2$

B13 $OH + NO_3 \longrightarrow HO_2 + NO_2$

B14 $OH + HNO_3 \longrightarrow H_2O + NO_3$

B15 $OH + HO_2NO_2 \longrightarrow NO_2 + H_2O + O_2$

B16 $HO_2 + NO \longrightarrow NO_2 + OJ$

B17 $HO_2 + NO_3 \longrightarrow NO_2 + OH + O_2$

B18 $NO + O_3 \longrightarrow NO_2 + O_2$

B19 $NO + NO_3 \longrightarrow NO_2 + NO_2$

B20 $NO_2 + O_3 \longrightarrow NO_3 + O_2$

B21 $OH + CO \longrightarrow CO_2 + H$

B22 $OH + CH_4 \longrightarrow H_2O + CH_3$

B23 $OH + HCHO \longrightarrow H_2O + HCO$

B24 $OH + CH_3OH \longrightarrow H_2O + HCHO + H$

B25 $OH + CH_3OOH \longrightarrow CH_3OO + H_2O$

B26 $OH + CH_3OOH \longrightarrow HCHO + OH + H_2O$

B27 $HO_2 + CH_3OO \longrightarrow CH_3OOH + O_2$

B28 $CH_3OO + CH_3OO \longrightarrow CH_3OH + HCHO + O_2$

B29 $CH_3OO + NO \longrightarrow NO_2 + HCHO + H$

B30 $CH_3OOH + Cl \longrightarrow HCl + HCHO + OH$

B31 $O(^3P) + ClO \longrightarrow Cl + O_2$

B32 $OH + Cl_2 \longrightarrow HOCl + Cl$

B33 $OH + ClO \longrightarrow HO_2 + Cl$

B34 $OH + ClO \longrightarrow HCl + O_2$

B35 $OH + HCl \longrightarrow H_2O + Cl$

B36 $OH + HOCl \longrightarrow H_2O + ClO$

B37 $HO_2 + Cl \longrightarrow HCl + O_2$

B38 $HO_2 + Cl \longrightarrow OH + ClO$

B39 $HO_2 + ClO \longrightarrow HOCl + O_2$

B40 $Cl + O_3 \longrightarrow ClO + O_2$

B41 $Cl + H_2 \longrightarrow HCl + H$

B42 $Cl + CH_4 \longrightarrow HCl + CH_3$

B43 $Cl + HCHO \longrightarrow HCl + HCO$

B44 $Cl + CH_3OH \longrightarrow HCl + HCHO + H$

B45 $Cl + OClO \longrightarrow ClO + ClO$

B46 $Cl + HOCl \longrightarrow Cl_2 + OH$

B47 $Cl + HOCl \longrightarrow ClO + HCl$

B48 $Cl + ClONO_2 \longrightarrow Cl_2 + NO_3$

B49 $ClO + NO \longrightarrow NO_2 + Cl$

B50 $ClO + CH_3OO \longrightarrow Cl + HCHO + HO_2$

B51 $O(^3P) + BrO \longrightarrow HOBr + HCO$

B52 $OH + HBr \longrightarrow H_2O + Br$

B53 $HO_2 + Br \longrightarrow HBr + O_2$

B54 $HO_2 + BrO \longrightarrow HOBr + O_2$

B55 $Br + O_3 \longrightarrow BrO + O_2$

B56 $Br + HCHO \longrightarrow HBr + HCO$

B57 $\mathrm{BrrO + NO \longrightarrow NO_2 + Br}$

B58 $\mathrm{BrO + ClO \longrightarrow Br + OClO}$

B59 $\mathrm{BrO + ClO \longrightarrow Br + Cl + O_2}$

B60 $\mathrm{BrO + ClO \longrightarrow BrCl + O_2}$

B61 $\mathrm{BrO + BrO \longrightarrow Br + Br + O_2}$

B62 $\mathrm{BrO + BrO \longrightarrow Br_2 + O_2}$

B63 $\mathrm{O(^3P) + HOBr \longrightarrow OH + BrO}$

B64 $\mathrm{OH + Br_2 \longrightarrow HOBr + Br}$

B65 $\mathrm{H + O_3 \longrightarrow OH + O_2}$

B66 $\mathrm{H + HO_2 \longrightarrow OH + OH}$

B67 $\mathrm{H + HO_2 \longrightarrow H_2O + O(^3P)}$

B68 $\mathrm{H + HO_2 \longrightarrow H_2 + O_2}$

B69 $\mathrm{H_2 + OH \longrightarrow H_2O + H}$

B70 $\mathrm{OH + O(^3P) \longrightarrow H + O_2}$

B71 $\mathrm{OH + OH \longrightarrow H_2O + O(^3P)}$

B72 $\mathrm{HO_2 + O(^3P) \longrightarrow OH + O_2}$

B73 $\mathrm{H_2O_2 + O(^3P) \longrightarrow OH + HO_2}$

B74 $\mathrm{O(^3P) + HOCl \longrightarrow OH + ClO}$

B75 $\mathrm{N_2O + O(^1D) \longrightarrow N_2 + O_2}$

B76 $\mathrm{N_2O + O(^1D) \longrightarrow NO + NO}$

B77 $\mathrm{CCl_3F + O(^1D) \longrightarrow ClO + 2\,Cl + products}$

B78 $\mathrm{CCl_2F_2 + O(^1D) \longrightarrow ClO + Cl + products}$

B79 $\mathrm{CHClF_2 + O(^1D) \longrightarrow ClO + H + products}$

B80	$CCl_3F_3 + O(^1D) \longrightarrow ClO + 2\,Cl + \text{products}$
B81	$CCl_4 + O(^1D) \longrightarrow 3\,Cl + ClO + \text{products}$
B82	$CHClF_2 + OH \longrightarrow Cl + H_2O + \text{products}$
B83	$CH_3Cl + OH\,(^+O_2) \longrightarrow ClO + CH_3OOH$
	Ternary Reaction
T1	$O(^3P) + O_2 + M \longrightarrow O_3$
T2	$OH + NO_2 + M \longrightarrow HNO_3$
T3	$HO_2 + NO_2 + M \longrightarrow HO_2NO_2$
T4	$HO_2NO_2 + M \longrightarrow HO_2 + NO_2$
T5	$NO_2 + NO_3 + M \longrightarrow N_2O_5$
T6	$N_2O_5 + M \longrightarrow NO_2 + NO_3$
T7	$CH_3OO + NO_2 + M \longrightarrow CH_3O_2NO_2$
T8	$CH_3O_2NO_2 + M \longrightarrow CH_3OO + NO_2$
T9	$ClO + NO_2 + M \longrightarrow ClONO_2$
T10	$ClO + ClO + M \longrightarrow Cl_2O_2$
T11	$Cl_2O_2 + M \longrightarrow ClO + ClO$
T12	$BrO + NO_2 + M \longrightarrow BrONO_2$
T13	$H + O_2 + M \longrightarrow HO_2$
	Photolysis Reaction
J1	$BrONO_2 + h\nu \longrightarrow BrO + NO_2$
J2	$BrONO_2 + h\nu \longrightarrow Br + NO_3$
J3	$BrCl + h\nu \longrightarrow Br + Cl$
J4	$Cl_2 + h\nu \longrightarrow Cl + Cl$

J5 $Cl_2O_2 + h\nu \longrightarrow Cl + ClOO$

J6 $ClNO_2 + h\nu \longrightarrow Cl + NO_2$

J7 $ClONO_2 + h\nu \longrightarrow Cl + NO_3$

J8 $ClONO_2 + h\nu \longrightarrow ClO + NO_2$

J9 $H_2O_2 + h\nu \longrightarrow OH + OH$

J10 $HCHO + h\nu \longrightarrow HCH + O$

J11 $HCHO + h\nu \longrightarrow H_2 + CO$

J12 $HO_2NO_2 + h\nu \longrightarrow HO_2 + NO_2$

J13 $HO_2NO_2 + h\nu \longrightarrow OH + NO_3$

J14 $HOBr + h\nu \longrightarrow OH + Br$

J15 $HOCl + h\nu \longrightarrow OH + Cl$

J16 $HNO_3 + h\nu \longrightarrow OH + NO_2$

J17 $CH_3O_2NO_2 + h\nu \longrightarrow CH_3OO + NO_2$

J18 $CH_3OOH + h\nu \longrightarrow HCHO + OH + H$

J19 $N_2O_5 + h\nu \longrightarrow NO_3 + NO_2$

J20 $NO_2 + h\nu \longrightarrow NO + O(^3P)$

J21 $NO_3 + h\nu \longrightarrow NO_2 + O(^3P)$

J22 $NO_3 + h\nu \longrightarrow NO_2 + O(^3P)$

J23 $O_2 + h\nu \longrightarrow O(^3P) + O(^3P)$

J24 $O_3 + h\nu \longrightarrow O_2 + O(^3P)$

J25 $O_3 + h\nu \longrightarrow O_2 + O(^1D)$

J26 $OClO + h\nu \longrightarrow O(^3P) + ClO$

J27 $Br_2 + h\nu \longrightarrow Br + Br$

J28	$HCl + h\nu \longrightarrow H + Cl$
J29	$H_2O + h\nu \longrightarrow H + OH$
J30	$CCl_3F + h\nu \longrightarrow 3\,Cl + \text{products}$
J31	$CCl_2F_2 + h\nu \longrightarrow 2\,Cl + \text{products}$
J32	$CHClF_2 + h\nu \longrightarrow Cl + H + \text{products}$
J33	$CCl_3F_3 + h\nu \longrightarrow 3\,Cl + \text{products}$
J34	$CH_3Cl + h\nu\,(^+O_2) \longrightarrow CH_3OO + Cl$
J35	$CCl_4 + h\nu \longrightarrow 4\,Cl + \text{products}$
J36	$N_2O + h\nu \longrightarrow O(^1D) + N_2$
	Heterogeneous Reaction
H1	$ClO_NO_2 + H_2O \longrightarrow HOCl + HNO_3$
H2	$ClO_NO_2 + HCl \longrightarrow Cl_2 + HNO_3$
H3	$HOCl + HCl \longrightarrow Cl_2 + H_2O$
H4	$N_2O_5 + H_2O \longrightarrow HNO_3 + HNO_3$
H5	$N_2O_5 + HCl \longrightarrow ClNO_2 + HNO_3$
H6	$ClONO_2 + HBr \longrightarrow BrCl + HNO_3$
H7	$BrONO_2 + HCl \longrightarrow BrCl + HNO_3$
H8	$HOCl + HBr \longrightarrow BrCl + H_2O$
H9	$HOBr + HCl \longrightarrow BrCl + H_2O$
H10	$HOBr + HBr \longrightarrow Br_2 + H_2O$
H11	$BrONO_2 + H_2O \longrightarrow HOBr + HNO_3$

A.2 Supplement to Chapter 4 Section 4.3

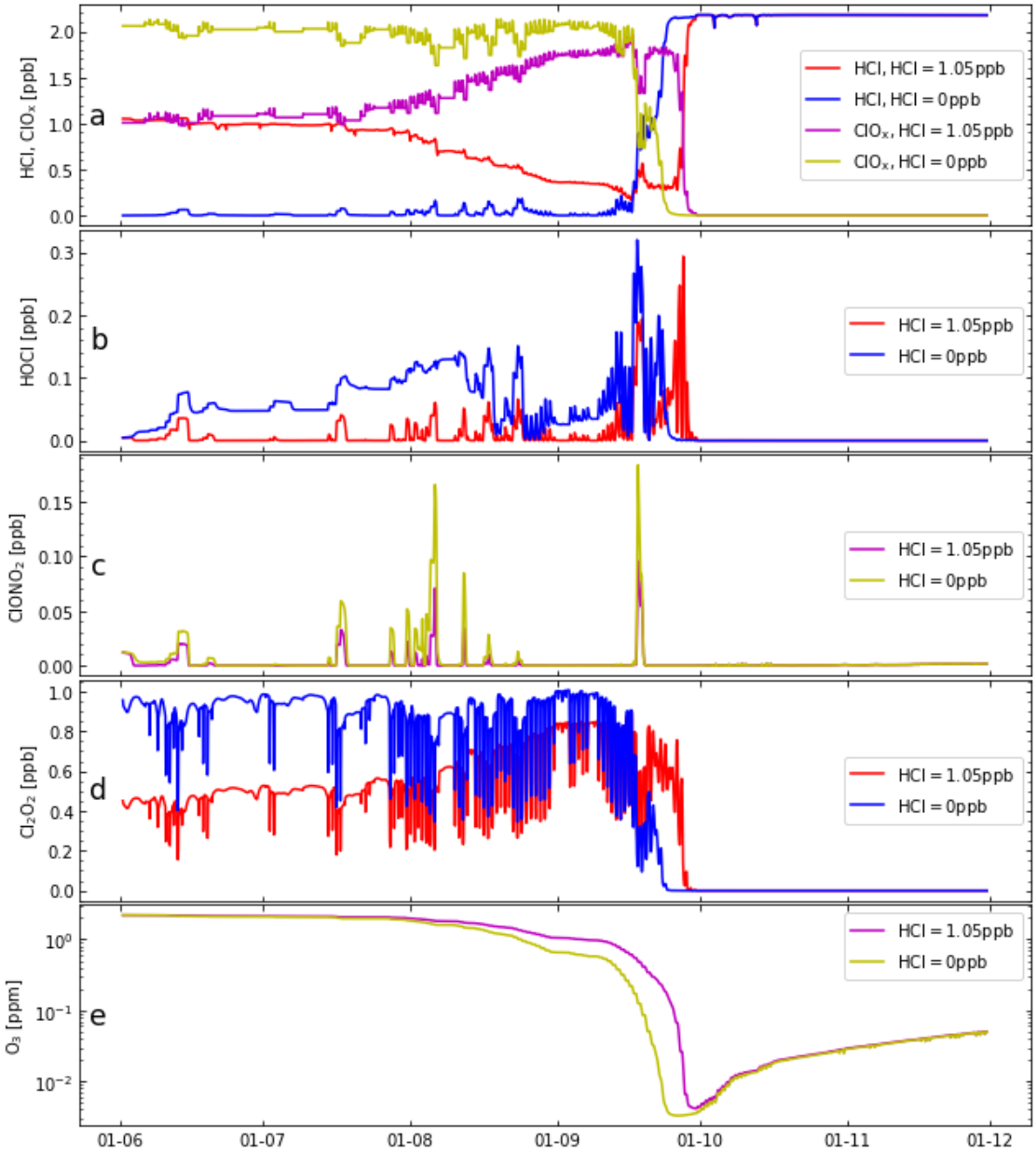

Figure A.1: Box-model simulations along a trajectory passing through the location of the ozone sonde observation at South pole of 14 ppbv on 740 hPa (391 K) on 24 September 2003 (Sander et al. 2011), Initial water vapour H_2O = 4.11 ppm. The results for initial value HCl = 1.05 ppb and HCl = 0 ppb are both presented in the plot: (a) HCl and ClO_x, (b) HOCl, (c) $ClONO_2$, (d) Cl_2O_2, (e) ozone.

A.3 Simulations with JPL2015

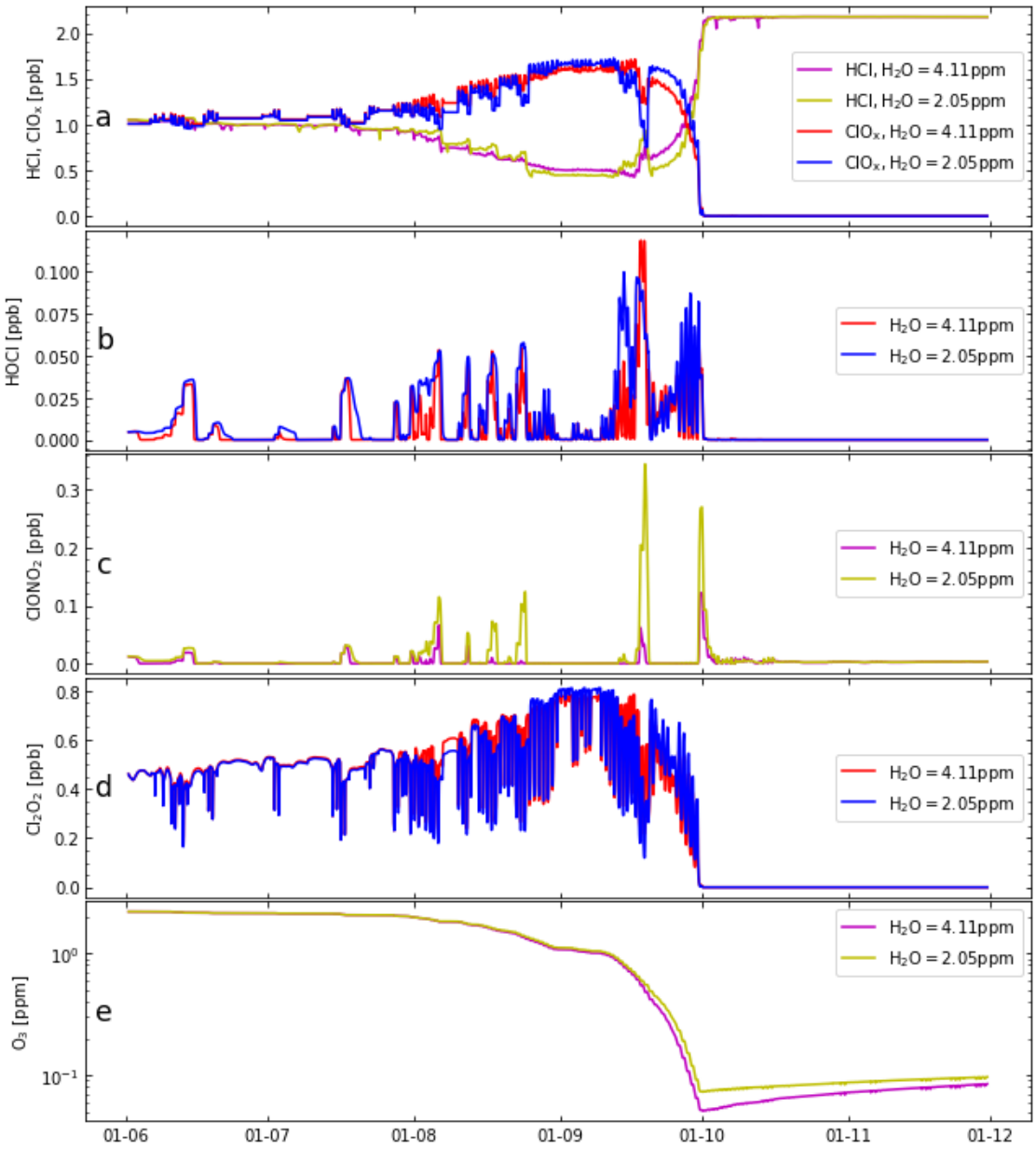

Figure A.2: Box-model simulations along a trajectory passing through the location of the ozone sonde observation at South pole of 14 ppbv on 740 hPa (391 K) on 24th September, 2003 (Burkholder et al. 2015), Initial water vapour H_2O = 4.11 ppm and H_2O = 2.05 ppm are both presented in the plot: (a) HCl and ClO_x, (b) HOCl, (c) $ClONO_2$, (d) Cl_2O_2, (e) ozone.

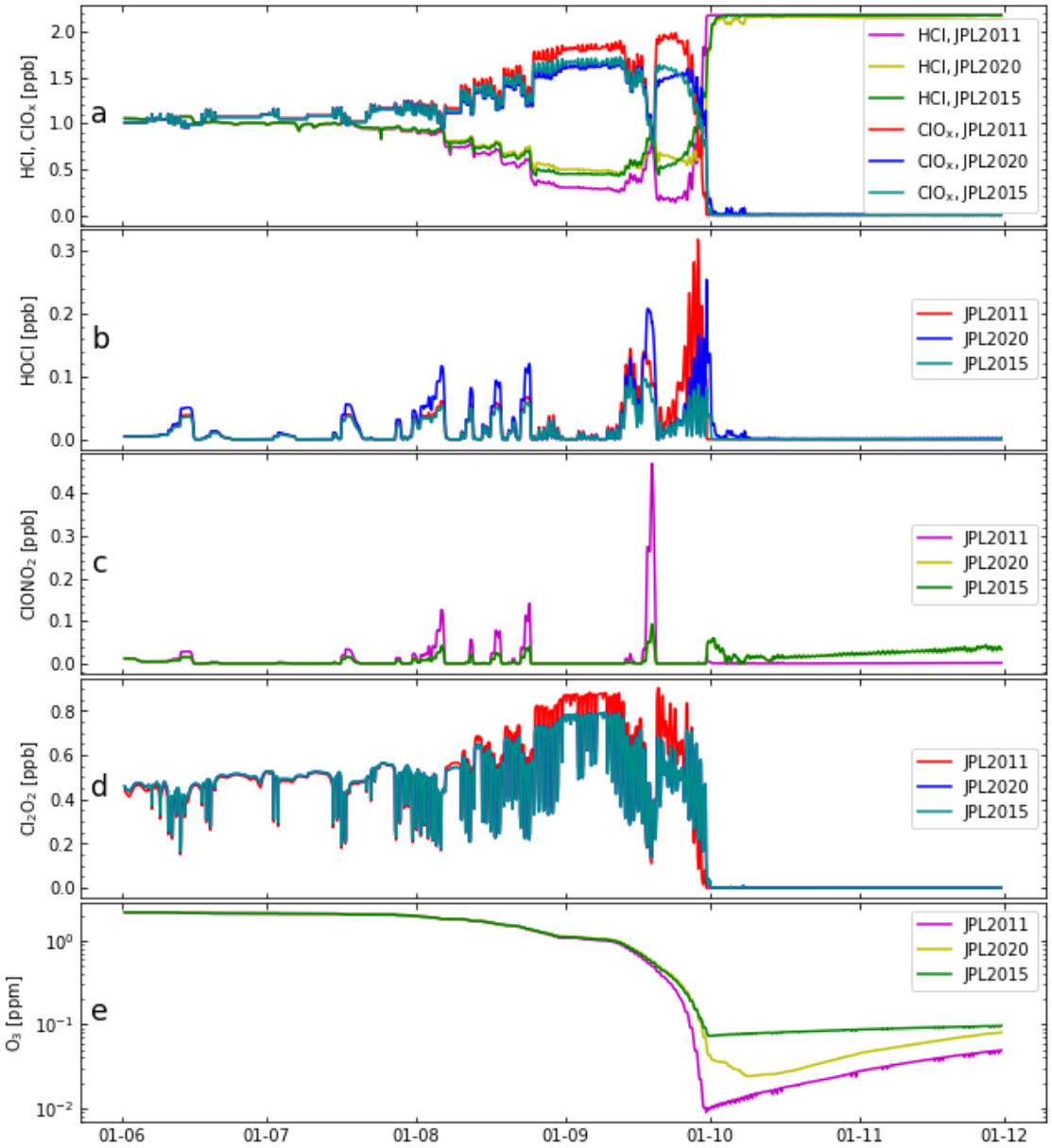

Figure A.3: Box-model simulations along a trajectory passing through the location of the ozone sonde observation at South pole of 14 ppbv on 740 hPa (391 K) on 24th September, 2003. Initial water vapour$H_2O = 2.05$ ppm for all simulations. Recommendation uses Sander et al. 2011, Burkholder et al. 2015 and Burkholder et al. 2020 respectively: (a) HCl and ClO_x, (b) HOCl, (c) $ClONO_2$, (d) Cl_2O_2, (e) ozone.

A.4 Supplement to Chapter 4 Section 4.4.1

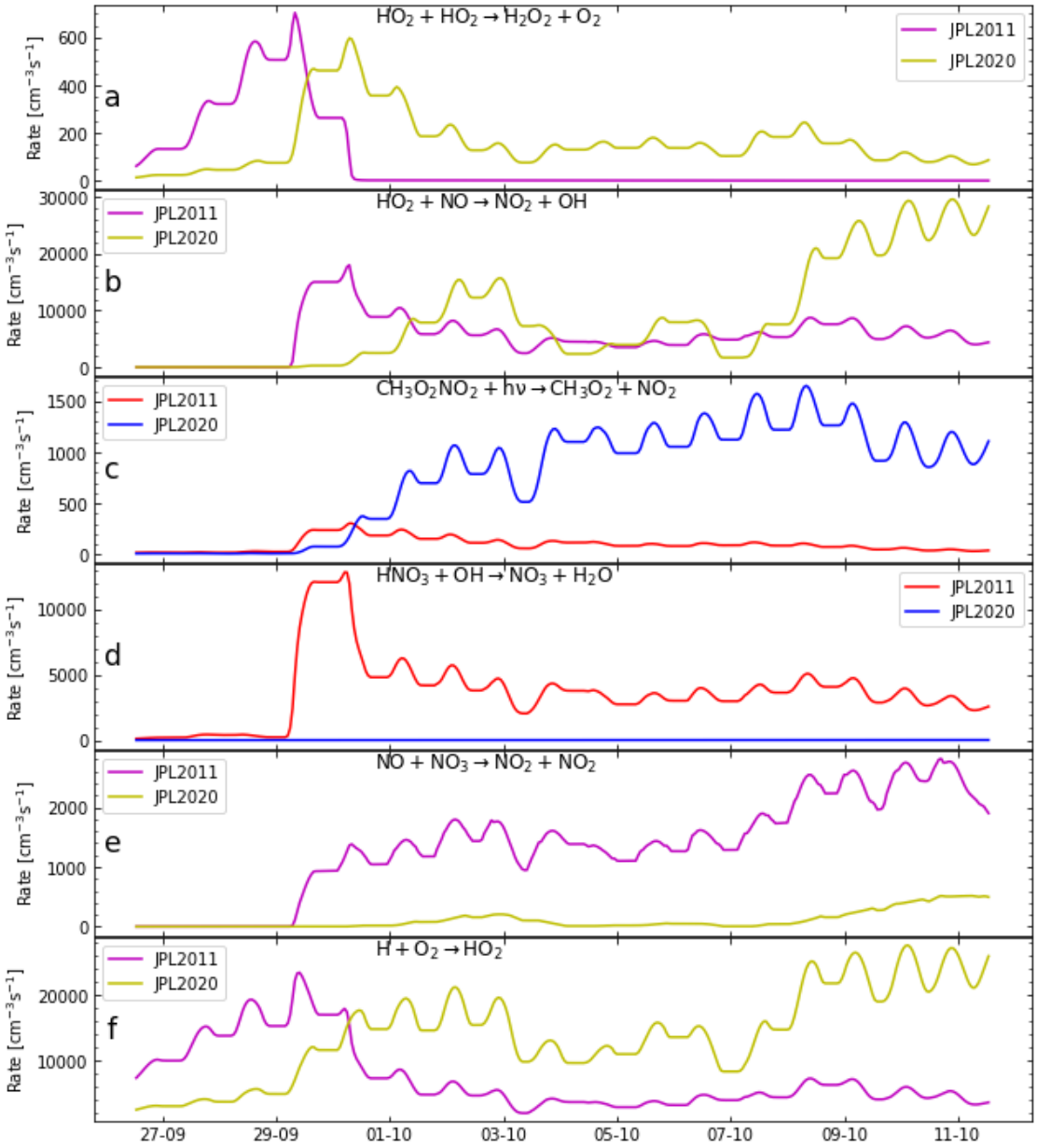

Figure A.4: Box-model simulations for initial value $H_2O = 2.05$ ppm, using recommendation Sander et al. 2011 and Burkholder et al. 2020 respectively, rates of selected reactions during 27th September to 11th October are shown. These reactions are changed in JPL2020 in comparison to JPL2011 and showed differences in the simulation. The reaction rates are plotted as 24 h running averages.